AFRL-RX-WP-TR-2012-0219

RESEARCH ON ADVANCED NONDESTRUCTIVE EVALUATION (NDE) METHODS FOR MATERIALS, PROCESS AND STRUCTURES
Delivery Order 006: Computed Radiography Crack Detection Validation Study - For Public Release

V. Kramb, C Buck, W. Hoppe, and R. Olding
University of Dayton Research Institute

JANUARY 2012

AIR FORCE RESEARCH LABORATORY
MATERIALS AND MANUFACTURING DIRECTORATE
WRIGHT-PATTERSON AIR FORCE BASE, OH 45433-7750
AIR FORCE MATERIEL COMMAND
UNITED STATES AIR FORCE

NOTICE AND SIGNATURE PAGE

Using Government drawings, specifications, or other data included in this document for any purpose other than Government procurement does not in any way obligate the U.S. Government. The fact that the Government formulated or supplied the drawings, specifications, or other data does not license the holder or any other person or corporation; or convey any rights or permission to manufacture, use, or sell any patented invention that may relate to them.

This report was cleared for public release by the USAF 88th Air Base Wing (88 ABW) Public Affairs (AFRL/PA) Office and is available to the general public, including foreign nationals. Copies may be obtained from the Defense Technical Information Center (DTIC) (http://www.dtic.mil).

AFRL-RX-WP-TR-2012-0219 HAS BEEN REVIEWED AND IS APPROVED FOR PUBLICATION IN ACCORDANCE WITH ASSIGNED DISTRIBUTION STATEMENT.

//signature//
CHARLES F. BUYNAK, Project Engineer
Nondestructive Evaluation Branch
Branch Metals, Ceramics & NDE Division
Division

//signature//
STEPHAN M. RUSS, Chief
Nondestructive Evaluation
Metals, Ceramics & NDE

//signature//
ROBERT T. MARSHALL, Deputy
Chief Metals, Ceramics & NDE
Division Materials &
Manufacturing Directorate

This report is published in the interest of scientific and technical information exchange, and its publication does not constitute the Government's approval or disapproval of its ideas or findings.

*Disseminated copies will show "//signature//" stamped or typed above the signature blocks.

REPORT DOCUMENTATION PAGE

Form Approved
OMB No. 0704-0188

1. REPORT DATE *(DD-MM-YY)*	2. REPORT TYPE	3. DATES COVERED *(From - To)*
January 2012	Technical Report	1 August 2009 – 1 April 2011

4. TITLE AND SUBTITLE
RESEARCH ON ADVANCED NONDESTRUCTIVE EVALUATION (NDE) METHODS FOR MATERIALS, PROCESS AND STRUCTURES
Delivery Order 006: Computed Radiography Crack Detection Validation Study - For Public Release

5a. CONTRACT NUMBER
FA8650-09-D-5224-0006

5b. GRANT NUMBER

5c. PROGRAM ELEMENT NUMBER
78070F

6. AUTHOR(S)
V. Kramb, C Buck, W. Hoppe, and R. Olding

5d. PROJECT NUMBER
2EDQ

5e. TASK NUMBER
00

5f. WORK UNIT NUMBER
LP106800

7. PERFORMING ORGANIZATION NAME(S) AND ADDRESS(ES)
University of Dayton Research Institute
300 College Park Drive
Dayton, OH 45469

8. PERFORMING ORGANIZATION REPORT NUMBER
AFRL-RX-WP-TP-2012-0219

9. SPONSORING/MONITORING AGENCY NAME(S) AND ADDRESS(ES)
Air Force Research Laboratory
Materials and Manufacturing Directorate
Wright-Patterson Air Force Base, OH 45433-7750
Air Force Materiel Command
United States Air Force

10. SPONSORING/MONITORING AGENCY ACRONYM(S)
AFRL/RXLP

11. SPONSORING/MONITORING AGENCY REPORT NUMBER(S)
AFRL-RX-WP-TP-2012-0219

12. DISTRIBUTION/AVAILABILITY STATEMENT
Approved for public release; distribution unlimited.

13. SUPPLEMENTARY NOTES
PA Case Number and clearance date: 88ABW-2011-5743, 27 Oct 2011. This report is the Public Release Version to AFRL-RX-WP-TR-2011-4187. If authorized also see ADB372128. This document contains color.

14. ABSTRACT
The University of Dayton Research Institute (UDRI) was awarded the Computed Radiography Crack Detection Validation Study Program in August 2009. This program was a follow-on effort to a smaller study that compared the capability of film and computed radiography (CR) for the detection of cracks in representative aerospace structures. The goals of the new program were to expand on the previous study to include additional experimental variables in the assessment of detection capability, as well as to develop the guidelines, procedures, training materials, validation testing, and probability of detection (POD) studies required for implementation of CR into Air Force radiographic procedures for crack detection. The testing and analysis performed in support of these program goals are divided into three parts. First was to develop and conduct system performance tests using radiographic standards that could distinguish between CR systems with differing crack detection capability. Second was to develop a test matrix and conduct the laboratory testing required to determine the relative crack detection capability of at least three different CR systems as compared to film. A third aspect of the program was to design and conduct a POD study that would provide a quantitative assessment of the crack detection capability of representative Air Force radiographers using both CR imaging and film. This report describes the specimens created and test procedures followed in conducting the laboratory testing. A summary of the laboratory data and analysis results is also provided. The complete procedures, guidelines, and POD analysis report can be found in the references listed at the end of this report.

15. SUBJECT TERMS
computed radiography, probability of detection, POD, crack detection

16. SECURITY CLASSIFICATION OF:			17. LIMITATION OF ABSTRACT:	NUMBER OF PAGES	19a. NAME OF RESPONSIBLE PERSON (Monitor)
a. REPORT	b. ABSTRACT	c. THIS PAGE			Charles Buynak
Unclassified	Unclassified	Unclassified	SAR	130	19b. TELEPHONE NUMBER *(Include Area Code)* N/A

TABLE OF CONTENTS

TABLE OF CONTENTS *(Cont'd.)*

Section **Page**

LIST OF FIGURES

LIST OF FIGURES *(Cont'd.)*

LIST OF TABLES

ABSTRACT

The University of Dayton Research Institute (UDRI) was awarded the Computed Radiography Crack Detection Validation Study Program in August 2009. This program was a follow-on effort to a smaller study that compared the capability of film and computed radiography (CR) for the detection of cracks in representative aerospace structures. The goals of the new program were to expand on the previous study to include additional experimental variables in the assessment of detection capability, as well as to develop the guidelines, procedures, training materials, validation testing, and probability of detection (POD) studies required for implementation of CR into Air Force radiographic procedures for crack detection. The testing and analysis performed in support of these program goals are divided into three parts. First was to develop and conduct system performance tests using radiographic standards that could distinguish between CR systems with differing crack detection capability. Second was to develop a test matrix and conduct the laboratory testing required to determine the relative crack detection capability of at least three different CR systems as compared to film. A third aspect of the program was to design and conduct a POD study that would provide a quantitative assessment of the crack detection capability of representative Air Force radiographers using both CR imaging and film.

In addition to the testing and analysis of the radiographic data; guidelines, procedures, and training materials were developed in support of the transition from film to CR for crack detection. A "Computed Radiography Qualification (Performance) Test Procedure for Crack Detection" was developed to characterize CR system performance and determine applicability for use in crack detection applications. The guidelines for technique development and validation testing of new inspection procedures were developed under this program and described in the document "Computed Radiography for Crack Detection Guidelines for Technique Development". Three training opportunities were offered for Air Force NDI personnel over the course of the program. Two of these programs were presented at the Joint AF/NAVAIR/Army Aviation NDI conference (commonly referred to as the Joint NDI Working Group Meeting (NDI WGM)) held in February 2010 and March 2011, and one extended training program was conducted at Mt. Home AFB in conjunction with the POD testing in September 2010. These training programs provided background information on the use of CR, as well as procedural training on technique development and system qualification processes for CR systems.

This report describes the specimens created and test procedures followed in conducting the laboratory testing. A summary of the laboratory data and analysis results is also provided. The complete procedures, guidelines, and POD analysis report can be found in the references listed at the end of this report.

ACKNOWLEDGEMENTS

UDRI would like to acknowledge and thank the many Air Force and contractor personnel who made this effort possible. Technical and managerial guidance provided by Kenneth LaCivita and Charles Buynak in the Air Force Air Force Research Laboratory (AFRL) at Wright-Patterson AFB is greatly appreciated. Technical guidance provided by Kenneth LaCivita at AFRL/RXSA has been invaluable throughout the program. Field inspections could not have been performed without the assistance and support of the Air Force NDI personnel located at Mt. Home and Tinker AFBs. Many thanks to TSgt Rodriguez and Mr. Brent Haynes for their support of the program and for allowing use of the Mt. Home and Tinker AFB NDI facilities. The help and support of Damaso Carreon with coordinating the field inspections is greatly appreciated. We would also like to thank Dan Laufersweiler, Dave Roberts, and Ed Porter of Universal Technology Corporation for their assistance with x-ray testing at AFRL, as well as assistance with testing provided by Brian Brown and Matt Simpson at Acuren. Technical support provided by Greg Mohr NDT with various aspects of the program is greatly appreciated. The primary program contributors from UDRI include Wally Hoppe, Chris Buck, Greg Hartman, Marylea Barlow, Ray Ko, Bob Olding, Ollie Scott, James Sebastian, Norm Schehl, Alan Gunderson, Dave Petricola, and Andrea Snell. The assistance of UDRI engineering and technical staff on this program was invaluable and their contributions to the success of the effort are greatly appreciated.

SUMMARY

This report summarizes the results of a study conducted by the University of Dayton Research Institute (UDRI) in conjunction with the Air Force Research Laboratory (AFRL) to quantitatively compare the crack detection capability of computed radiography (CR) to that of x-ray film for the detection of cracks in aircraft structures. The study included the creation of fatigue crack specimens to be used in simulated aircraft structures. The simulated structures were radiographed using a variety of CR systems and the digital images compared to conventional film images to determine the relative crack detection capability of the two techniques. A design of experiments approach was used with the laboratory testing to evaluate the crack detection capability of the various CR systems relative to film, and relative to various CR system variables. In addition to the laboratory testing, a probability of detection (POD) test was conducted to evaluate the effect of operator variability on the detection of cracks in the digital CR images and film images. The POD test was conducted following recommendations in MIL-HDBK 1823 [1].

Based on the results of laboratory and POD testing, guidelines and procedures were developed that would provide guidance for use of CR systems in crack detection of U.S. Air Force structures. These guidelines include a "CR System Qualification and Performance Test Procedure" and "Guidelines for CR System Technique Development". Training materials were also developed for users of these two guidelines, as well as training materials for all CR users on general background information for CR instrumentation and software. Training for Air Force NDI personnel was conducted on three separate occasions, twice at the NDI WGM in February 2010 and March 2011, and once at Mt. Home AFB as a foundation component of the POD testing.

Three specific high-priority inspection applications were also evaluated and techniques developed for conducting CR inspections of these specific components. Stack-ups representing the structures were tested in the laboratory and the techniques were validated on actual aircraft structures for two of the components. Drafts of the technical orders (T.O.s) needed to perform the inspections were developed for the two structures that were validated.

The following report provides a description of the fatigue crack specimens created, the CR systems studied, the laboratory and field x-ray testing performed, results of statistical and POD analysis, and recommendations for future work. Copies of the guidelines and procedures developed, as well as the POD analysis report, are included as appendices at the end of the report. Training materials are provided on CD.

Note: This report provides invaluable information to support the transitioning of traditional x-ray film methods to computed radiography. As such, it provides AFRL and ALC NDI managers the resources to amend Technical Orders (TOs) to initiate qualification and utilization of these emerging systems. Please note that standard USAF TO inspection processes must be adhered to and changes to the Technical orders can only be made by approved authorities.

1.0 INTRODUCTION

The University of Dayton Research Institute (UDRI) submits this report to the U.S. Air Force, which describes an extensive comparative evaluation of computed radiography (CR) imaging systems to that of film (F)-based x-ray inspections for the detection of cracks in aerospace relevant structural components. The test plan followed in this program was created based on input from 22 Air Force (AF) military and civilian personnel provided at the program kick-off meeting held on September 17, 2009. As a result of input provided at the kickoff meeting, a program test plan was created and distributed to the AF on October 6, 2009, shown in Appendix A.

Also discussed at the kickoff meeting was a request for input regarding which high-priority inspections should be the focus of the program development. The three high-priority inspections were selected and UDRI was notified by email on November 17, 2009 that the specific applications would be the F-15 Outboard Torque Box, the B-52 Flap Track, and the C-5 Upper Lobe Truss Splice. These specific inspection applications were chosen to span the range of crack detection applications within the AF and should provide a good indication of the applicability of CR for crack detection applications. Inspections were developed for all three applications using laboratory testing on simulated structures. Validation testing was performed at Mt. Home AFB in September 2010 on the F-15 Torque Box application and at Tinker AFB on the B-52 Flap Track application in October 2010. Validation testing was not performed on the C-5 inspection application because the radiographic inspection requirement was eliminated in December 2010.

This report provides details regarding the specimens used in testing and the x-ray tests performed in the laboratory at the Air Force Research Laboratory (AFRL), as well as the AF field sites. All references in this report to laboratory x-ray testing were conducted in the systems support laboratory at AFRL. CR systems used in the testing are described and the data acquired on the systems are summarized. However, to protect the various CR manufacturers‟ proprietary information, all CR system components are arbitrarily renamed (e.g. Scanner A, Type I imaging plate, etc.) and briefly described where applicable. Results of analysis and recommendations for future work are presented. All guidelines and procedures developed under the program are included at the end of the report in the appendices or delivered as standalone documents and referenced within the text of the final report.

2.0 METHODS, ASSUMPTIONS, AND PROCEDURES

2.1 Test Plan Development

The program was executed in phases following the test plan approved by the AF NDI personnel. The first phase of the program was to define the CR system components and variables to be studied. Similarly, the range of crack specimen variables was defined based on those AF structures with radiography inspection requirements. Once the range of specimen variables was established, fatigue crack specimens were created that could be used in x-ray testing. The second phase of the program was to characterize CR system performance using radiographic standards. The third phase of the program was to conduct x-ray testing on crack specimens and correlate the crack detection capability of the different CR systems to the performance characterized using

standards. The fourth phase of the program was to conduct the POD testing using AF operators and analyze the results. Following these testing and analysis phases of the program, procedures and guidelines were developed that would provide AF NDI personnel with the information needed to implement CR into radiographic inspections for crack detection. The following sections describe the methods, assumptions, and procedures used in conducting the studies during each phase of the program.

2.2 Phase 1: CR System and Crack Specimen Variables Definition

2.2.1 CR System Variables. The CR systems available in the USAF NDI facilities vary with regard to manufacturer, software, and age. Most are used exclusively for detection of foreign object damage or water. Both of these high-contrast radiographic inspection applications are low-risk and do not test the limits of detection capability for the CR systems. The CR systems chosen for evaluation under this program include those which are currently available in the AF depot and maintenance facilities, but are also expected to provide the highest level of performance. By limiting the testing to only CR systems with the best performance, the program was able to conduct a more-limited and efficient test matrix, as well as be more likely to identify CR systems that exhibit detection capability comparable to film. The CR system components tested under this program are listed in Table 1. Not all system variables were tested with all possible combinations of system components. The specific CR system components evaluated as part of the laboratory study are discussed in the following sections under each test type as the results are presented.

2.2.2 Film Radiography. All film radiographs used for comparison with CR images were obtained using M-type film. Laboratory testing utilized manual film processing, while field tests used local automated film processors. Image quality was assessed using film density readings made in the area of interest, typically on a penetrameter. Density readings between 1.5 and 3.0 were considered adequate for crack detection.

2.2.3 Fatigue Crack Specimen Variables. Fatigue crack specimens were created following the design developed during the first phase of the program [2]. Flat panel, center notched aluminum and steel panels were fatigue loaded until a crack grew to the desired length from the center notch. These center crack specimens were then machined so that the center portion of the specimen that contained the fatigue crack was removed. The center notch was then machined so that a center hole 10 mm in diameter remained, with a fatigue crack emanating from both sides of the hole. Final dimensions of the crack specimens are 3.85 in wide by 2.0 in high. Additional flat panel specimens with the same dimensions and center hole were machined from the excess material remaining from the fatigue specimens. These additional un-cracked specimens, referred to in this document as “spacers”, were used as additional stack-up material in order to represent a range of aircraft structure thicknesses. Figure 1 shows a schematic of the center-notched fatigue specimen and the center-hole crack specimen created from the center portion of the specimen.

The materials and thickness ranges selected for creation of the crack specimens were based on a survey of the current x-ray inspections conducted by the USAF. A summary of these inspections requirements is listed in Appendix A. Two materials, aluminum and steel, were used to create flat panel crack specimens. Panel thicknesses used in this study to create the crack specimens ranged

from 0.040-0.375 in. Table 2 lists the crack parameters for all flat panel aluminum specimens used in the study.

Table 1. CR System Variables Examined

X-Ray Tube	CR Scanner	Imaging Plate	Sample Size	Software Applications	Monitor
Phillips 0.4 mm focal spot	Scanner A	Type III (high resolution)	50 micron	Software A	Monitor A 3MP
Phillips 3.0 mm focal spot	Scanner B	Type II (standard resolution)	100 micron	Software B	Monitor B 3MP
Lorad 1.5 mm focal spot	Scanner C	Type I (coarse grain)		Image J	Monitor C 3MP

All fatigue cracks generated in flat panels grew as through-thickness cracks. The lengths reported in Table 2 were measured using optical microscopes mounted to the test machine. Each crack length was measured from the notch tip and extends out to the crack tip. The crack openings were measured on the crack specimens after machining using a microscope with 10 or 20X magnification under a no-load condition, as it would appear during an x-ray inspection. The table shows that most of the crack openings are less than 0.001 in. Cracks in actual components which would encounter a free surface, such as a fatigue crack spanning two fastener holes, would exhibit a significantly larger crack opening, even when not under load. A few cracks with larger crack openings were created to simulate this condition by applying an overload to the specimen after reaching the desired crack length. These cracks are identified by crack openings greater than 0.001 in. Additional details regarding the crack specimens, including micrographs of the crack initiation area, are included in Appendix B of this report.

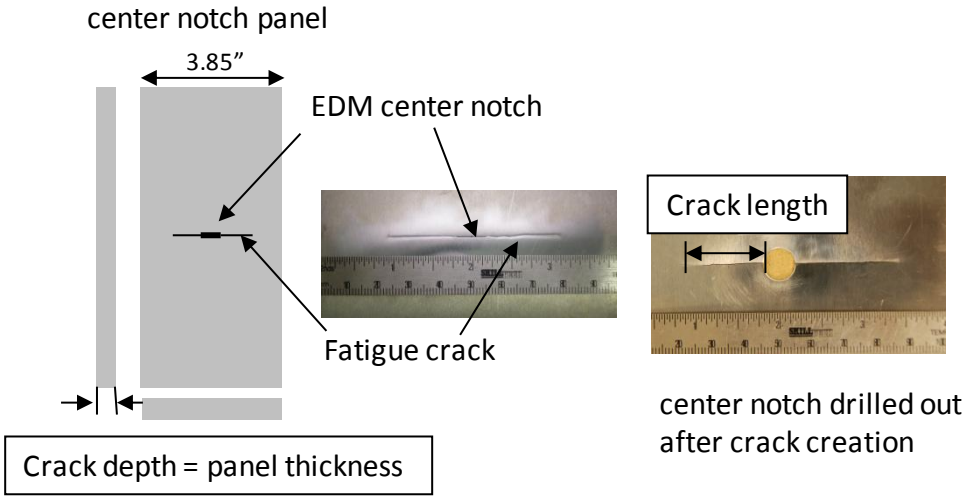

Figure 1. Fatigue Crack Specimen Design and Relevant Dimensions

Table 2. Aluminum Flat Panel Crack Specimens Used in the CR Study

	Specimen Number	Nominal Thickness (in)	Crack Length (left, in)	Crack Length (right, in)	Approx. Crack Opening (in)
1	Al-040-1	0.040	0.320	0.318	0.0002
2	Al-040-2	0.040	1.028	0.940	0.0007
3	Al-040-3	0.040	1.121	1.123	0.0300
4	Al-050-1	0.050	0.308	0.312	0.0001
5	Al-050-2	0.050	0.987	0.926	0.0004
6	Al-050-3	0.050	Fractured	1.880	0.0300
7	Al-050-4	0.050	0.522	0.492	0.0005
8	Al-050-5	0.050	0.621	0.609	0.0005
9	Al-063-1	0.063	0.650	0.720	0.0005
10	Al-063-2	0.063	0.490	0.470	0.0006
11	Al-063-3	0.063	0.780	0.730	0.0010
12	Al-100-1	0.100	0.300	0.300	0.0010
13	Al-100-2	0.100	0.969	0.932	0.0001
14	Al-100-3	0.100	0.234	0.222	0.0006
15	Al-100-4	0.100	0.573	0.542	0.0001
16	Al-100-5	0.100	0.524	0.507	0.0001
17	Al-125-1	0.125	0.309	0.298	0.0001
18	Al-125-2	0.125	0.968	0.945	0.0000
19	Al-125-3	0.125	Fractured	Fractured	
20	Al-125-4	0.125	0.532	0.514	0.0000
21	Al-125-5	0.125	0.554	0.550	0.0000
22	Al-125-1-1	0.125	0.320	0.320	0.0000
23	Al-125-2-1	0.125	0.670	0.750	0.0000
24	Al-125-3-1	0.125	1.090	0.950	0.0000
25	Al-189-1	0.189	0.293	0.308	0.0001
26	Al-189-2	0.189	1.009	0.899	0.0005
27	Al-189-3	0.189	1.063	1.017	0.0131
28	Al-189-4	0.189	0.308	0.301	0.0000
29	Al-189-5	0.189	0.974	0.958	0.0002
30	Al-189-6	0.189	0.299	0.307	0.0001
31	Al-189-4-1	0.189	0.318	0.323	0.0001
32	Al-189-5-1	0.189	0.671	0.680	0.0001
33	Al-189-6-1	0.189	1.046	1.016	0.0001
34	Al-250-1	0.250	0.08	0.300	0.0001
35	Al-250-2	0.250	0.953	0.950	0.0001
36	Al-250-3	0.250	1.185	1.122	0.0001
37	Al-250-4	0.250	0.305	0.305	0.0001
38	Al-250-5	0.250	0.947	0.934	0.0006
39	Al-250-6	0.250	0.315	0.293	0.0197
40	Al-375-1	0.375	0.328	0.336	0.0000
41	Al-375-2	0.375	1.081	0.977	0.0002
42	Al-375-3	0.375	Not used	Fractured	
43	Al-375-4	0.375	0.296	0.299	0.0003
44	Al-375-5	0.375	0.974	0.940	0.0010
45	Al-375-6	0.375	Fractured	Fractured	

In addition to the aluminum flat panel specimens, steel center-notched crack specimens were created to support steel inspection applications. The steel crack specimens were created following the same procedures as were used for aluminum, with thicknesses and crack lengths shown in Table 3 below. Additional information, including micrographs of the cracks, is also included in Appendix B of this report.

Table 3. Stainless Steel Crack Specimens Used in the CR Study

Specimen Number	Nominal Thickness (in)	Left Crack Length (in)	Right Crack Length (in)	Average Crack Opening (x1000 in)	Material
ST-050-1	0.050	0.299	0.302	0	304 SS
ST-050-2	0.050	0.946	0.803	1	304 SS
ST-050-3	0.050	0.896	0.917	5	304 SS
ST-063-1	0.063	0.318	0.193	0	304 SS
ST-063-2	0.063	0.608	0.585	0	304 SS
ST-063-3	0.063	0.886	1.014	0	304 SS
ST-125-4	0.125	0.109	0.093	0	304 SS
ST-125-5	0.125	0.238	0.305	0	304 SS
ST-125-6	0.125	0.83	0.5819	0	304 SS
ST-250-1	0.250	0.30	0.3077	1	304 SS
ST-250-2	0.250	0.85	0.8830	18	304 SS
ST-250-3	0.250	0.148	0.151	2	304 SS
ST-250-4	0.250	0.307	0.299	1	304 SS
ST-250-5	0.250	0.942	0.941	2	304 SS
ST-250-6	0.250	0.149	0.143	1	304 SS
ST-350-1	0.350	0.303	0.302	1	304 SS
ST-350-2	0.350	0.958	0.957	1	304 SS
ST-350-3	0.350	0.150	0.152	1	304 SS
ST-350-4	0.350	0.305	0.303	1	304 SS
ST-350-5	0.350	0.951	0.947	10	304 SS
ST-350-6	0.350	0.151	0.150	1	304 SS

Additional crack specimens were created from “L”-shaped aluminum panels that could be used to simulate cracks growing in rib or spar flange radius. Previous x-ray testing conducted during the first phase of the program showed that tight, penny-shaped cracks originating from the radius of the component were not detected using x-ray film or CR imaging. The specimens created under this program were designed to initiate from the flange radius, then grow to lengths which were expected to be detectable using x-rays. However, it was found during testing, that all cracks that initiated in the flange radius penetrated through the thickness of the flange, before propagating visibly from the starter notch. These through-cracks propagated through the thinnest portion of the structure, in the flange web area near, but not inside, the radius. Cracks which grew to lengths greater than 1.0 inch exhibited a very large crack opening. Smaller cracks exhibited characteristics resembling the flat panel fatigue cracks. Since all angle beam cracks were shown to grow as through-cracks in the web portion of the structure, these specimens were not used for additional tests. Rib and spar inspection applications were simulated during x-ray testing using

flat panel stack-ups with appropriate flat panel crack specimens within the stack-up. Potential influence of rib and spar geometries and other internal structures were simulated in lab testing by placing additional plates on the flat panel crack specimens, in the appropriate orientations and locations, and found to produce insignificant effects (*i.e.*, no detectable effects from x-ray scatter). Table 4 lists the crack lengths for the angle beam specimens created under this program. Note that the crack lengths listed in the table are the total length of the crack from crack tip to crack tip.

Table 4. L-Shaped Crack Specimens Used in the CR Study

Specimen I.D.	Length (in)	Width (in)	Height (in)	Thickness (in)	Crack Length (in)
LC-1	6	2.5	2.5	0.187	2.28
LC-2	6	2.5	2.5	0.187	4.69
LC-3	6	2.5	2.5	0.187	4.69
LC-4	6	2.5	2.5	0.187	1.76
LC-5	6	2.5	2.5	0.187	2.31
LC-6	6	2.5	2.5	0.187	1.59
TLC-1	6	2.5	2.5	0.125	1.00
TLC-2	6	2.5	2.5	0.125	2.48
TLC-3	6	2.5	2.5	0.125	2.54
TLC-4	6	2.5	2.5	0.125	1.38
TLC-5	6	2.5	2.5	0.125	3.39
TLC-6	6	2.5	2.5	0.125	3.74
RTLC-1	6	2.5	2.5	0.072	2.92
RTLC-2	6	2.5	2.5	0.072	0.90
RTLC-3	6	2.5	2.5	0.072	2.71
RTLC-4	6	2.5	2.5	0.072	2.01
RTLC-5	6	2.5	2.5	0.072	1.03
RTLC-6	6	2.5	2.5	0.072	2.09

2.3 Phase 2: Characterization of CR System Performance Using Standards

2.3.1 CR System Performance Metrics. Performance of a CR system in radiographic inspections depends in part, on the individual contributions of each component in that specific system. Therefore, in the following discussions, the performance of an individual CR system will include a description of the four major system components being used: the x-ray tube, CR scanner, imaging plate (IP) type, and scanner sample resolution. IP orientation relative to the laser scan direction is also included as a system parameter in reporting performance since there is an inherent orientation effect in the CR image retrieval process and its effect on image quality is not known a priori. In all discussions of system performance, the A orientation refers to that which is parallel to the IP feed direction, and the B orientation is perpendicular to the feed direction (Figure 4).

CR system performance will be discussed in terms of image noise and image resolution. Since one goal of the study was to develop performance test procedures that could be applied to any CR system, independent of specific software tools, a visual test of system performance was needed. Therefore, the Equivalent Penetrameter Sensitivity (EPS) standard (ASTM E-746-07 [3]) was selected for use in the measurement of image noise and the Air Force Computed Radiog-

raphy Process Control Specimen (AF CRPCS [4]) line pair gauges were selected for evaluation of image resolution. The standards used for measuring image noise and image resolution are discussed in Section 2.3.2 below. Other image quality standards not discussed in this report were also evaluated early on in the program. However, their ability to discriminate between CR systems with differing image quality was not demonstrated for the particular range of detection sensitivities needed for crack detection.

2.3.2 Performance Standards. Image noise was characterized for the CR systems using EPS standards described in ASTM E-746-07, and shown schematically in Figure 2. However, due to the low-energy applications for this study, aluminum was used as the standard material instead of steel as called out in ASTM E746-07. The standard consists of four separate plaques mounted on a solid piece of 2024-T3 aluminum, 0.75 in thick. The four plaques are made of the same aluminum alloy, with thicknesses: 0.015, 0.010, 0.008 and 0.005 in, respectively. Each of the three thickest plaques is machined with six rows of holes, arranged in three duplex rows. The thinnest plaque is 0.005 in thick and has 10 rows of holes arranged in five duplex rows. The holes in each duplex row have the same diameter. Each duplex row contains a total of 30 holes. Using the actual hole diameters, plaque thickness, and absorber plate thickness, an "equivalent" penetrameter sensitivity (or EPS), can be calculated per ASTM E1025. The schematic drawing in Figure 3 shows the EPS values obtained by calculating the EPS value for the absorber plate, plaque thicknesses, and hole diameters used in the AF performance testing.

The principle behind the EPS standard is that, when mounted on a 0.75-in-thick block, the sets of holes will represent equivalent penetrameter sensitivity values ranging from nearly a Number 2-T hole at the top (largest holes) to just smaller than a Number 1-T hole at the bottom (smallest holes). One advantage of the EPS plaque standard is that a finer measurement of penetrameter sensitivity is provided by 13 EPS values between 1.0 and 2.0. Also, by presenting the operator with 30 holes of equal size, spread across the width of the specimen, a better assessment of image quality can be obtained than if a standard "hole type" penetrameter containing one each 1T, 2T, and 4T hole were used. Also shown in the figure is a representative CR image of one EPS plaque, with the rows of duplex holes clearly visible. By using the EPS standard, the effects of image noise are presented over a larger region, so that localized effects are minimized. By determining rows where 20 out of the 30 holes are visible to the operator, a more-robust measurement of image quality can be made than when a single penetrameter is used in a single area of the specimen.

The image spatial resolution was characterized using the line pair targets mounted within the Air Force Process Control Standard, or CRPCS, shown in Figure 4. The line pair targets consist of parallel slits of narrowing width, cut into a lead film that produce an image of three dark lines on a light background when radiographed. The three dark lines become more narrowly spaced as the slits become more narrow and closer together, eventually becoming un-resolvable as distinct lines when they are more closely spaced than the resolution of the image or viewing system. On most CR systems, when a 14 in X 17 in imaging plate is used the two line pair targets are mounted such that the gauge in the A orientation provides a measure of the image spatial resolution in the laser scan direction (fast scan) and the gauge oriented in the B direction provides a measure of image spatial resolution in the imaging plate feed direction (slow scan). The resolution measurement is

reported in units of line pair per millimeter (lp/mm). Further details of the line pair targets and their use in CR system process control can be found in Technical Order 33B-1-2 [4].

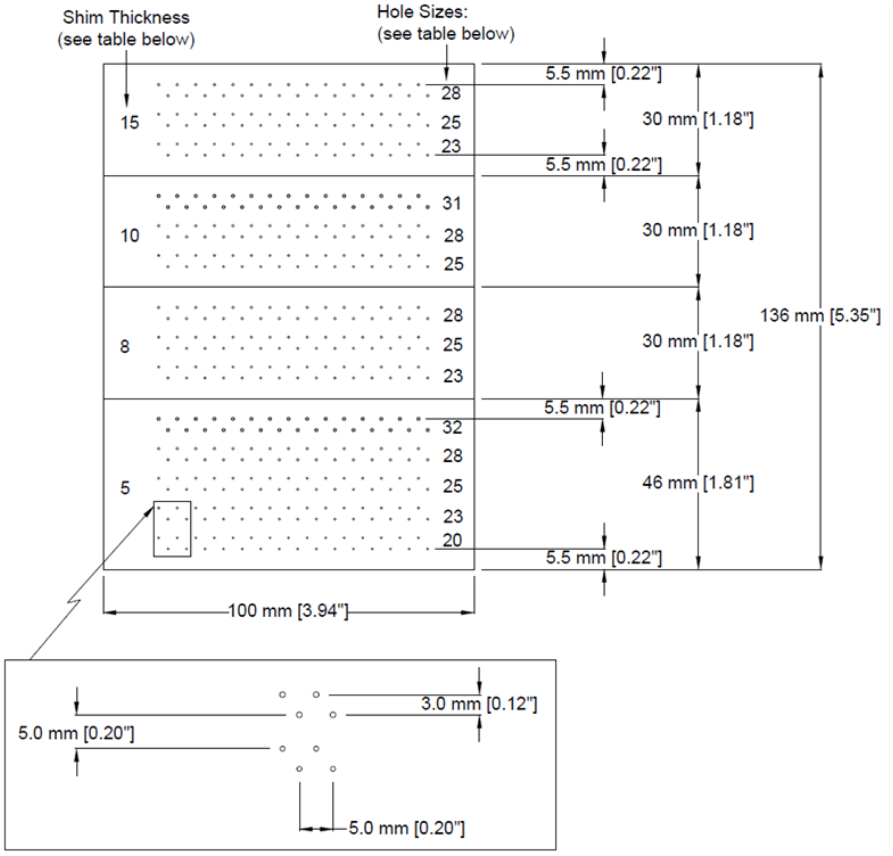

(a)

Step Identification	Shim Thickness, mm (in.)
15	0.38 ± 0.012 (0.015 ± 0.0005)
10	0.25 ± 0.012 (0.010 ± 0.0005)
8	0.20 ± 0.012 (0.008 ± 0.0005)
5	0.13 ± 0.012 (0.005 ± 0.0005)

(b)

Hole Identification	Hole Size, mm (in.)
32	0.81 ± 0.025 (0.032 ± 0.001)
31	0.79 ± 0.025 (0.031 ± 0.001)
28	0.71 ± 0.025 (0.028 ± 0.001)
25	0.64 ± 0.025 (0.025 ± 0.001)
23	0.58 ± 0.025 (0.023 ± 0.001)
20	0.50 ± 0.025 (0.020 ± 0.001)

(c)

Hole Spacing (horizontal): 5 ± 0.1 mm (0.2 ± 0.004 in.) Noncumulative
Row Spacing: 3 ± 0.1 mm (0.2 ± 0.004 in.)
Spacing between hole sets: 5 ± 0.1 mm (0.2 ± 0.004 in.)
All other dimensions shall be in accordance with standard engineering practice.

(d)

Figure 2. (a) EPS Plaques Made to Specifications and Tolerances: (b) Plaque Thicknesses, (c) Hole Diameters, and (d) Hole Spacing

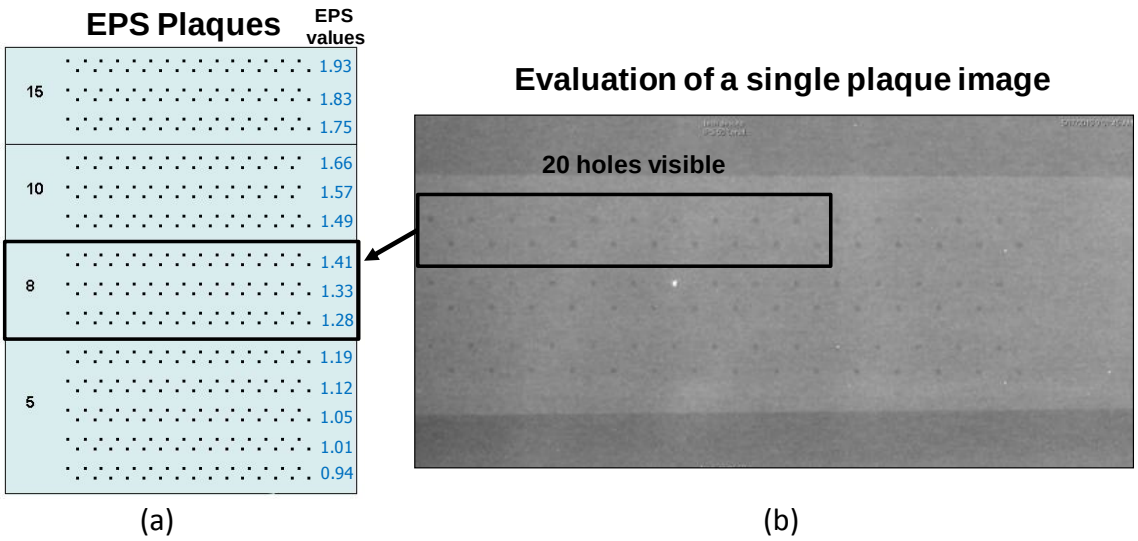

Figure 3. (a) Schematic of EPS Specimen Showing Individual Plaques, Thicknesses (in mils), and Equivalent EPS Values, (b) CR Image of Individual EPS Plaque Showing Holes with Properly Set Window and Level for Evaluating Image. EPS Value for Duplex Row in Box is 1.41%EPS

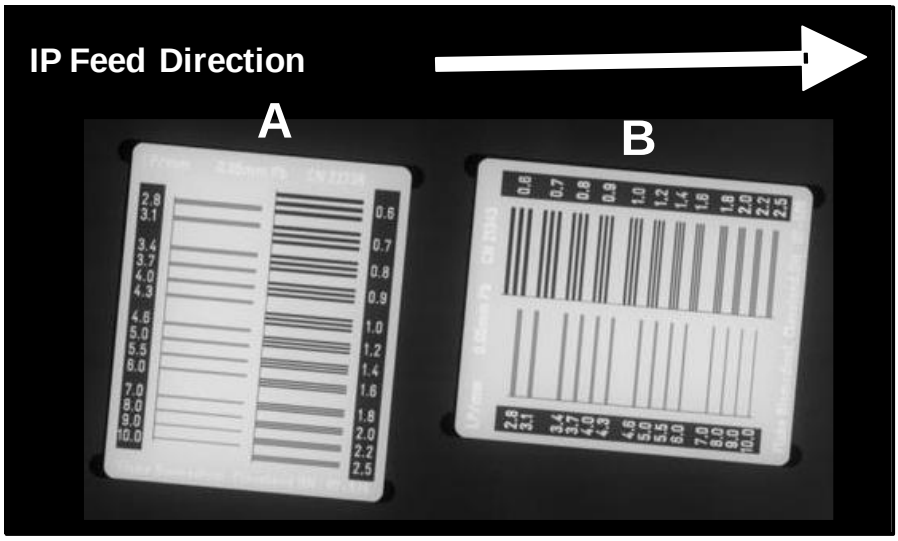

Figure 4. Line Pair Targets Used to Measure Image Spatial Resolution During System Performance Testing

2.3.3 Performance Test Execution. Performance tests were conducted on each CR system in the AFRL laboratory using the same set of EPS and line pair standards. Image resolution tests were conducted following procedures described in T.O. 33B-1-2 [4]. Images of the EPS specimen were acquired over a range of technique settings. Since radiographic image noise improves with increasing exposure (tube current multiplied by exposure time) up to a point, the EPS tests

were conducted over a large enough range of exposures that the minimum image noise achievable by the CR system could be evaluated. Typically, images were acquired over a range of exposure times from 15 sec to 240 sec, with a constant current setting of 5 mA. A constant energy (kV) was selected for all exposures that would not result in a saturated (i.e. overexposed) image, typically around 65kV. Average image intensity values were recorded along with the technique and CR system settings. All performance tests were conducted at a distance of 48 in, measured from the x-ray tube focus to the IP or film.

2.3.4 Performance Test Evaluation. Evaluation of the CR images was performed using four different operators working on three different CR image processing workstations running software native to the CR scanner. Operators were instructed regarding use of the software tools for adjusting image brightness/contrast and proper magnification settings to be used for CR images with different pixel resolutions. Use of software filters during image evaluation was not permitted. The minimum EPS reading and maximum image resolution results for each system configuration were manually recorded in a binder. The results for each test condition were then averaged for the four operators and the average value used to assess system performance.

Evaluation of film images was performed using a light box. Use of 5× hand magnifiers or a 7× loupe was left to the discretion of the operator. As with the digital images, the image spatial resolution and minimum EPS readings were recorded for each operator in a binder.

2.4 Phase 3: Characterization of Crack Detection Capability for CR Systems and Film

2.4.1 Test Matrix Development. Two types of comparative testing were performed under the study. First, a few tests of specific CR system configurations were examined to identify potential variables for the comparative study. Second, a Design of Experiments approach was used to develop a test matrix that could be conducted on a specific set of CR system configurations to assess crack detection capability and compare that capability to film. Due to the large number of variables being examined under the program, it was necessary to limit the number of x-ray tests performed under the comparative study to a tractable number so that data acquisition and analysis could be completed under the time constraints of the program. Therefore, after preliminary testing, some of the test variables for both the CR systems and crack specimens were eliminated from the study. The list of test matrix variables examined under the capability study is shown in Table 5. These CR system variables are a subset of the total shown previously in Table 1. Preliminary testing also indicated that improvements in image resolution (*i.e.*, 50 micron) provided benefit in the detection of linear indications, such as cracks. Also, it was decided that, in the interest of time, if high-quality Type III imaging plates were available for testing, then, most likely, higher-resolution, 50-micron scanning would also be employed to obtain the highest quality image possible. As will be discussed later in Section 3.2, results of the capability study later indicated that for some CR system configurations a higher quality image may be obtained when using a scan resolution larger than 50 micron (*i.e.*, 100 micron). In addition, when selecting the test variables particular consideration was paid to the immediate concerns of USAF NDI community. Type II plates were the only type of IP that was common to all USAF NDI shops, therefore, while Type III imaging plates were evaluated using only 50 micron scan resolutions, the Type II plates were scanned using both 50 and 100 micron resolutions.

Table 5. CR System Variables Evaluated in the Laboratory Capability Study

X-Ray Tubes/ Focal Spots	CR Scanners	Imaging Plate Types	CR Scanner Resolutions	Orientations
Phillips/0.4mm Lorad/1.5mm	Scanner A Scanner B Scanner C	Type III Type II	50 micron 100 micron	A B

The laboratory testing of crack specimens was conducted using a window frame structure that was designed to accept 15 "specimen stacks" of a specific total thickness. The specimen stacks were created by combining cracked and un-cracked (referred to as "spacers") aluminum panels arranged in such a way that the cracked panel was always located on the bottom of the stack and nearest to the film or IP during exposure. It should be noted that the effects of un-sharpness were evaluated in separate laboratory testing and were not added into the laboratory test matrix in order to keep the number of inspections manageable. Laboratory testing to compare CR system capability utilized a frame and corresponding specimen stacks with a total stack-up thickness of 0.375 in. During x-ray testing, specific crack specimen stacks were placed in specific locations within the frame. Figure 5(a) shows a typical frame with crack specimens in place. Figure 5(b) illustrates the numbering scheme used to identify the location of the cracked specimens within each exposure. The pattern of crack specimens shown in Figure 5 will be referred to in this report as "Test Matrix 2", or TM2. Additional information regarding the specimen stacks used in TM2 can be found in Table 6.

The crack specimens selected for TM2 are characterized by crack length and crack depth. Since all cracks were through-cracks, depth is equivalent to the crack panel thickness. Due to the time constraints of the program and the need to improve statistics for the final comparative analysis, two groups of crack lengths were examined in the capability study, which will be referred to in the analysis as "short" and "long". The short cracks refer to specimens whose fatigue crack extension from the notch is approximately 0.3 in. The long cracks are those in which the crack extension was approximately 1.0 in from the notch. Test Matrix 2 was designed to contain eight short and seven long crack specimens. These particular crack lengths were chosen based on the inspection applications. Since many radiographic inspections are to detect cracks growing from or near fastener holes, a minimum crack length that would be detected using x-rays would be one which protrudes from a fastener head. Therefore, for a fastener head overhang of approximately 0.1 in and a crack growth beyond the fastener head of 0.2 in, a total crack length of 0.3 in was a reasonable estimate as the minimum crack length that would be reliably detected using x-rays. The maximum crack length was chosen similarly. Fatigue cracks that grow between fastener holes, typically, remain tight and closed until reaching an open surface, at which time, the crack opening can become significantly larger. Since typical fastener hole spacing is 1.0 in, a maximum crack length that would be expected for tightly closed fatigue cracks is approximately 1.0 in. Therefore, the long crack condition tested in the capability study contained specimens whose crack growth was approximately 1 in from the center notch. Keep in mind that each specimen contained a crack of approximately equal length growing from both sides of the notch. Therefore, later in the results section of this report, the analysis will refer to the 16 short and 14 long cracks contained in TM2, which includes both the right and left sides of the crack specimen separately. For simplicity, Table 6 lists the average crack length for each specimen in the TM2 arrangement, but Tables 2

and 3 list the specific crack lengths measured for the right and left side of the crack for all specimens created in the study.

In order to evaluate the effect of crack specimen position relative to the x-ray beam center, two other arrangements of these same 15 crack specimen stacks were tested during the program, referred to as Test Matrix 1 (TM1) and Test Matrix 4 (TM4). The arrangement of crack specimens utilized with these two test matrices are shown in Figure 6. The corresponding information for specimen stacks in TM1 and TM4 is the same as for TM2, with the specific frame locations changed according to the arrangement of crack specimens.

The same frame design was also used to test an arrangement of 15 steel crack specimens, referred to as Test Matrix 3 (TM3). Figure 7 shows the arrangement of crack specimens in TM3 with the specific specimen stack information. Note that TM3 utilized a steel frame that was 0.250 in thick. Therefore, the steel specimen stacks in TM3 are also 0.250 in thick. Due to the more-limited application of steel in radiographic inspections, the crack lengths selected for steel specimens are more varied than those used in the laboratory testing of aluminum. Due to the interest expressed within the AF for the assessment of crack detection capability for smaller crack lengths, several specimens were created with lengths in the 0.10 in range.

The effect of additional obstruction layers on crack detection was evaluated by adding layers of aluminum on top of the crack specimen frames prior to x-ray exposures. In all cases, the frame containing the crack specimens was on the bottom of the stack-up next to the imaging plate or film. For the aluminum specimens, three total stack-up thicknesses were tested: 0.375, 0.625, and 1.125 in of aluminum. For the steel specimens, only two stack-up thicknesses were evaluated: 0.250 in of steel, and 0.250 in of steel with an additional 0.250 in of aluminum added.

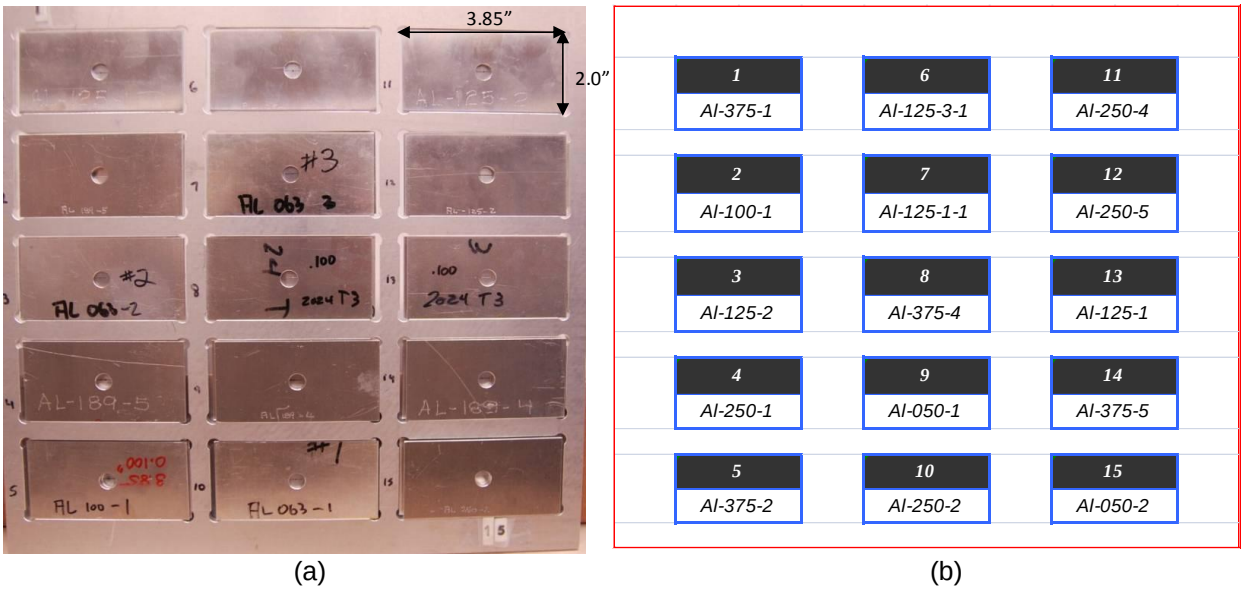

(a) (b)

Figure 5. (a) Panel Layup Containing Cracked Specimens for Laboratory Testing, (b) TM2 Panel Layup Record Identifying Specimen Locations Within the Frame

Table 6. TM2 Specimen Stack Information – Total Stack-Up 0.375 in

TM2 Position	Crack Specimen Number	Avg. Crack Length (in)	Thickness (in)	Crack Layer % Total	Spacers Used
1	Al-375-1	0.32	0.375	100	none
2	Al-100-1	0.31	0.1	27	Al-125-1, Al-100-2, Al-050-2
3	Al-125-2	0.96	0.125	33	Al-250-2
4	Al-250-1	0.30	0.25	67	Al-040-2, 2 x Al-040-1
5	Al-375-2	1.03	0.375	100	none
6	Al-125-3-1	1.02	0.125	33	Al-250-1
7	Al-125-1-1	0.32	0.125	33	Al-250-4
8	Al-375-4	0.29	0.375	100	none
9	Al-050-1	0.31	0.05	13	Al-125-2, 2 X Al-100-2
10	Al-250-2	0.95	0.25	67	Al-125-1
11	Al-250-4	0.31	0.25	67	Al-125-2
12	Al-250-5	0.94	0.25	67	Al-063-1, Al-063-3
13	Al-125-1	0.30	0.125	33	Al-250-1
14	Al-375-5	0.96	0.375	100	none
15	Al-050-2	0.96	0.05	13	Al-250-2, 2 X Al-040-2

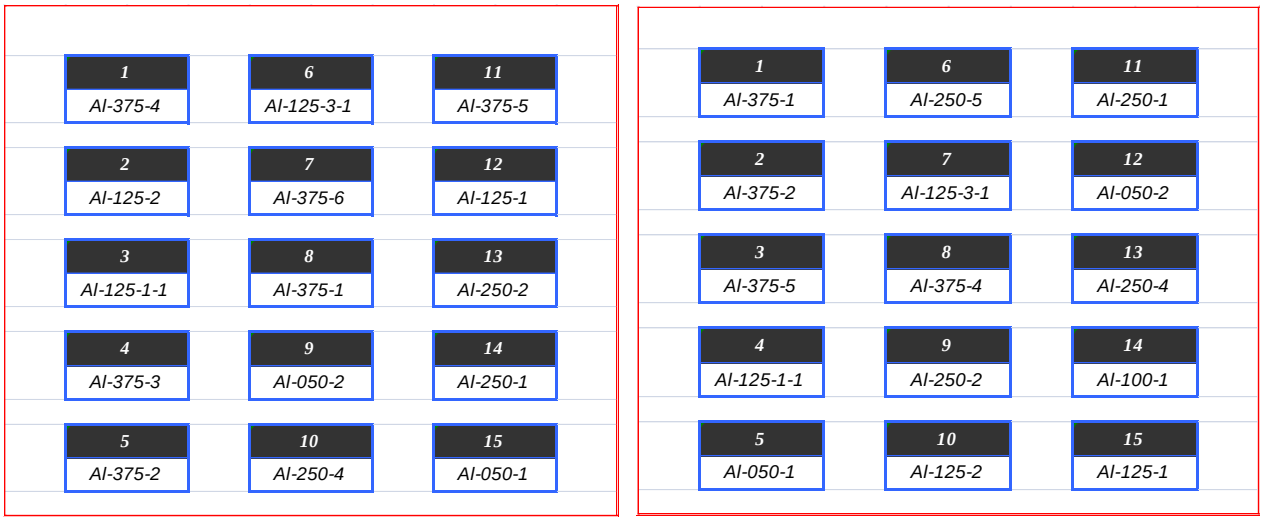

(a) (b)

Figure 6. Crack Specimen Arrangements Used in (a) Test Matrix 1 and (b) Test Matrix 4

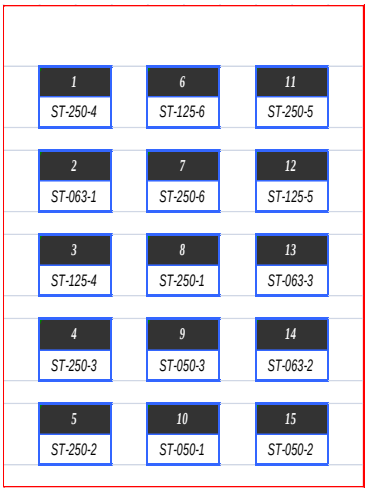

(a)

Test Matrix 3-Steel					
test matrix position	Specimen number	Avg. crack length (in.)	Thickness (in.)	% total stack-up	spacers used
1	ST-250-4	0.31	0.25	100	none
2	ST-063-1	0.26	0.063	25	ST-063-3, ST-125-6
3	ST-125-4	0.10	0.125	50	ST-125-5
4	ST-250-3	0.15	0.25	100	none
5	ST-250-2	0.87	0.25	100	none
6	ST-125-6	0.70	0.125	50	ST-125-4
7	ST-250-6	0.15	0.25	100	none
8	ST-250-1	0.30	0.25	100	none
9	ST-050-3	0.91	0.05	20	ST-050-1, ST-050-2, 2 X ST-050-3
10	ST-050-1	0.30	0.05	20	4 X ST-050-1
11	ST-250-5	0.94	0.25	100	none
12	ST-125-5	0.27	0.125	50	ST-125-6
13	ST-063-3	0.95	0.063	25	ST-063-3, ST-125-5
14	ST-063-2	0.60	0.063	25	ST-063-2, ST-125-4
15	ST-050-2	0.88	0.05	20	3 X ST-050-2, ST-050-3

(b)

Figure 7. (a) Crack Specimen Arrangement Used in Test Matrix 3 and (b) Specimen Stack Information by Test Matrix Location

2.4.2 Laboratory X-Ray Testing. As previously discussed in Section 2.4.1, x-ray testing performed as part of the study to evaluate CR system capability primarily utilized the TM2 arrangement of crack specimens. Limited testing was conducted using the TM1 and TM4 arrangement. The tests were conducted using three total stack-ups: 0.375, 0.625, 1.125 in. The 0.375 in stack-up consisted of the test matrix frame of specimens alone, with no additional obstruction layers. Table 7 shows the distribution of crack layer thicknesses used for all three stack-ups.

Table 7. TM2 Crack Layer Percent of Total Stack-Up

Test Matrix Position	Crack Specimen Number	Avg. Crack Length (in)	Thickness (in)	Crack Layer % Total Stack-Up		
				0.375 in	0.625 in	1.125 in
1	Al-375-1	0.32	0.375	100	60	33
2	Al-100-1	0.31	0.1	27	16	9
3	Al-125-2	0.96	0.125	33	20	11
4	Al-250-1	0.30	0.25	67	40	22
5	Al-375-2	1.03	0.375	100	60	33
6	Al-125-3-1	1.02	0.125	33	20	11
7	Al-125-1-1	0.32	0.125	33	20	11
8	Al-375-4	0.29	0.375	100	60	33
9	Al-050-1	0.31	0.05	13	8	4
10	Al-250-2	0.95	0.25	67	40	22
11	Al-250-4	0.31	0.25	67	40	22
12	Al-250-5	0.94	0.25	67	40	22
13	Al-125-1	0.30	0.125	33	20	11
14	Al-375-5	0.96	0.375	100	60	33
15	Al-050-2	0.96	0.05	13	8	4

TM3 containing steel specimens was also evaluated using the laboratory CR and film systems. TM3 was evaluated using only the steel specimens with a total stack-up thickness of 0.250 in steel, and also with an additional layer of 0.250 in of aluminum.

All laboratory testing of crack specimens was conducted with a focus-to-IP distance equal to 60 in. This distance provided a cone of detection of 5 degrees, which included the 11 central crack specimens. The 4 outermost crack specimens were within 7.5 degrees of the central beam. T.O. 33B-1-1 implies a 5 degree maximum for crack detection using film.

Laboratory testing of the crack specimens was conducted with the cracks oriented in both the A and B directions of the CR scanner. Results will be presented for both orientations and the effect of crack orientation on detection capability discussed. Due to the homogeneous nature of film and manual processing used at AFRL, films were assumed to have no orientation effects. A limited evaluation of film images verified this assumption. Film images were, therefore, evaluated with cracks oriented in only one direction, visually equivalent to the A orientation of the CR radiographs.

All CR and film images used in the comparative study were obtained using a medium exposure level. For the CR systems tested, a minimum exposure level of 900 mAs (180 sec at 5 mA) was adequate to achieve a medium level of exposure. Film exposures were obtained with a nominal exposure of 900mAs with the Lorad tube and 1200mAs with the Phillips tube. In order to obtain a complete data set, it was necessary to include one Lorad film exposure in the analysis that was acquired with a exposure level of 550 mAs. Although a complete assessment of CR system performance had not been completed at the time of the comparative study or POD testing, preliminary testing indicated that these exposure levels would result in images that were representative of the system capability. In addition, these exposure levels were comparable (or longer) than nearly all crack detection applications for the F-15, C-130, and T-38 aircraft and, therefore, considered to be reasonable representation of field level inspections.

2.4.3 CR and Film Crack Image Evaluation Procedures. Crack images were evaluated on campus at UDRI using ImageJ software on two image processing workstations [5]. ImageJ is an open-source software application that was developed by the National Institute of Health so that medical images could be viewed using an independent software application that was system- and manufacturer-independent. Using ImageJ, operators adjusted window and level (brightness and contrast) and magnification of the CR images through mouse and menu controls. Image transformations, such as rotations and panning the images, could also be performed. Cracks which were visible in the image were measured using a measurement tool that calculated length based on pixel size. All CR crack images analyzed were stored in DICOM formats, which is a nonproprietary image data format that can be opened using ImageJ. The DICOM-formatted images also contain embedded tags which provide information regarding the x-ray technique used to acquire the image, CR scanner settings, and other information that the operator may choose to enter at the time of data acquisition.

During crack image evaluation, the crack lengths were measured on both the right and left sides of the center hole for each specimen in the matrix. The crack length measurements were then compared to the optical crack lengths to determine errors in crack measurements. An effective "hit/miss" assessment was also obtained from the crack length measurements by assigning a "hit"

to all crack lengths measured which were larger than a specific minimum value, typically, 0.050 in or 25 pixels of a 50 micron CR image. This criterion was established based on the minimum crack length that could be reliably measured on film images by the lab data operators. Using magnifiers and a ruler, a minimum crack length was determined to be approximately 1 mm, or 0.040 in. Therefore, in the evaluation of hit-miss data, all crack length measurements that were greater than 0.050 in were considered a "hit". Although hit/miss analysis provides a measure of detection capability for comparing CR systems, ideally an analysis of the errors in the actual crack length measurements should be performed on the data to compare inspection accuracy and false calls. Due to time constraints under the program, the error analysis was not completed. Other options are also possible for hit/miss data analysis by imposing different criteria for the minimum crack length used to define a "hit".

Additional capability was provided within the ImageJ software through the use of customized "Plugins" developed by UDRI. These plugins provide image analysis tools that can be used to obtain image statistics such as signal-to-noise ratio (SNR), contrast-to-noise ratio (CNR), line profiles, and auto adjust the image brightness and contrast using image statistics. Details of the ImageJ Plugins developed under the CR program are discussed in Appendix C.

Film images were evaluated using a light box with adjustable brightness. Crack lengths were measured on the films using a ruler. Operators were permitted to use hand magnifiers or a 7× loupe. Crack length measurements were recorded in a binder and later tabulated into spreadsheets for evaluation and comparison with CR measurements.

2.4.4 CR and Film Crack Measurement Analysis Procedures. Analysis of the crack length measurements was performed using three methods. First, a direct comparison of the hit/miss results were made for all CR systems and film. Second, a paired t-test was employed as one measure of statistical significance of the observed differences in the hit/miss performance for specific crack lengths and stack-up thicknesses. Third, a z-test was used to compare the proportion of hits between the different CR systems and to film. Additional details of the analysis used in the comparative study will be discussed in Section 3.

2.4.5 Correlation of Crack Detection Capability with System Performance. Comparisons were made between the hit/miss crack detection results and the system performance data to determine if a qualification criterion could be found that characterized CR systems performing at a level that was equal to or the same as film for crack detection. These comparisons were also compared with statistical analysis of the data to determine a level of confidence that can be assessed to the qualification criteria. Additional details of the methods used to determine CR system performance and how the performance correlated with crack detection capability will be discussed later in Section 3.

2.5 Phase 4: POD Testing

2.5.1 POD Test Matrix Development. One goal of the POD testing was to assess the variability introduced into the x-ray inspection process due to evaluation of the CR images by human operators and compare that to the variability in evaluation of film images. Although human operators currently evaluate film based radiographs, it was not known a priori whether or not the

variability in the evaluation of CR images would be greater than, less than, or the same as that observed with film image evaluations. Due to the large number of variables being tested in the laboratory CR capability study, it was necessary to limit the POD testing to a single CR system, and a single IP orientation, for acquisition of the CR images. The CR system chosen was based on preliminary data that suggested Scanner A, with Type III imaging plates, scanned with a 50-micron resolution, in the A orientation provided the optimum detection capability. Although some differences in detection capability due to image orientation had been previously observed, preliminary testing of crack specimens showed that for the CR system used in the POD study the effect was marginal. Therefore, all POD images were acquired using a single IP orientation. Both IP orientations were evaluated in the laboratory study, and the effects of IP orientation on overall system capability are discussed later in Section 3. Due to availability, the Phillips 0.4mm focal spot tube was used with both film and CR. Therefore, all POD images were acquired using this same CR system. All CR images were also acquired using M-type film. All exposures were obtained using a medium exposure level, as previously discussed in Section 2.4.2.

The POD test matrix was developed following guidelines in MIL-HDBK 1823 as closely as possible. The test matrix of crack specimens included those used in the laboratory testing, plus additional crack specimens with crack lengths between 0.3 and 1.0 in so that a sufficient range of crack lengths and crack thicknesses were represented. A list of all the crack specimens used in the POD study was shown in Table 2. Additional details of the POD analysis processes and results obtained are contained in [6].

2.5.2 Correlation of POD Results with Laboratory Studies. Although the POD images were evaluated using field AF operators, it is still possible to correlate the results with that of the laboratory capability study. By allowing the operators that evaluated the images for the laboratory CR capability study to also evaluate the set of POD images, a comparison can be made between the POD of the AF operators and that of the capability study evaluators. Also, since the CR system that was used to acquire the POD images is also one of the systems used in the capability study, a direct comparison can be made between the performance of all other CR systems and that of the POD system. These results and the process used to make the comparisons will be discussed in more detail in Section 3.4.

2.6 Application-Specific Testing

Under the CR program, inspection procedures were developed for the use of CR in crack detection for three specific applications selected from those listed in Appendix A by Air Force NDI personnel. The three applications, announced to UDRI on November 17, 2009, included: the F-15 Outboard Torque Box Upper Spar, the B-52 Flap Track, and the C-5 Upper Lobe Truss Splice. Each of these applications was tested in the laboratory using simulated stack-ups that represented the total beam path thickness and the crack layer thickness of the actual structure, as well as unsharpness as defined by the focus to detector distance and object to detector distance. Later in the program, inspection procedures developed for the F-15 and B-52 applications were tested in the field on actual aircraft structures. In December 2010, UDRI was notified that the C-5 inspection application was no longer being conducted and, therefore, validation testing on an actual component would not be conducted under the program. Based on the results of laboratory and the limited field testing, drafts of a test procedure for each of the specific applications were developed and can be found in [7-9]. A brief summary of each application is included below for completeness.

2.6.1 F-15 Outboard Torque Box Upper Spar. One unique aspect of the F-15 inspection application is that the cracks originate from fatigue loading in the radius of the spar structure. It was initially assumed that the cracks were propagating within and parallel to the radius, however, laboratory testing discussed in Section 2.2.3 showed that the cracks generated in the radius quickly grew to through-thickness cracks which propagated in the thinner web portion of the spar structure. Therefore, it was determined that a valid approach to inspection technique development for the F-15 Outboard Torque Box Upper Spar would be to use flat panel aluminum specimens equal to the total stack-up, with crack layers located at the appropriate depths for the actual component cross section. Figure 8 shows a schematic of the structure cross section and the representative stack-up used to develop the technique.

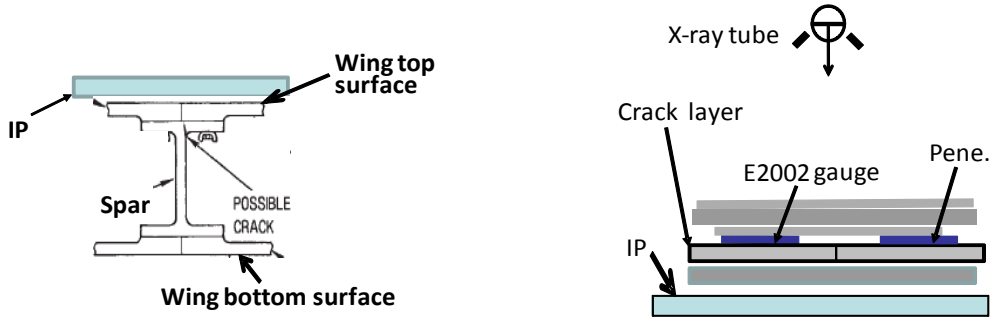

Figure 8. (a) F-15 Outboard Torque Box Spar Schematic Cross Section and (b) Specimen Stack-Up Used in Laboratory Testing

The laboratory testing included evaluation of the image un-sharpness present in the actual inspection due to the distance between the crack layer structure and the position of the IP, and the distance between the tube focus and IP. A duplex wire gauge, described in ASTM standard E2002 [10], was utilized for the measurement of total image un-sharpness. Also, visualization of a 2-T penetrameter hole was used in technique development to verify beam penetration and intensity levels on the image. Crack layers were placed at the position of the crack layer in the structure as a check for how the crack images might actually appear during an inspection.

The technique was validated in the field at Mt. Home AFB in September 2010 using the CR scanner, workstation, and x-ray tube available at the maintenance facility. To simulate the cracked structure, three cracked plates of the approximate thickness of the spar flange were placed on top of the aircraft wing and positioned such that the cracks would appear in the radiograph as though they were in the radius geometry oriented parallel to the radius (Figure 9). The imaging plate was then laid on top of the wing and crack specimens for imaging. This configuration, with imaging plate immediately next to the crack specimens, resulted in an unconservative assessment of unsharpness, but the purpose of this test was only to evaluate the effects of structural geometry, scatter and to confirm adequate x-ray penetration. The x-ray testing on the aircraft showed no unusual effects due to scatter or unexpected obstructions in the CR images. Development of the T.O. for inspection of the F-15 Outboard Torque Box Spar was based on that validation testing at Mt. Home AFB, information contained in the existing film T.O., and following the procedures

described in the Computed Radiography for Crack Detection Guidelines for Technique Development [11] developed under this program. The entire F-15 Outboard Torque Box Spar inspection T.O. can be found in [7].

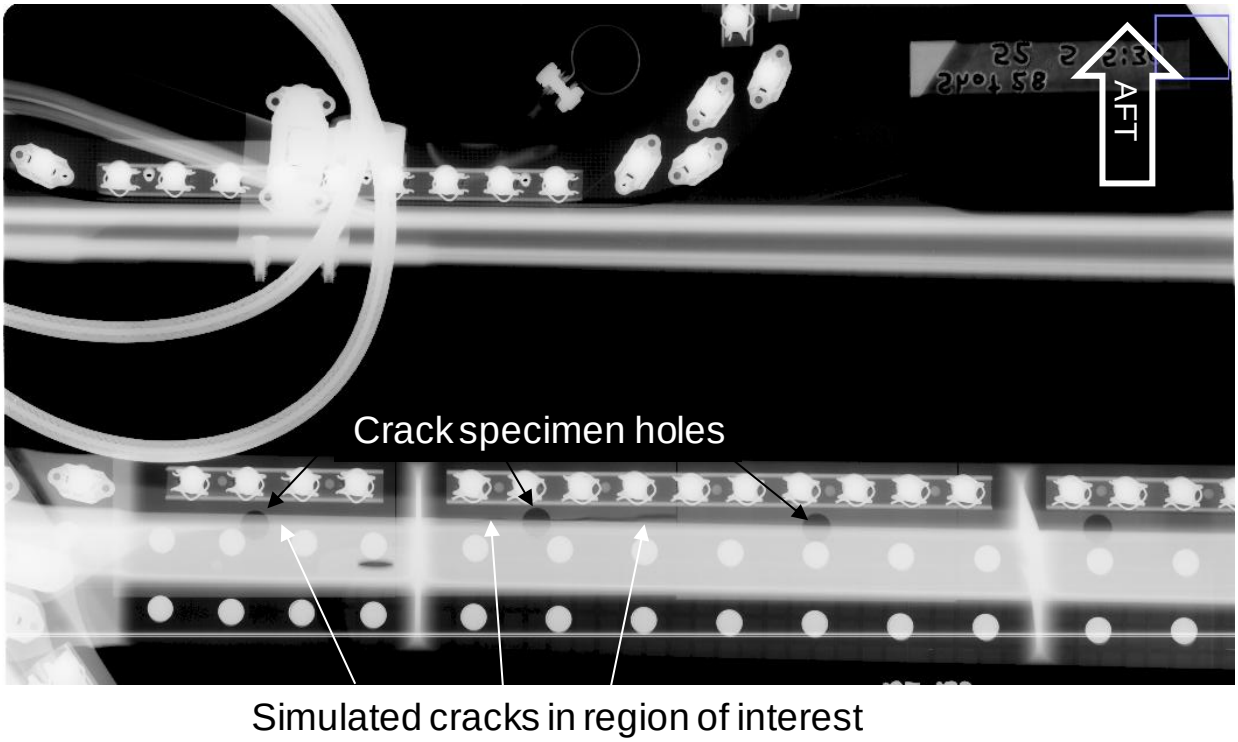

Figure 9. CR image of F-15 Outboard Torque Box Spar On-Wing Testing

2.6.2 B-52 Flap Track. The B-52 Flap Track application is one of the few USAF aircraft radiography inspections that involves cracks growing within a steel structure. The steel support structure is hidden on both sides by an aluminum doubler, so that the total stack-up consists of approximately 0.250 in of steel with 0.250 in of aluminum. Another challenging aspect of the flap track inspection is that access to the structure is limited due to the location of the other flap tracks and supporting struts on the wing (Figure 10). As a result of the limited access, the tube-to-IP distance is either 15 or 17 in and, thus, shots must be acquired at 2-in intervals to maintain the appropriate cone of radiation for the inspection. Due to the limited access and shape of the flap track components, the IP used for validation testing must be cut to fit the shape of the region of interest. All of these specific details of the flap track inspection were accounted for in the development of an inspection technique. Steel crack specimens 0.25 in thick were used with the aluminum spacers to simulate the total stack up in the laboratory. In addition, actual flap track components that were made available for testing during the study were used to verify detection capability. Some of these components contained naturally occurring fatigue cracks, which were detected in the laboratory using both CR and film.

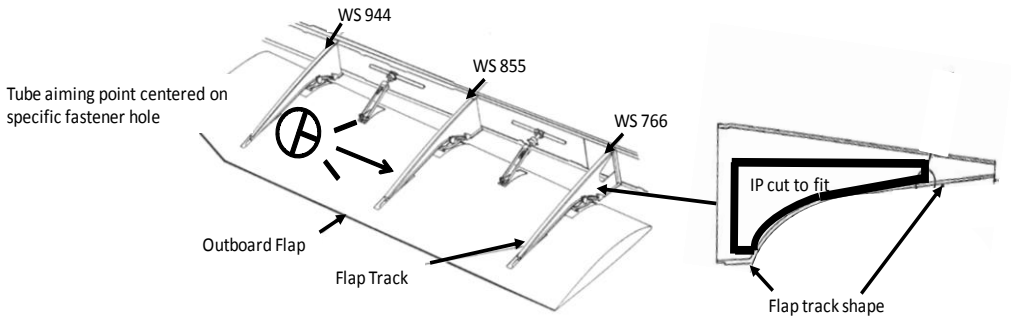

Figure 10. B-52 Flap Track Structure Location On-Wing and Component Shape

Validation testing for the B-52 flap track inspection was performed at Tinker AFB, OK in October 2010. The aircraft that was available for testing was known to contain naturally occurring fatigue cracks within one of the flap track components. Therefore, testing at Tinker AFB was limited to laboratory testing to characterize CR and film system performance, and on-wing testing at the Wing Station (WS) locations known to contain cracks. The CR system demonstrated equivalent capability to that of film in the detection of the naturally occurring fatigue crack shown in Figure 11.

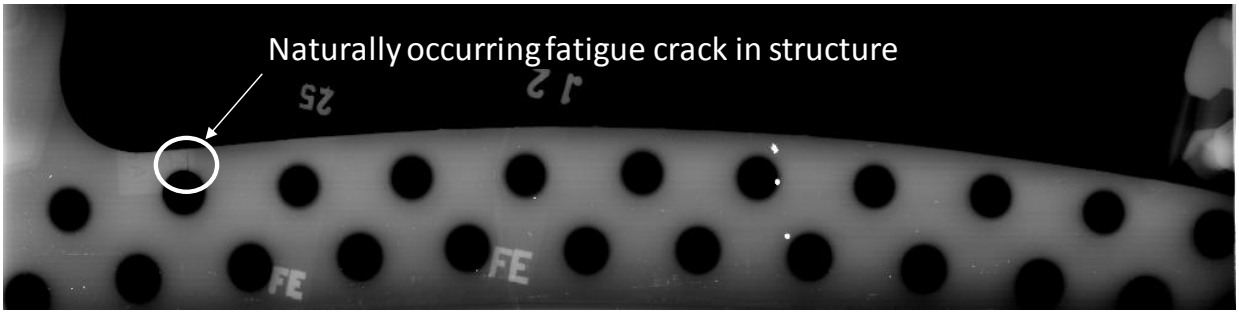

Flap track at WS 855

Figure 11. CR image of B-52 Flap Track On-wing Testing

Based on the laboratory testing using actual and simulated components, validation testing on-wing, and the guidelines for CR technique development in [11], a draft of the T.O. for the B-52 Flap Track inspection was developed. The entire T.O. can be found in [8].

2.6.3 C-5 Upper Lobe Truss Splice. The C-5 Upper Lobe Truss Splice is unique, in that the structure consists of very thick (≈0.75-2.0 in) stack-ups of aluminum and, because of access limitations, the inspection must be conducted with a very small IP-to-tube distance on one side of the part and very long IP-to-tube distance on the opposing side of the part. A schematic of the structure and inspection setup is shown in Figure 10.

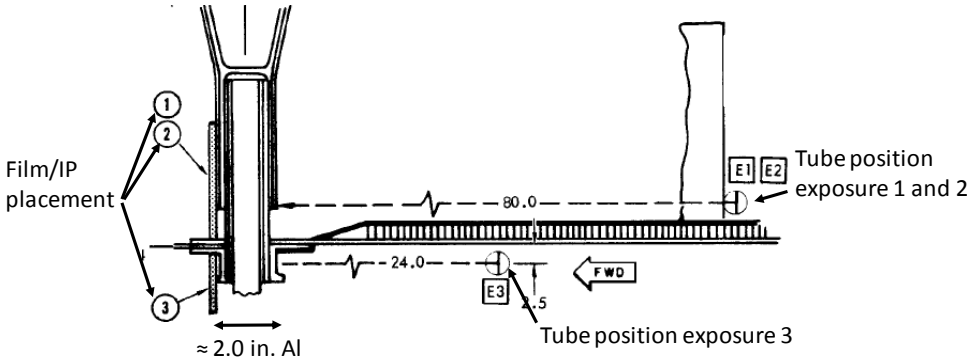

Figure 12. C-5 Upper Lobe Truss Splice Inspection Schematic

The C-5 inspection was simulated in the laboratory using a stack-up of flat plate aluminum with the TM2 crack panels. Up to 2.0 in of total aluminum stack-ups were tested. Although the 1-T penetrameter hole could be imaged using both CR and film, the only cracks that could be seen reliably in the images were the 1-in cracks that were more than 0.25 in. in depth. As previously mentioned in Section 2.6, the C-5 inspection application was eliminated prior to validation testing and, therefore, a complete T.O. could not be developed under this program. However, x-ray testing for thicknesses of aluminum up to 2.0 in demonstrated that crack detection capability for CR systems are provided on some level beyond that which was tested in this capability study A draft of the T.O. for the C-5 application, but without validation testing, can be found in [9].

2.7 CR Training Opportunities

In order to reach the largest possible audience, CR training sessions were held at the NDI WGM in February 2010 and, again, in March 2011. Additional training was provided at Mt. Home AFB September 20-25, 2010. Training materials were developed in the form of slide presentations, tutorials, and computer-based training interactive programs. A summary of the training opportunities, the specific goals of the training programs, and audience participation is discussed below. The details of training materials and deliverables are discussed in Section 3.7. The entire training manual, including slides and tutorial, can be found in [12].

The first training session was held in March 2010 at the NDI WGM in Ft. Worth, TX. The training session was designed to provide background material on CR theory of operation, usage, and image evaluation principles. This first two-hour training session became the foundation of the training module on CR Background, as well as the tutorial on use of CR for crack detection. The session was attended by approximately 30 civilian and military personnel in attendance at the WGM.

The second training session was held at Mt. Home AFB, attended by the eight field-level operators participating in the POD study, and conducted in two separate four-hour sessions. This training session focused on the needs of the field-level operator and included discussions on image processing and system performance testing. The training slides were later used as the basis of the training provided to the field-level operators at the NDI WGM in March 2011.

The third training session was at the NDI WGM in March 2011. This training program was divided into two separate programs designed to address the specific needs of the field-level inspectors and the ALC NDI technical order writers in separate sessions. Each of these two programs were offered on two separate occasions during the week-long conference, so that as many participants as possible could attend. In all, 47 attendees participated in the ALC training and 19 attended the field-level training. The training program presented at the NDI WGM in 2011 became the basis for the training materials contained in [12].

3.0 RESULTS AND DISCUSSION

The results of the laboratory testing part of the program are presented in three parts. First, the results of the CR system performance testing are presented and the performance parameters that are significant for crack detection are defined and evaluated for the different CR systems. Second, the results of x-ray testing on fatigue crack specimens are presented and the effect of system variables on crack detection capability discussed. Third, correlation of system performance with crack detection capability is presented, which will be used to later define the system qualification requirements for CR systems used in crack detection.

The results of POD testing are summarized in Section 3.4 below which highlights some of the significant findings of the POD study relevant to the development of guidelines and procedures delivered under the program. Additional details of the POD study results and discussion can be found in [6].

3.1 CR System Performance

3.1.1 Image Spatial Resolution. CR system performance was characterized using the EPS specimens and the line pair targets, and reported in terms of image spatial resolution and %EPS, as previously discussed in Section 2.3. The image spatial resolution was evaluated using one technique setting per T.O. 33B-1-2 (SWP 106 01 paragraph 2) for each CR system configuration and the values obtained for each operator averaged. Table 8 contains a summary of the individual operator readings for each of the image resolution measurements. Due to time constraints under the program, not all configurations were analyzed by all operators. A summary of the average spatial resolution for each CR system is shown in Table 9.

A comparison of the measurements for individual operators shows certain trends in the data. First, the variability due to operator visual acuity can be estimated from the range of readings in Table 8. The typical range of readings between operators is within 2 line pairs for a particular system configuration. However, if the standard deviations of readings are compared, systems using a 100-micron scan resolution exhibit lower variability than the same system using a 50-micron scan resolution. Nevertheless, if the ranking of operator measurements is compared, their readings remain fairly consistent, indicating that the operator readings may be consistently higher or lower than another operator, but are, most likely, not randomly higher or lower.

Table 8. Image Spatial Resolution Measurements for All Operators

					lp/mm (A)					lp/mm (B)				
Tube	focal spot (mm)	CR system	IP Type	scan res (microns)	Operator 1	Operator 2	Operator 3	Operator 4	average	Operator 1	Operator 2	Operator 3	Operator 4	average
			III	50	6.0	5.0	6.0	7.0	6.0	8.0	7.0	6.0	6.0	6.8
			III	100	4.3	3.7	4.0	2.8	3.7	4.0	4.0	4.0	3.1	3.8
			II	50	6.0	5.0	6.0	6.0	5.8	7.0	6.0	7.0	7.0	6.8
			II	100	4.3	4.0	4.0	4.0	4.1	4.0	3.7	4.0	4.0	3.9
		System A	I	50	5.5	3.7	5.0	6.0	5.1	6.0	4.0	6.0	7.0	5.8
			I	100	4.0	3.1	4.0	3.7	3.7	4.0	3.7	4.3	3.4	3.9
			IV	50	8.0	6.0	7.0	7.0	7.0	8.0	7.0	8.0	6.0	7.3
			IV	100	4.0	3.7	4.0	3.4	3.8	4.0	4.3	3.4	3.1	3.7
			III	50	5.5	4.6	4.6	5.5	5.1	7.0	5.0	5.0	6.5	5.9
			III	100	3.4	3.7	2.8	3.4	3.3	2.5	2.8	2.5	3.1	2.7
Phillips	0.4	System B	II	50	5.5	4.3	4.6	6.0	5.1	7.0	6.0	5.0	4.6	5.7
			II	100	4.0	3.7	3.1	3.7	3.6	2.5	2.5	2.8	3.7	2.9
			I	50	5.0	3.7	4.0	5.0	4.4	6.0	4.6	4.6	4.3	4.9
			I	100	4.0	3.1	3.1	3.4	3.4	4.0	3.7	4.0	3.4	3.8
			III	50	4.3	3.1	4.0	3.7	3.8	8.0	5.0	7.0	4.6	6.2
			III	100	3.7	2.8	3.7	3.4	3.4	4.0	3.4	3.4	2.5	3.3
		System C	II	50	4.0	3.1	4.0	4.0	3.8	8.0	6.0	7.0	7.0	7.0
			II	100	3.7	3.1	3.7	3.1	3.4	3.7	3.1	3.7	2.8	3.3
			I	50	3.7	3.1	3.4	3.4	3.4	7.0	4.3	6.0	5.5	5.7
			I	100	3.7	2.5	3.4	3.1	3.2	4.0	2.8	3.7	3.4	3.5
			III	50	6.0	5.0	5.0	6.0	5.5	7.0	5.5	4.6	6.0	5.8
			III	100	4.0	4.0	4.3	3.7	4.0	4.0	4.0	4.0	3.7	3.9
			II	50	6.0	5.0	5.5	6.0	5.6	7.0	5.0	7.0	7.0	6.5
			II	100	4.0	3.7	3.4	3.7	3.7	4.0	3.7	4.0	3.4	3.8
		System A	I	50	5.5	4.0	4.6	5.0	4.8	6.0	4.0	5.5	5.5	5.3
			I	100	4.0	3.4	4.3	3.7	3.9	4.3	3.7	4.0	4.0	4.0
			IV	50	8.0	7.0	7.0	6.0	7.0	8.0	7.0	7.0	7.0	7.3
			IV	100	4.0	3.7	4.3	3.7	3.9	4.0	4.3	4.3	3.2	4.0
			III	50	5.5	4.6	4.6	4.6	4.8	7.0	6.0	5.5	6.0	6.1
			III	100	4.0	4.0	3.7	3.7	3.9	2.2	2.5	2.2	2.5	2.4
Phillips	3.0		II	50	5.5	4.3	4.3	6.0	5.0	7.0	5.5	5.5	5.5	5.9
		System B	II	100	3.7	2.8	3.1	4.0	3.4	2.8	2.8	2.0	2.5	2.5
			I	50	4.6	3.4	3.7	4.6	4.1	6.0	4.6	4.3	4.0	4.7
			I	100	4.0	3.4	3.4	3.1	3.5	3.4	2.5	2.5	3.4	3.0
			III	50	4.3	3.7	4.0	3.7	3.9	8.0	5.5	7.0	7.0	6.9
			III	100	3.7	2.8	3.7	3.4	3.4	3.7	3.1	3.4	2.8	3.3
			II	50	4.0	3.4	4.0	3.7	3.8	8.0	5.5	7.0	7.0	6.9
		System C	II	100	3.7	2.8	3.7	3.4	3.4	4.0	3.1	3.7	2.8	3.4
			I	50	3.7	3.1	3.4	3.4	3.4	7.0	5.0	6.0	6.0	6.0
			I	100	3.4	2.5.	3.1	3.1	3.2	4.0	3.1	4.3	3.7	3.8
			III	50	6.0				6.0	7.0				7.0
			III	100	4.0				4.0	4.0				4.0
			II	50	7.0				7.0	7.0				7.0
		System A	II	100	4.0				4.0	4.3				4.3
			I	50	6.0				6.0	6.0				6.0
			I	100	4.0				4.0	4.3				4.3
			IV	50	7.0				7.0	8.0				8.0
Lorad	1.5		IV	100										
			III	50	5.5				5.5	6				6.0
		System B	III	100	4				4.0	2.5				2.5
			II	50	5.5				5.5	6				6.0
			II	100	4				4.0	2.5				2.5
			III	50	4.6	4.0	4.0	4.3	4.2	8.0	6.0	5.0	7.0	6.5
			III	100	3.7	3.4	3.1	3.4	3.4	2.5	3.1	3.1	3.1	3.0
		System C	II	50	4.6	3.4	3.7	4.0	3.9	7.0	4.6	5.0	6.0	5.7
			II	100	3.7	2.8	3.4	3.4	3.3	2.5	3.1	3.4	3.1	3.0

Table 9. Image Spatial Resolution Average Measurements

CR System	Detector	Scan Res (microns)	Phillips 0.4mm Average lp/mm (A)	Phillips 0.4mm Average lp/mm (B)	Phillips 3mm Average lp/mm (A)	Phillips 3mm Average lp/mm (B)	Lorad 1.5mm Average lp/mm (A)	Lorad 1.5mm Average lp/mm (B)
	Type III	**50**	**6.0**	**6.8**	**5.5**	**5.8**	**6.0**	**7.0**
	Type III	100	3.7	3.8	4.0	3.9	4.0	4.0
	Type II	**50**	**5.8**	**6.8**	**5.6**	**6.5**	**7.0**	**7.0**
	Type II	100	4.1	3.9	3.9	3.8	4.0	4.3
Scanner A	**Type I**	**50**	**5.1**	**5.8**	4.8	**5.3**	**6.0**	**6.0**
	Type I	100	3.7	3.9	3.9	4.0	4.0	4.3
	Type IV	**50**	**7.0**	**7.3**	**7.0**	**7.3**	**7.0**	**8.0**
	Type IV	100	3.8	3.7	3.9	4.0		
	Type III	**50**	**5.1**	**5.9**	4.8	**6.1**	**5.5**	**6.0**
	Type III	100	3.3	2.7	3.9	2.4	4.0	2.5
Scanner B	**Type II**	**50**	**5.1**	**5.7**	**5.0**	**5.9**	**5.5**	**6.0**
	Type II	100	3.6	2.9	3.4	2.5	4.0	2.5
	Type I	50	4.4	4.9	4.1	4.7		
	Type I	100	3.4	3.8	3.5	3.0		
	Type III	**50**	3.8	**6.2**	3.9	**6.9**	4.2	**6.5**
	Type III	100	3.4	3.3	3.4	3.3	3.4	3.0
Scanner C	**Type II**	**50**	3.8	**7.0**	3.8	**6.9**	3.9	**5.7**
	Type II	100	3.4	3.3	3.4	3.4	3.3	3.0
	Type I	**50**	3.4	**5.7**	3.4	**6.0**		
	Type I	100	3.2	3.5	3.2	3.8		

Other observations can be made by examining the average spatial resolutions for the different CR systems. First, it should be noted that, for all CR systems, the A orientation results in lower image spatial resolution than the B orientation. This is an inherent limitation of the CR scanning process, due in large part to the size of the laser spot used to scan the image and the relaxation time of the phosphor material in the imaging plate. This tendency is largely a characteristic of the CR scanner design. For some CR systems the magnitude of the difference may also depend on the scan resolution used to extract the image. For Scanner C, the difference in A and B orientation spatial resolutions are <10% when scanning at 100 micron, but the difference can be as high as 80% when scanning with a 50 micron resolution. In contrast, the difference between A and B orientation resolutions are <20% for both 50 and 100 micron scan resolutions for the Scanner A and Scanner B systems tested.

Another observation that can be made from a review of the data in Table 9 is that, for 50-micron scan resolutions, an average image spatial resolution of 5.0 lp/mm or higher was obtained for nearly all CR systems evaluated. Line pair readings equal to or greater than 5.0 lp/mm are highlighted in red. The exceptions are Scanner A, which does not achieve a 5.0 lp/mm average resolution with the Type I plate, and the Phillips 3.0 mm tube in the A direction. Similarly, the Scanner B with the Type I plate does not achieve a 5.0 lp/mm with either of the Phillips tubes. The Type I plate is a very coarse grain imaging plate that is intended for rapid exposure industrial radiography and is

not intended to be used in a high-resolution mode; therefore, these results are not unexpected. The resolution measured for Scanner B with Type III plate at 50-micron scan with the Phillips/3.0 mm tube was somewhat low at 4.8 lp/mm. Although there did not appear to be a large dependency of spatial resolution on x-ray tube or spot size, the resolutions obtained were somewhat lower for Scanner B with the Phillips 3.0 mm spot. It is possible that this particular measurement is an outlier and a re-examination of the images might be recommended.

Another trend was that observed in the image spatial resolution data was that the Scanner C did not achieve a 5.0 lp/mm image spatial resolution in the A direction using any IP, scan resolution, or x-ray tube. The source of the large discrepancy between the image spatial resolution in the A and B direction when scanning at 50 microns is not clear and the effect was observed on all Scanner C systems tested throughout the program.

3.1.2 Image Noise Measurements. CR system image noise was evaluated using the EPS image quality standard previously discussed in Section 2.3.2. The EPS images were acquired over a range of exposure settings and the minimum value determined following the recommended procedure described in the CR system qualification and performance test procedure [13]. The procedure used to determine the minimum EPS for a particular CR system is summarized briefly, as follows: After acquiring the EPS images over a range of exposure settings, the operators examined each image and recorded the minimum EPS value defined by the duplex row of holes where 20 out of 30 holes were visible. The criteria for "visible" was defined as the holes must appear round and be clearly distinguishable from the background image noise before they could be counted. The EPS values were tabulated for each operator and each CR system. Table 10 shows EPS values obtained from all four operators for one example CR system: Scanner A, with IPS plates, 50-micron scan resolution, with the Phillips 0.4 mm tube. The techniques used to acquire the images utilized 65 kV at 5 mA with the exposure times shown in the table. The maximum pixel value for all images is 65535, which was used with the intensity on the absorber plate in the image to calculate the percentage of maximum pixel value (%MPV) shown in the table.

Table 10. EPS Readings for Each Operator on a Single CR System: Phillips/0.4 mm tube, Scanner A, Type III Imaging Plate, 50-Micron Scan Resolution

Exposure Time (sec)	% MPV	%EPS				
		Reader 1	Reader 2	Reader 3	Reader 4	Avg.
12	7%	1.41	1.49	1.41	1.28	1.40
24	13%	1.19	1.28	1.19	1.19	1.21
48	28%	1.12	1.12	1.12	1.19	1.14
72	42%	1.12	1.12	1.12	1.12	1.12
90	50%	1.19	1.19	1.12	1.12	1.16
114	47%	1.12	1.12	1.05	1.12	1.10
138	59%	1.12	1.12	1.05	1.12	1.10
162	68%	1.01	1.19	1.05	1.05	1.08
186	80%	1.05	1.12	1.12	1.01	1.08
210	86%	1.05	1.19	1.12	1.05	1.10

A review of the data shows that the expected trend of decreasing EPS value with increasing exposure time was observed for all four operator"s readings and is reflected in the average EPS values. Following the procedure described in the CR System Qualification (Performance) Test Procedure [13], a local minimum EPS regime was defined where the EPS value reached a relatively stable value of EPS. This local minimum in EPS values is referred to as the plateau level and is characterized by the average value of four consecutive EPS readings where the individual values do not vary by more than 0.09 %EPS. The allowable variability of 0.09 %EPS was based on the maximum difference between the EPS values for two consecutive duplex rows on the EPS standard. For the performance data shown in Table 10, the EPS plateau region could be defined as beginning with an exposure time of 48 sec and extending out to 210 sec. The average of four successive EPS readings, beginning with the value at 48 sec, would, therefore, be 1.13 %EPS. Following the performance test procedure, a value of 1.13 %EPS would then be recorded as the minimum EPS value for the specific CR system.

The overall behavior of the image noise in terms of EPS can also be illustrated by plotting the values as a function of exposure (exposure time at constant filament current setting) and %MPV, as shown in Figure 13. The plots show that, for Scanenr A with Phillips 0.4 mm tube, the EPS values are significantly higher at very low exposures, but that the EPS value decreases and levels off to some relatively low value. This behavior is observed for all four imaging plate and scan resolution settings shown. Similarly, the EPS values are higher for very low image intensities, represented by %MPV in Figure 13b. These plots help to illustrate that the lowest noise CR images are those obtained using the longest exposure and highest pixel value practical.

Table 11 shows a summary of the EPS values for each CR system tested. The EPS values were calculated using the average EPS values for all four operators. An overview of the results shows that, in general, the Type III plates produce images that result in lower EPS values when compared to the same system setup using Type II plates. These results would indicate that lower image noise is obtained by the use of Type III plates. A smaller difference in EPS values is observed when using 50-micron or 100-micron scanning with all other system parameters remaining the same. These performance data will be compared with crack detection capability to determine qualification criteria for CR systems in Section 3.3.

3.2 Crack Detection Capability Comparative Study – CR Systems and Film

3.2.1 Hit/Miss Comparison – Aluminum. The most direct method of comparing the crack detection capability of CR systems to that of film is through the use of hit/miss data generated from the crack length measurements obtained from evaluation of the TM2 images. However, it was not clear at the onset of the analysis how the crack detection capability would vary with crack parameters. Therefore, the analysis was divided into two groups. First, the data was divided by crack length into "short" cracks (≈0.3 in. in length) and "long" cracks (≈1.0 in. in length). Second, the data was divided by total stack-up thickness into the three groups tested: 0.375, 0.625, and 1.125 in thickness. The following discussion will present the results of the hit/miss analysis based on the combined results from three different operators. In all cases, the hit/miss data will be compared to that obtained from evaluation of the corresponding film image of the same cracks.

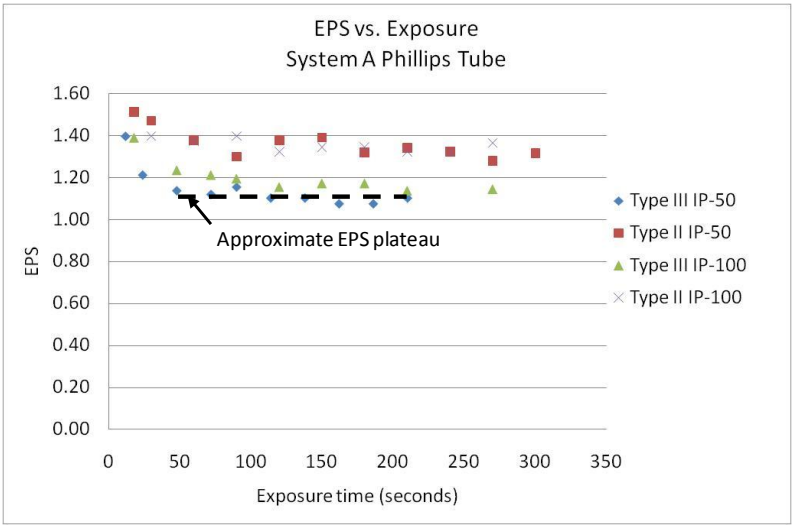

(a)

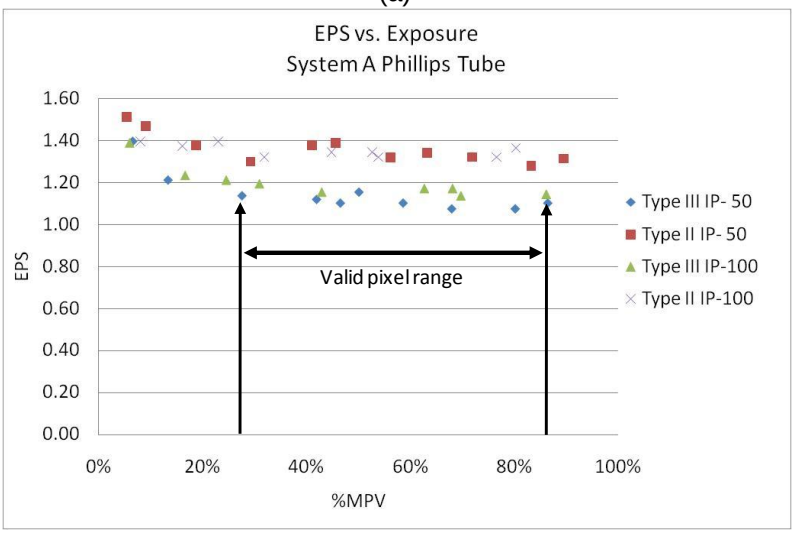

(b)

Figure 13. Image Noise Evaluation Based on %EPS: (a) EPS Dependence on Exposure Time and (b) EPS Variation with Image Intensity (%MPV)

Table 11. Minimum EPS for Each CR System Calculated from the Average EPS for All Four Operators

				%EPS	
Tube/ Focal spot	**Detector**	**Scan Res. (microns)**	**Scanner A**	**Scanner B**	**Scanner C**
Phillips/0.4mm	Type III	50	1.13	1.32	1.13
	Type III	100	1.18	1.20	1.10
	Type II	50	1.35	1.40	1.26
	Type II	100	1.33	1.40	1.31
Lorad/1.5mm	Type III	50	1.19	1.33	1.18
	Type III	100	1.20	NA	1.28
	Type II	50	1.28	1.34	1.34
	Type II	100	1.37	1.40	1.42

An overall review of the hit/miss data can be obtained by combining all the results using both the Lorad and Phillips x-ray tubes into one set of summary charts. After presenting the summary data, specific details regarding differences in results due to the different system parameters will be discussed. Figure 14 shows the hit/miss comparisons in bar chart form for short cracks with all three stack-up thicknesses. A summary review of the hit/miss results for short cracks reveals some trends in the data. First, the orientation dependency that was observed in the system performance tests for image resolution can be observed in the crack detection tests also. A comparison of the data obtained for both the A and B orientations using the same CR system shows that, in general, the number of hits is lower for the B than the A orientation. In the B orientation, the cracks are oriented so that they are perpendicular to the feed direction or, more significantly, parallel to the laser scan direction within the scanner. This results in a smearing of the fine, low-contrast linear indications. This reduction in crack detection capability is observed on some level with all CR systems tested, however, the effect is much-more pronounced with some systems. In particular, Scanner C exhibits as much as a 54% decrease in hits between the A and B orientations when using the IPS plate at a scan resolution of 50 microns. This large discrepancy in crack detection capability for the two orientations correlates with the 80% difference in image spatial resolution for the two directions as discussed in Section 3.1.1. For Scanner A using Type II plates at a 50-micron resolution, a reduction of 32% in hits was observed between the A and B orientations. This particular reduction in capability is somewhat significant, since the reduced detection capability in the B orientation is below that of film for the same stack-up thickness (Figure 14a). Further discussion of the statistical significance of differences between detection capability of film and the CR systems will be discussed in Section 3.3.

A similar assessment of the long crack detection capability can be obtained from plots of the hit/miss data for the CR systems and film shown in Figure 15. An initial review of the long crack data shows that the proportion of hits using all systems is higher for the long cracks than the short, thus confirming that crack length is, in fact, a relevant metric for crack detection. However, unlike the short crack hit/miss results, the differences in crack detection capability for the CR systems is less evident, since there are fewer misses, in general, with the long crack data. The differences in hit/miss data for the two orientations is also less-pronounced, with all ratios greater than 0.93 (with the exception of the Scanner A/Type II plates/50-micron scan resolution/B

orientation) where the ratio was 0.80. Of the 18 different CR system configurations, 15 reported a proportion of hits equal to 95% or more than film, with roughly 12 out of 18 reporting a higher proportion of hits than film. The results of the hit/miss comparisons for both the long and short cracks for all three stack-up thicknesses are summarized in Table 12.

Table 12 lists the ratio of hits using each specific CR system to that of film for the combined Lorad and Phillips data acquired using TM2. Shaded green are ratios greater than or equal to 1.0, indicating that the specific CR system listed generated as many, or more, hits than film. For the CR system to be considered "as good or better than" film, the system would need to demonstrate crack detection capability equivalent to film for all crack lengths and stack-up thicknesses, as well as for both A and B orientations. Only one system, Scanner A with Type III plates at 50-micron scan resolution, satisfied all of these requirements. Scanner B with Type III plates at 50 microns is very nearly the same as film, with the exception of a 4% difference in hits for the short cracks in the 0.625-in stack-up. All other systems fall short of the film hit/miss results for four or more detection conditions. Although these results are not a definitive assessment of crack detection capability, they provide a starting point for a comparison of CR system capability.

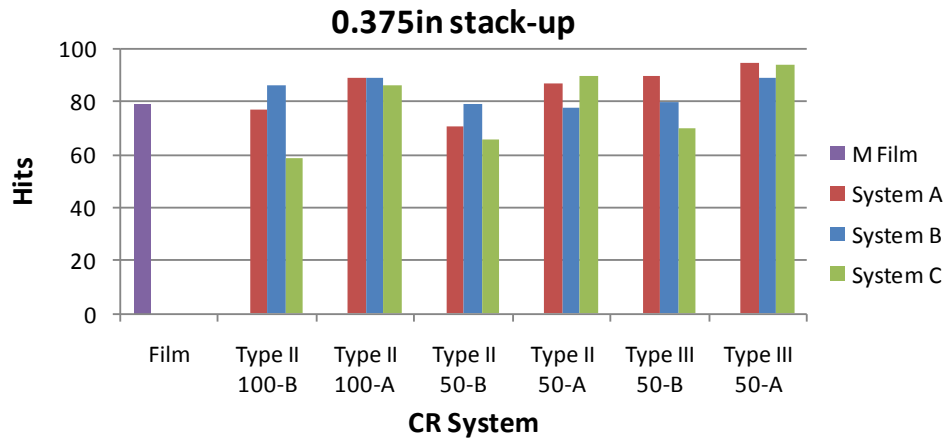

(a)

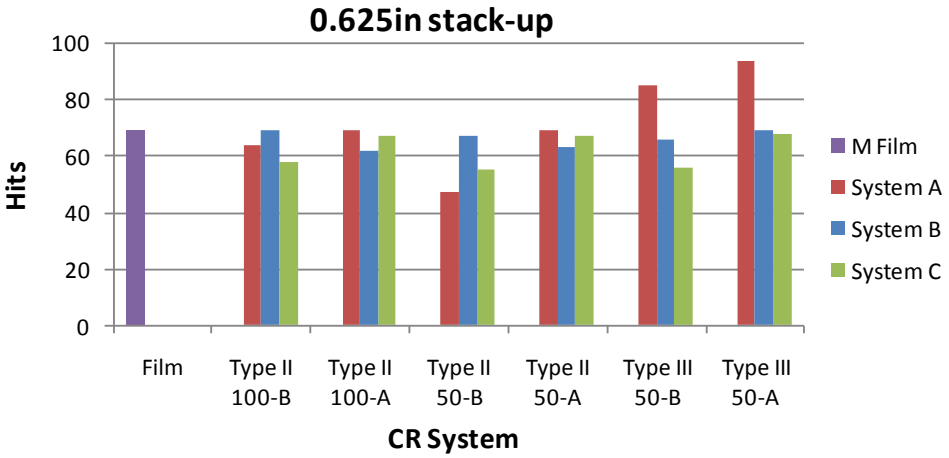

(b)

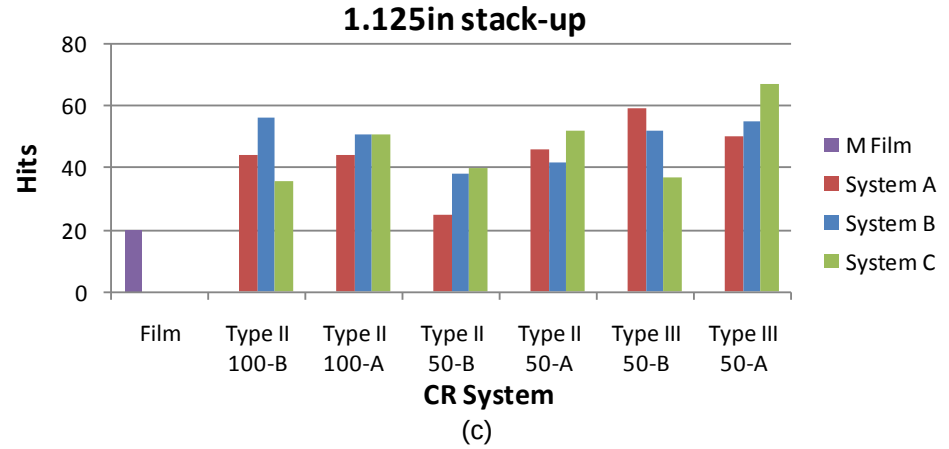

(c)

Figure 14. Hit/Miss Summary Data for Short Cracks in Aluminum (a) Total Stack-Up Thickness 0.375 in, (b) 0.625 in, and (c) 1.125 in. Results from Lorad and Phillips Tubes Combined

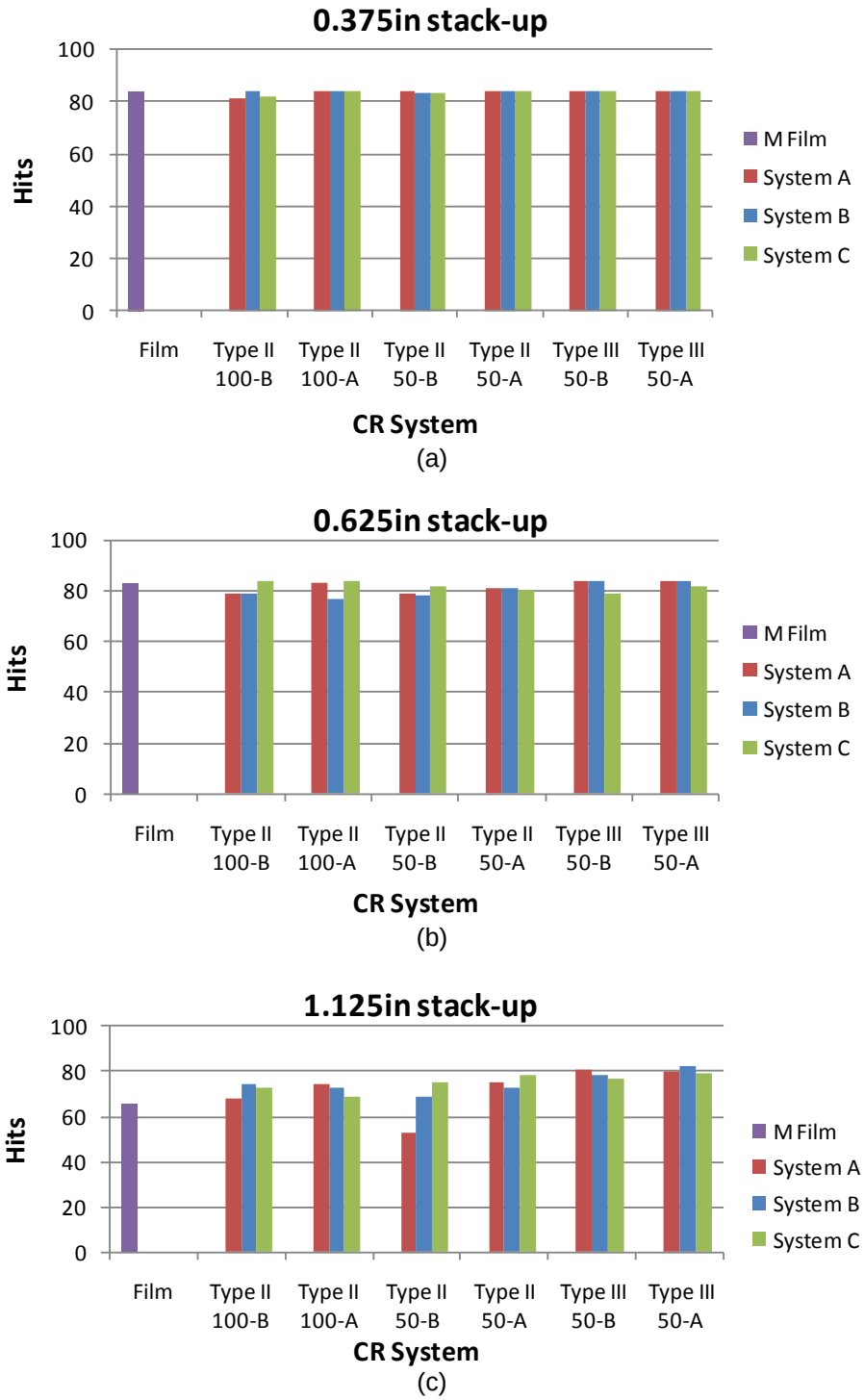

Figure 15. Hit/Miss Summary Data for Long Cracks in Aluminum (a) Total Stack-Up Thickness 0.375 in, (b) 0.625 in, and (c) 1.125 in. Results from Lorad and Phillips Tubes Combined

Table 12. Hit/Miss Ratios for CR and Film – Combined Summary for Both Lorad and Phillips Tubes with Cracks in Aluminum

		Scanner B		Scanner A		Scanner C	
		Short	Long	Short	Long	Short	Long
Type II 100-B	0.375	1.09	0.96	0.97	0.96	0.75	0.98
	0.625	0.93	0.95	0.93	0.95	0.84	1.01
	1.125	2.80	1.12	2.20	1.03	1.80	1.11
Type II 100-A	0.375	1.13	1.00	1.13	1.00	1.09	1.00
	0.625	0.90	0.93	1.00	1.01	0.97	1.01
	1.125	2.55	1.11	2.20	1.12	2.55	1.05
Type II 50-B	0.375	1.00	0.99	0.90	1.00	0.84	0.99
	0.625	0.97	0.94	0.68	0.95	0.80	0.99
	1.125	1.90	1.05	1.25	0.80	2.00	1.14
Type II 50-A	0.375	0.99	1.00	1.10	1.00	1.14	1.00
	0.625	1.00	0.98	0.97	0.96	0.97	0.96
	1.125	2.10	1.11	2.30	1.14	2.60	1.18
Type III 50-B	0.375	1.01	1.00	1.14	1.00	0.89	1.00
	0.625	0.96	1.01	1.23	1.01	0.81	0.95
	1.125	2.60	1.18	2.95	1.23	1.85	1.17
Type III 50-A	0.375	1.13	1.00	1.20	1.00	1.19	1.00
	0.625	1.00	1.01	1.36	1.01	0.99	0.99
	1.125	2.75	1.24	3.35	1.21	3.35	1.20

3.2.2 Hit/Miss Comparison – Steel. Since the steel specimen crack lengths are more widely distributed over the range between 0.1-1.0 in, the crack lengths cannot be broken up into short and long categories as can the aluminum specimens. In addition, due to time constraints of the program, the CR data acquired on the steel specimens was limited to only a few test conditions, and a full analysis of the steel CR images was not possible. However, a preliminary analysis of the steel hit/miss results can be discussed in terms of a direct comparison between CR and film detection of all the cracks as a group, followed by a discussion of the detection of specific cracks. The results that will be discussed were obtained from inspections using the Lorad tube only. Images were evaluated by two operators. In addition, due to the limited number of tests conducted using

steel crack specimens, any applicable data sets were used to improve the statistical analysis. As a result, the number of possible hits for all film and CR systems are not the same. Therefore, the data is presented as a proportion (*i.e.*, the ratio of the number of hits to the total number of possible hits). Figure 16 shows the proportion of hits using each of the CR systems and film for steel cracks, both with and without the additional 0.25- in aluminum layer. Note that the Scanner A was only tested using the IPS plate at a 50-micron resolution for the case of steel with aluminum.

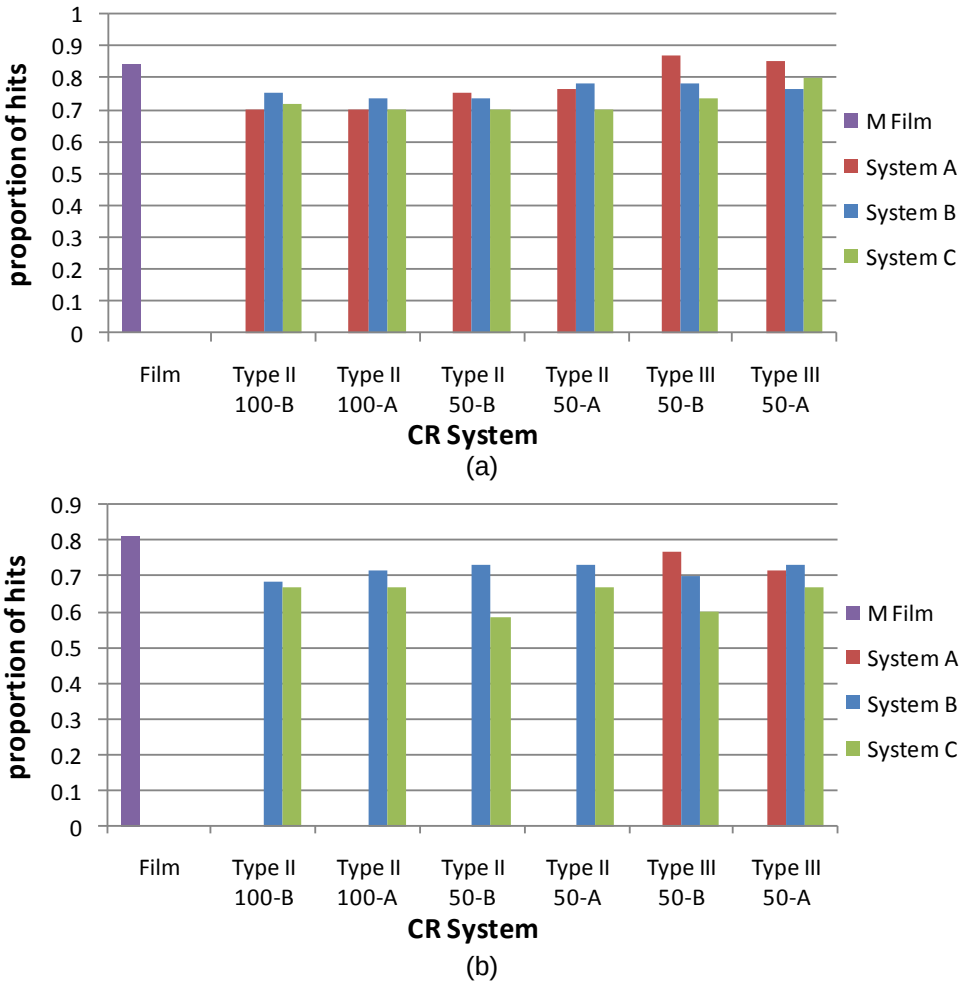

Figure 16. Proportion of Hits for Steel Cracks: (a) 0.25-in-Thick Steel Only, (b) 0.25-in Steel with an Additional 0.25-in Layer of Aluminum. Results from Lorad Tube Only

A comparison of the proportion data in the plots shows that there is not a profound difference between the results obtained using the different CR systems. However, trends in the data suggest that the CR systems, in general, are less-effective than film at detecting cracks in steel. The only CR system that provided an equivalent proportion of hits to film in steel was the Scanner A system with Type III plates at 50-micron scan resolution. The proportion data can also be compared between CR and film by taking the ratio of the proportion of hits. Table 13 lists the ratio of proportion of hits with CR to proportion of hits with film. The table shows that the performance of

all the systems using Type II plates is less than that of film. Using the Type III plate at a 50-micron scan resolution shows that the ratio of hits in steel only (without additional aluminum layer) for Scanner A is equivalent to film. However, with the additional aluminum layer, the proportion of hits falls short of the film results. No other CR system demonstrated a proportion of hits for both orientations and both stack-ups within 5% of film. The differences in detection capability for CR and film can be further studied by comparing the cracks parameters for those cracks that were easily detected to those that were missed.

Table 13. Hit/Miss Ratios for Cracks in Steel CR and Film – Results for Lorad Tube Only

	Scanner B		Scanner A		Scanner C	
	Steel Only	+0.25 in. Al	Steel Only	+0.25 in. Al	Steel Only	+0.25 in. Al
Type II 100-B	0.89	0.85	0.83		0.85	0.82
Type II 100-A	0.87	0.89	0.83		0.83	0.83
Type II 50-B	0.87	0.91	0.89		0.83	0.72
Type II 50-A	0.93	0.91	0.91		0.83	0.82
Type III 50-B	0.93	0.87	1.03	0.95	0.87	0.74
Type III 50-A	0.91	0.91	1.01	0.89	0.95	0.82

An analysis of the 30 steel cracks detected and those that were missed showed that:

- 15 of the 30 cracks were detected by all CR systems and film, both with and without aluminum layers.
- An additional four cracks were detected by all CR systems except Scanner C when scanning at 50-micron resolution.
- 5 of the 30 cracks were not detected by CR or film, with or without aluminum layers.

Of the 6 cracks detected using film, but only sometimes detected with CR:

- 2 of the cracks were 0.1 in long and 0.125 in in depth.
- 4 of the cracks were 0.6-0.9 in in length, but only 0.063 in. in depth (25% or less of the total stack-up thickness.)

Consideration of the specific information about cracks that are detected and those that are missed is significant for evaluating the effectiveness of CR for use in AF-relevant inspections. In particular, the cracks that were detected with all CR systems include all cracks that were 0.25 in. in depth. These cracks range in length from 0.15-1.0 in, which encompasses the range of cracks currently being inspected on AF structures. In addition, those cracks were detected equally well with and without the additional layer of aluminum added to the steel stack-ups. Cracks that were missed

specifically by Scanner C when scanning at 50 microns were 0.125 or 0.050 in. in depth, less than 50% of the total stack-up. These cracks were however, within the capability of the other CR systems for detection. Previous discussions regarding the differences in detection capability of Scanner C when using a 50-micron scan resolution suggest that a higher variability in detection of these cracks may be observed. Since those same cracks that were missed using a 50-micron scan resolution were detected using the Type II plate at a scan resolution of 100 microns, it might be suggested that Scanner C would be more reliable for the inspection of steel cracks using the 100-micron scan resolution. In summary, the results of the comparative study indicate that, for the specific steel inspection application that is needed by the AF, namely the inspection of B-52 Flap Track components, CR detection capability for steel cracks that are 0.25 in. in depth is equivalent to film for all CR systems evaluated. The hit/miss data presented here further suggests that for the CR systems tested, with the exception of the Scanner C with 50 micron scan resolution, cracks which are greater than 0.3 inches in length and are more than 0.125 inches in depth exhibit detection capability equivalent to film. Any more detailed analysis of CR system detection capability for steel cracks would require further testing and analysis.

3.3 Correlation of Crack Detection Capability to CR System Performance

Section 3.1 discussed the results of system performance testing conducted on multiple CR systems. Those results show how image spatial resolution and image noise depended on CR system parameters such as imaging plate type, scan resolution, and orientation relative to the scanner feed direction. Section 3.2 presented results that show the crack detection capability of several CR systems is comparable to film, but on different levels. By correlating crack detection capability for each system with its corresponding performance during standardized testing, a qualification criteria may be developed that can distinguish between CR systems that perform as well as film for crack detection.

3.3.1 Hit/Miss Results Separated by X-Ray Tube. Tables 14 and 15 show summaries of the hit/miss ratios for each CR system tested separated by the individual tubes that were used in testing. The tables both show that the only system which demonstrated crack detection capability consistently equal to or better than film was Scanner A with Type III plates scanned at 50 microns. This result is independent of the x-ray tube used in testing. Scanner B is somewhat comparable to film when using the Type III plates at 50-micron scan resolution, but falls short of the film results in detection of short cracks in the thinnest stack-ups. For both the Scanner A and Scanner B systems with Type III plates at 50-micron scan resolution, more long cracks were detected than with film, possibly due to the ability to magnify the images and enhance contrast in the CR images. These results indicate that further analysis of the existing data may be able to establish additional crack detection limits for CR systems meeting the performance of Scanner B used in this study.

Tables 14 and 15 also show the differences in inspection capability using Scanner C. A comparison of the hit/miss ratios for the A and B orientations shows that, for short cracks, detection capability varies significantly from that of film. As an example, using the Type III plate at a scan resolution of 50 micron results in short crack detection capability more than 3 times that of film in the A orientation, but 50% less than film in the B orientation. As previously discussed in Section 3.2, the large differences in image spatial resolution for the two orientations of Scanner C may be directly influencing the difference in inspection capability for cracks. Although the

orientation differences in crack detection capability are greatly reduced when using the Type II plate and scanning at 100 micron, the ratios for short cracks still fall short of film. As previously mentioned, the long crack data does not clearly demonstrate the differences in CR systems and their limitations as well, since nearly all the long cracks were detected most of the time. Nevertheless, use of Scanner C systems that are used for detection of cracks in aluminum that are known to be 1.0 in. in length or longer, may demonstrate sufficient capability for these applications. A brief discussion of the statistical significance of the differences in hit/miss data will be included in Section 3.3.2 below.

3.3.2 CR System Performance. CR system performance was assessed in Section 3.2 based on image spatial resolution in terms of line pairs/mm and image noise in terms of %EPS. A summary of those performance results for the CR systems used in crack detection are shown in Table 16. Note that, in listing the performance data for each system, the minimum %EPS value is shown, which was calculated as described in Section 3.2.2 and in [13]. The line pair resolution reported is the minimum for each system, considering both the A and B directions. Although, in many crack detection applications, the direction of crack growth is known based on stress analysis, a minimum level of performance for the entire system must be established for the entire system, independent of preferential detection orientations. Therefore, only the minimum resolution that was measured for the system is listed in Table 16. The performance data for CR systems that performed as well or better than film for all crack detection scenarios are highlighted in bold type.

Table 14. Hit/Miss Ratios for Cracks in Aluminum CR and Film – Results for Phillips 0.4 mm Tube Only

CR Film Comparison--Phillips 0.4mm tube only							
		Scanner B		Scanner A		Scanner C	
		Crack Length		Crack Length			
IP/Res./Orientation	Stack-Up (in)	Short	Long	Short	Long	Short	Long
Type II 100-B	**0.375**	1.21	1.00	1.00	1.00	0.66	1.00
	0.625	0.97	0.95	0.86	1.00	0.72	1.02
	1.125	2.80	1.09	2.70	1.06	2.10	1.13
Type II 100-A	**0.375**	1.18	1.00	1.11	1.00	1.05	1.00
	0.625	0.92	0.93	1.00	1.00	0.86	1.02
	1.125	2.60	1.09	2.50	1.31	2.90	1.09
Type II 50-B	**0.375**	1.05	0.98	0.79	0.98	0.84	0.98
	0.625	1.03	0.95	0.50	1.00	0.69	1.02
	1.125	2.30	0.97	1.10	0.84	1.40	1.13
Type II 50-A	**0.375**	1.03	1.00	1.11	1.00	1.13	1.00
	0.625	0.89	0.95	1.03	1.00	0.92	1.02
	1.125	2.10	1.13	2.40	1.22	2.10	1.19

Type III 50-B	**0.375**	1.11	1.00	**1.21**	**1.00**	0.74	1.00
	0.625	1.00	1.02	**1.25**	**1.02**	0.86	1.00
	1.125	2.90	1.19	**3.20**	**1.28**	0.50	1.09
Type III 50-A	**0.375**	1.08	1.00	**1.24**	**1.00**	1.24	1.00
	0.625	0.97	1.02	**1.28**	**1.02**	0.97	1.02
	1.125	2.90	1.25	**3.20**	**1.31**	3.20	1.25

Table 15. Hit/Miss Ratios for Cracks in Aluminum CR and Film – Results for Lorad 1.5 mm Tube Only

CR Film Comparison--Phillips 0.4mm tube only							
		Scanner B		Scanner A		Scanner C	
		Crack Length		Crack Length			
IP/Res./Orientation	Stack-Up (in)	Short	Long	Short	Long	Short	Long
Type II 100-B	**0.375**	0.98	1.00	0.90	0.93	0.83	0.95
	0.625	1.03	0.95	1.00	0.90	1.12	1.00
	1.125	2.80	1.15	1.70	1.12	1.50	1.09
Type II 100-A	**0.375**	1.07	1.00	1.15	1.00	1.12	1.00
	0.625	0.88	0.93	1.00	1.00	1.09	1.00
	1.125	2.40	1.12	1.90	1.24	2.20	1.00
Type II 50-B	**0.375**	0.95	1.00	1.02	1.00	0.83	1.00
	0.625	0.91	0.93	0.88	0.90	0.91	0.95
	1.125	1.50	1.12	1.40	1.12	2.60	1.15
Type II 50-A	**0.375**	0.98	1.00	1.10	1.00	1.15	1.00
	0.625	0.94	1.00	0.97	0.95	1.03	0.90
	1.125	2.10	1.12	2.20	1.18	3.10	1.18
Type III 50-B	**0.375**	0.93	1.00	**1.07**	**1.00**	1.02	1.00
	0.625	0.88	1.00	**1.21**	**1.00**	0.76	0.90
	1.125	2.30	1.18	**2.70**	**1.24**	3.20	1.24
Type III 50-A	**0.375**	1.17	1.00	**1.17**	**1.00**	1.15	1.00
	0.625	1.03	1.00	**1.45**	**1.00**	1.00	0.95
	1.125	2.60	1.24	**1.80**	**1.24**	3.50	1.15

Table 16. Minimum EPS and Image Resolution for CR Systems Used in Crack Detection

Tube/ Focal Spot	Detector	Scan Res. (microns)	Scanner A		Scanner B		Scanner C	
			%EPS	lp/mm	%EPS	lp/mm	%EPS	lp/mm
Phillips/ 0.4 mm	Type III	50	**1.13**	**6.0**	1.32	5.1	1.13	3.8
	Type III	100	1.18	3.7	1.20	2.7	1.10	3.3
	Type II	50	1.35	5.8	1.40	5.1	1.26	3.8
	Type II	100	1.33	3.9	1.40	2.9	1.31	3.3
Lorad/ 1.5 mm	Type III	50	**1.19**	**6.0**	1.33	5.5	1.18	4.2
	Type III	100	1.20	4.0	NA	2.5	1.28	3.0
	Type II	50	1.28	7.0	1.34	5.5	1.34	3.9
	Type II	100	1.37	4.0	1.40	2.5	1.42	3.0

Based on these data, it could be argued that only CR systems meeting a minimum level of performance equal to 1.19 %EPS and 6.0 lp/mm should be used in crack detection. POD testing and analysis discussed in [6] and Section 3.4 below are also in agreement with these results. Nevertheless, some considerations for other systems that are very close in performance and crack detection capability to Scanner A with IPS plates at 50 micron may be considered for some crack detection applications as well. For example, Scanner B, when used with an Type III plate at a 50-micron scan resolution, also performed as well as film for all crack detection conditions except for the short cracks with the thinnest stack-ups (Tables 14 and 15). These data indicate that the limitations of image noise are more significant when detecting small cracks.

Additional statistical analysis of limited hit/miss data was also performed under the program. Results of some paired t-tests and two proportion z-tests comparing the CR results to film suggests that the observed differences in performance between some CR systems and film may not be statistically significant. However, significance tests comparing the performance of Scanner A using Type III plates and 50-micron scan resolution to all other CR systems suggested that there is a real performance improvement for crack detection obtained with Scanner A for all crack detection scenarios investigated except the short cracks in the 1.125-in stack-up. Due to time constraints under this program, additional statistical analysis of the CR and film data could not be presented.

Other factors, such as system reliability and false calls, should also be considered when determining qualification criteria. It was noted during the image analysis that image artifacts occurred more often with some CR systems than others. For example, ghost images that appeared in CR images acquired using Scanner C sometimes required a second erasure step using another manufacturer"s scanner before proceeding with the testing. Incomplete erasure processes can result in significant loss of IP usefulness and throughput in an inspection process. Another example are the dark lines oriented in the laser scan direction that occasionally appeared in CR images. These dark lines were observed in CR images acquired using all three scanners to some degree. With sufficient training and experience the operators could learn to distinguish between the linear artifacts and cracks. However, if the lines were oriented parallel to the crack growth direction the artifacts could obscure the cracks or result in a false crack length measurement. These types of image artifacts were noted on the data sheets, but no quantitative assessment of the effect of these linear artifacts on crack detection could be determined under the constraints of the current program.

Additional data collected under the CR program included the Test Matrix 1 and Test Matrix 4 images. The purpose of these images was to assess the variability of crack detection capability with crack orientation relative to the x-ray beam. Additional analysis of crack orientation dependence could also be obtained from comparison of selected POD crack images with those of the same cracks at different locations within the frames. Due to time constraints under the program, this analysis was not completed.

3.4 Comparison of POD Data with Laboratory Results

All discussion of results presented in this report thus far describe the tests conducted to characterize differences in detection capability between different CR systems and how that capability compares to film. In addition, test results were presented which were used to establish optimized inspection equipment, settings, and procedures. In order to characterize the effect of operator varia-

bility on crack detection using CR and film however, a POD study was conducted using a representative pool of USAF operators as discussed in Sections 2.5 and 3.6. The results of this POD study and the corresponding analysis have been documented in a detailed POD report [6]. It is of interest however to relate the results of the POD study conducted at Mt. Home and the comparative study conducted by UDRI engineers and technicians. Consequently, a small study was conducted in which one of the two UDRI engineers and one UDRI technician who participated in the laboratory comparative study evaluated the same POD images used at Mt. Home by AF personnel. The evaluation of the POD images followed the same procedures as were used in the Mt. Home study. The operators evaluated images and reported "hit" or "miss" for each inspection opportunity. Facilitators were used to record the hit/miss results as they were reported in a binder. The hit/miss data was then entered into spreadsheets and processed using the identical software routines previously described for the Mt. Home POD analysis. Therefore, the POD evaluations conducted at UDRI using the operators who evaluated the laboratory data followed the POD procedures used at Mt. Home as closely as possible. One difference between the two studies pertains to time constraints. Although the Mt. Home POD study was limited to the one week at that location, the UDRI POD study was conducted over several weeks, as availability permitted. Other differences between the AF operators and the UDRI evaluators are discussed below.

The main purpose of this section is to provide a correlation between the POD analysis conducted using the hit/miss data from Mt. Home operators and the hit/miss data from the UDRI operators. The POD study could not be conducted using all CR systems available, therefore it is of interest to compare the detection capability of the UDRI operators to a representative pool of AF operators, so that the results of the POD study can be related to that of the laboratory capability study. For additional details concerning the specimens, data collection, and interpretation, as well as POD analysis methodology please see the complete POD analysis report [6].

3.4.1 Comparative POD Analysis for UDRI Operators. The UDRI test results have been processed in the same manner as was done with the Mt. Home data. POD parameters were calculated and the resulting POD curves were plotted against the various detection metrics. These plots are contained in Figures 17-19. The figures contain plots of POD results for the individual operators used in the Mt. Home test (exactly the same results reported in the official POD report [6]) as well as the POD results from the UDRI operators. In each of the figures, the left-hand plots show analysis results for computed radiography, while the right-hand plots show the results for film. The top figures plot POD versus the depth; the middle plots are POD versus length, and the bottom plots are POD versus length times depth divided by stack up thickness. In Figure 20, the depth metric is divided by stack-up thickness for the top plots, the length metric is divided by stack-up thickness for the middle plots, and the bottom plots are, again, for POD versus length times depth divided by stack-up thickness. In each plot, the Mt. Home operators" results are in black, while the UDRI operators" results are in color. It should be noted that the film data for the UDRI operators failed to converge for the 1.125-in stack-up. Consequently, a comparison cannot be made for this data set and the plots are not shown.

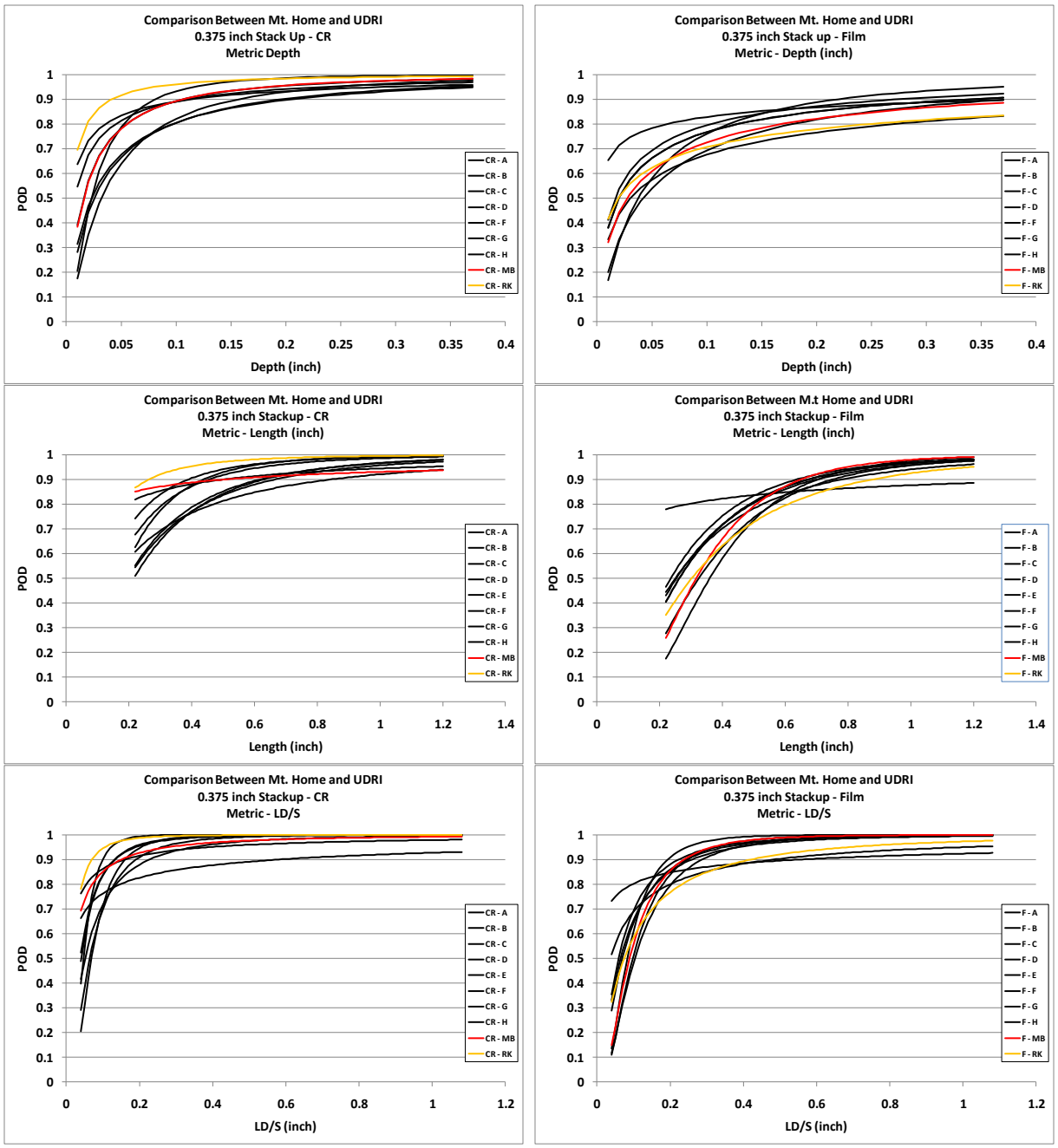

Figure 17. Comparison Between Mt. Home and UDRI POD Plots for Various Metrics for CR and Film for 0.375-in Stack-Up for (left) CR and (right) Film for Three Metrics: (top) Depth (D), (middle) Length (L), and (bottom) LD/S, where S Is Stack-Up Thickness

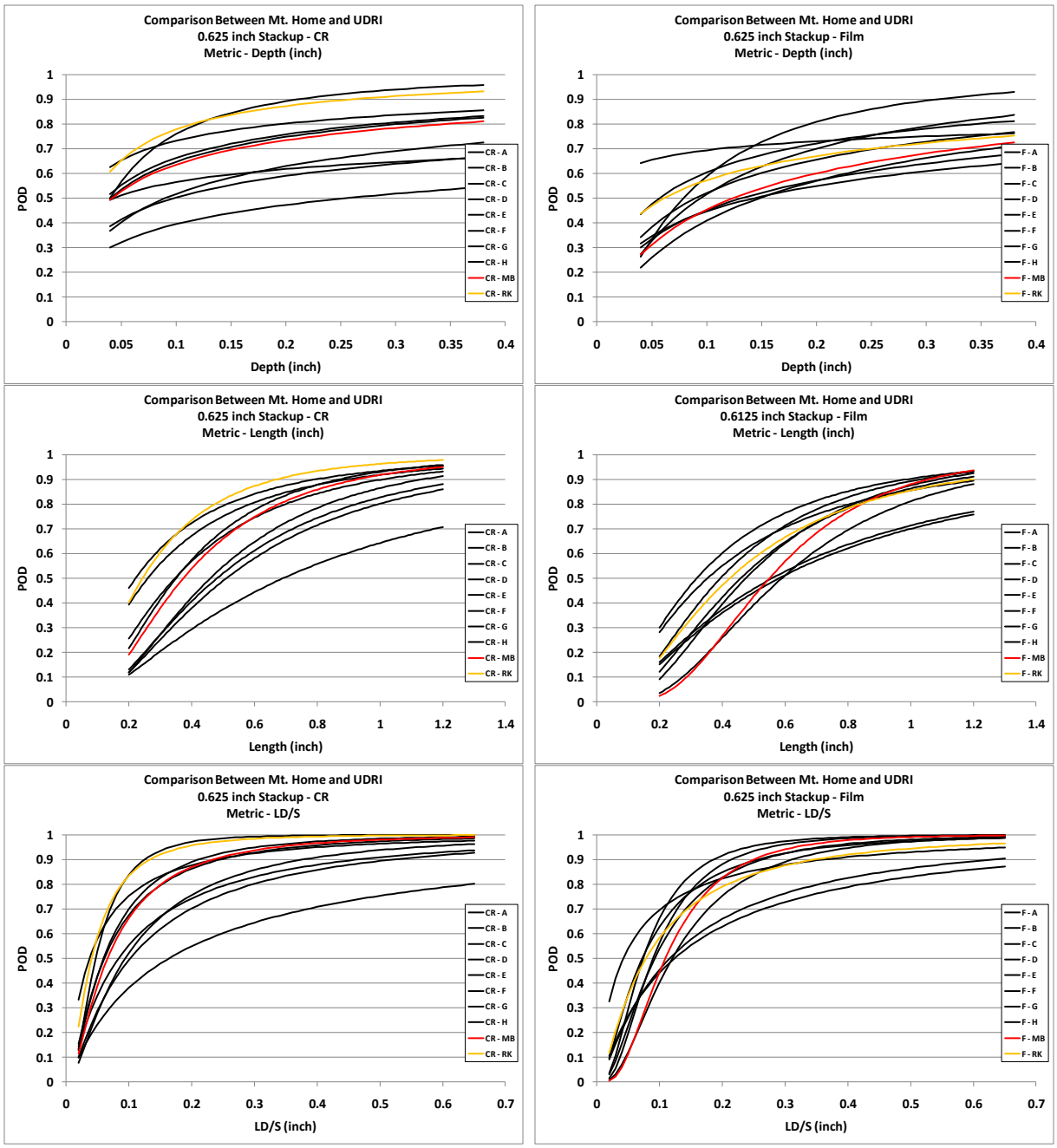

Figure 18. Comparison Between Mt. Home and UDRI POD Plots for Various Metrics for CR and Film (F) for 0.625-in Stack-Up for (left) CR and (right) Film, for Three Metrics: (top) Depth (D), (middle) Length (L), and (bottom) LD/S, where S Is Stack-Up Thickness

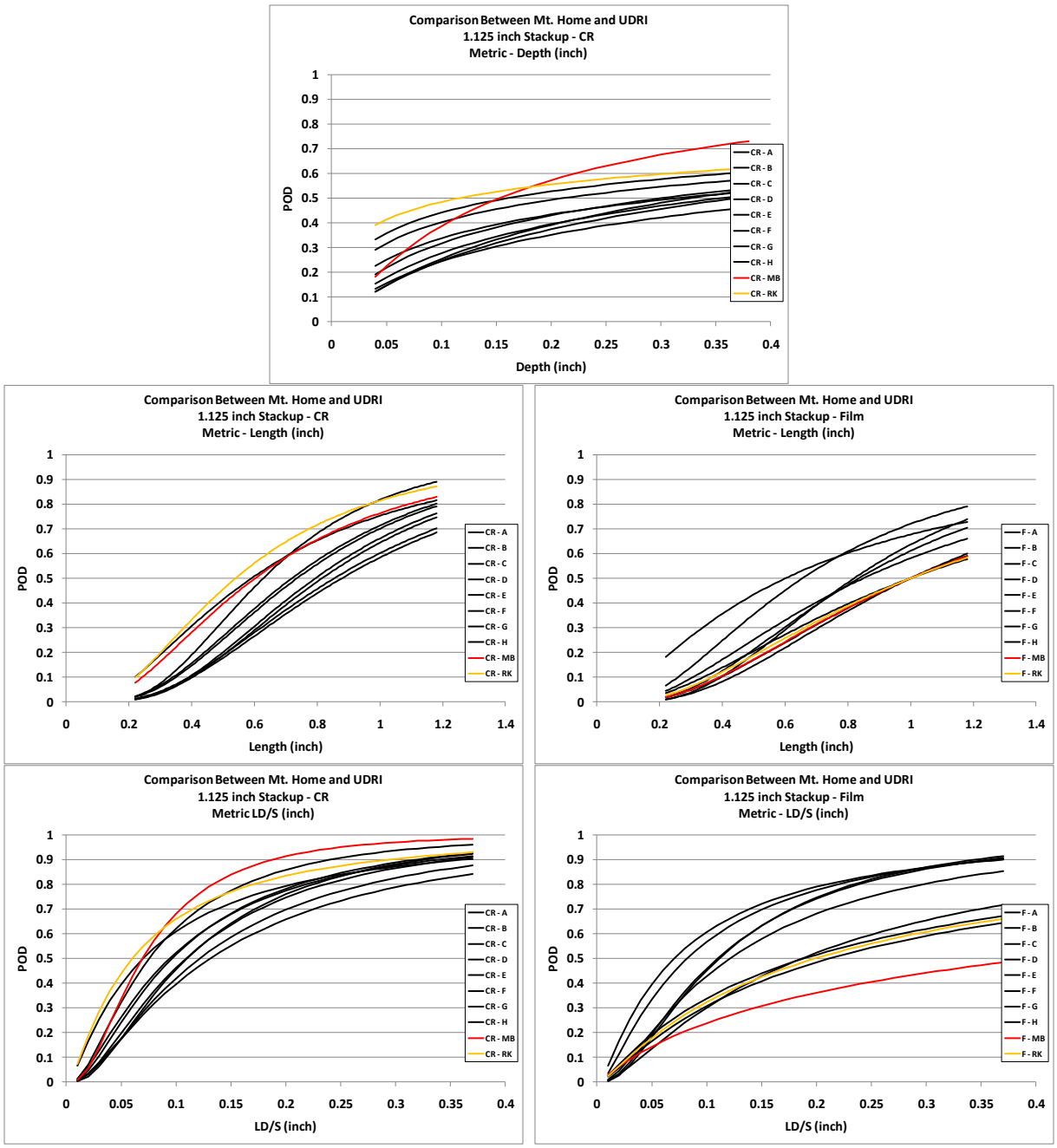

Figure 19. Comparison Between Mt. Home and UDRI POD Plots for Various Metrics for CR and Film (F) for 1.125-in Stack-Up for (left) CR and (right) Film, for Three Metrics: (top) – Depth (D), (middle) – Length (L), and (bottom) LD/S, where S is Stack-Up Thickness. Note the Film Data for Depth Did Not Converge for the UDRI Operators and No Plots Are Shown for This Case

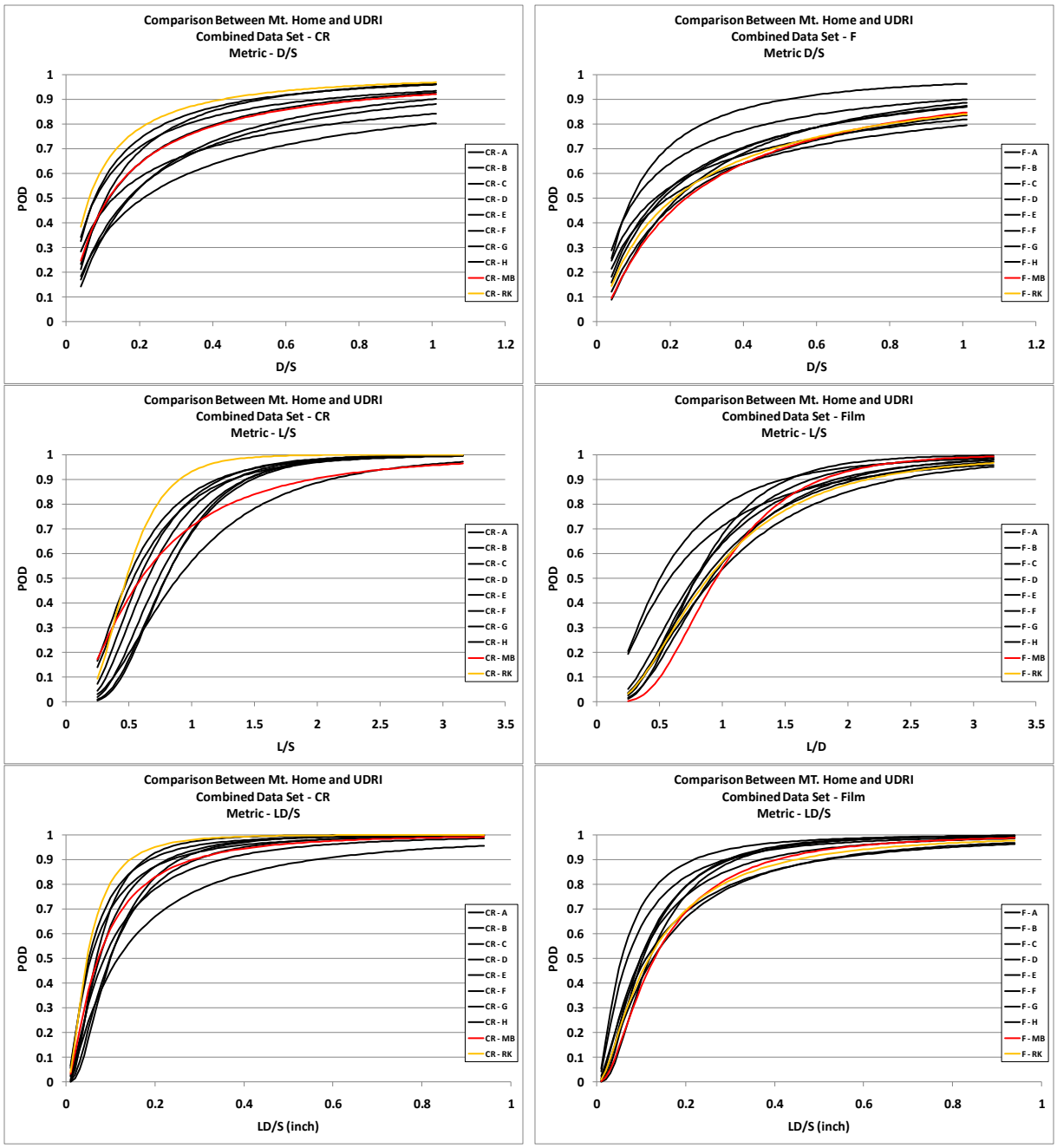

Figure 20. Comparison Between Mt. Home and UDRI POD Plots for Various Metrics for CR and Film (F) for Combined Stack-Up for (left) CR and (right) Film, for Three Metrics: (top) Depth (D) Divided by Stack-Up (S), (middle) Length (L) divided by Stack-Up, and (bottom) DL/S

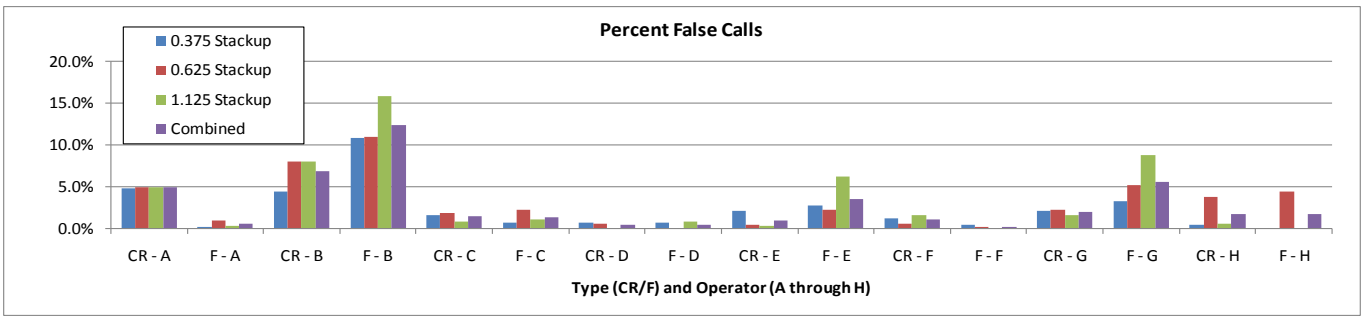

Figure 21. Chart of False Call Results from Data Collected at Mt. Home for the Various Stack-Up Thicknesses and Operators (A-H) for CR and Film (F)

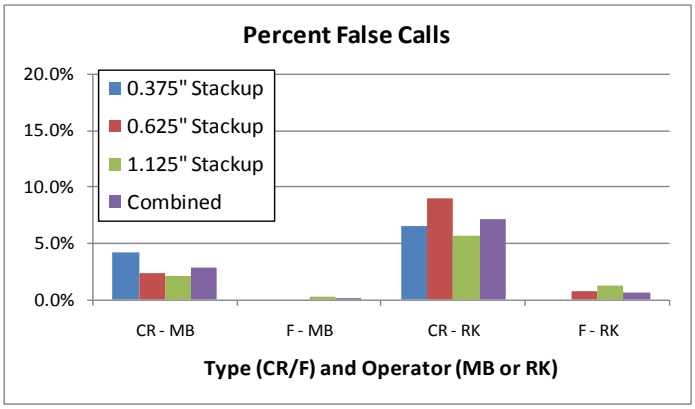

Figure 22. Chart of False Call Results from Data Collected at UDRI for the Various Stack-Up Thicknesses and Operators (MB and RK) for CR and Film (F)

In each plot, it is apparent that there are, essentially, no significant differences between the POD plots for the Mt. Home operators and the UDRI operators, except perhaps in the lower right-hand plot in Figure 19. One UDRI operator produced a POD result that is poorer than the other UDRI and Mt. Home operators. This is unexplained, but not totally unexpected. Occasionally, an operator‟s capability will vary with fatigue and other unpredictable and uncontrollable factors. In general, though, these results visually confirm that the UDRI operators have similar detection capabilities as the operators at Mt. Home.

3.4.2 Comparison of False Call Results. The capability of the Mt. Home and UDRI operators can also be compared using the false call rates recorded for these operators. Figure 21 is a chart of the false call results extracted from the POD report for the data collected at Mt. Home. Figure 22 is a similar chart of the results from UDRI. It is interesting that the UDRI operators recorded a significantly larger number of false calls for computed radiography than for film; however, the UDRI rates seem to be typical of those seen at Mt. Home.

3.4.3 Comparison Between UDRI and Mt. Home Operators – Summary. In summary, there does not seem to be any significant difference between the POD results derived from the

data collected at UDRI and that derived from the Mt. Home data. In addition, there does not seem to be any significant difference between the false call rates seen at UDRI and those at Mt. Home.

3.5 Application-Specific Testing

As previously discussed in Section 2.6, three specific x-ray inspection applications were selected for testing under the CR program. Simulated component tests were conducted in the laboratory using flat panel stack-ups of appropriate thicknesses to determine approximate techniques that could be used to validate the inspection. During laboratory testing, crack specimens were also used in the stack-ups to verify the ability to image cracks within the region of interest for the application. Although use of these crack specimens cannot be used to confirm or deny crack detection capability for any system or application, the appearance of the cracks in the actual stack-up can help to determine how the cracks may actually appear or provide the T.O writer with some additional confidence in the technique developed. The crack specimens that were selected for testing were as close as possible to the actual crack layer thickness. In addition, the cracks selected were of at least three different profiles that included cracks which were: short-tight (0.30 in), long-tight (1.0 in, closed) and long-open (1.0 in, opened). These three crack profiles could be used to obtain an idea of how difficult it might be to image cracks of a certain type within the actual component. The long-open crack could be used to more easily identify the region of interest within the component, while the short-tight crack would provide feedback on the worst-case imaging conditions that might be encountered on the structure. The x-ray tests were also conducted using film following the procedures in the existing T.O.s to verify that the images obtained using both film and CR produced similar results.

In addition to the crack specimens, duplex wire gauges were included in the simulated stack-ups at the actual crack layer position relative to the film or IP. The duplex wires were used to verify minimum un-sharpness levels necessary for the inspection application. Baseline un-sharpness levels required for the laboratory testing are discussed in detail in [11]. In addition, limited tests were conducted using the TM2 crack specimens with the CR system used in the POD study to identify the unsharpness levels where crack detection capability was affected. These test results showed that for object to detector distances > 0, detection of the #9 wire pair on the E2002 gauge was required to insure that crack detection capability was the same as without unsharpness. The unsharpness levels where crack detection was adversely affected correlated well with prior studies using duplex wire gauges.

3.5.1 Application-Specific Laboratory Testing. As previously discussed in Section 2.6, the three application-specific inspections were tested in the laboratory using simulated flat panel stack-ups, or actual components, if possible. Table 17 summarizes the laboratory tests conducted on application-specific stack-ups. For all applications, a simulated stack-up was created using cracked and un-cracked panels of aluminum. The table lists the thickness of the crack layers used in laboratory testing. Crack layers as thick as the actual crack component, or thinner, were used in testing. Since a crack panel with a depth smaller than the actual component would be more difficult to detect, testing with a thinner specimen was considered to be somewhat conservative.

Table 17. Application-Specific Tests Conducted in the Laboratory at AFRL

Specific Application	Shot Number	Total Stack-Up Thickness (in. Aluminum)	Simulated Stack-Up Crack Layers Tested	Actual Components Tested
F-15 Outboard Torque Box Upper Spar	1	0.45	Crack Layers: 0.050 and 0.100 in	F-15 Closure Rib
	2	0.35		F-15 " Closure Rib
B-52 Flap Track	1	0.25 in Steel, 0.25 in Aluminum	Crack Layers: 0.250 in Steel	B-52 Flap Track Component
C-5 Upper Lobe Truss Splice	1	1.5, 2.0 in Aluminum	0.375 in Aluminum	None

Techniques developed in the laboratory for these applications were used as starting points for field-level validation testing on the actual components. Due to limitations from building restrictions, not all inspections could be simulated exactly in the lab. For example, a distance of 90 in from the x-ray tube to the IP could not be simulated in the lab due to ceiling height limits. However, testing on the simulated components did provide an excellent starting point for the techniques to be used in field-site validation testing.

In addition to the simulated stack-ups, some actual aircraft components were available for testing in the lab. Testing conducted using the F-15 closure ribs provided valuable information regarding the position of fastener holes and radii within the flange/web transition region. The B-52 flap tracks provided for laboratory testing were invaluable test articles that contained, not only actual components with correct thicknesses and structures, but also contained naturally occurring fatigue cracks which were imaged using laboratory equipment. The detection of the cracks in all cases were verified using both CR and film in the laboratory.

3.5.2 Field Validation Testing. Validation tests were conducted on two of the three specific applications. As discussed in Section 2.6, the C-5 application was eliminated in December 2010, so validation testing was not conducted on that structure. Validation tests conducted at Mt. Home AFB were in support of the F-15 Outboard Torque Box Upper Spar inspection. Validation tests conducted at Tinker AFB were in support the B-52 Flap Track inspection application.

3.5.3 Creation of Inspection Procedures for Specific Applications. Inspection procedures were created for each of the three specific applications discussed above. Details of the procedures for the F-15 application are contained in [7] and for the B-52 application in [8]. Inspection procedures developed in the laboratory at AFRL for the C-5 Fuselage Upper Lobe Splice Plate can be found in [9].

3.6 POD Results and Analysis

Section 2.5 of this report presented a brief overview of the POD testing that was conducted under the CR program. Section 3.4 presented a comparison of the POD results obtained from the UDRI operators that also evaluated the POD data, and how UDRI POD compared with that obtained

from the AF operators at Mt. Home AFB. The discussion in Section 3.4 was based on a basic understanding of the POD data and results contained in the actual POD analysis report [6]. A brief summary of the results of the Mt. Home POD study are included below. The complete POD analysis report can be found in [6].

3.6.1 Overview of POD Experiment. An experiment was conducted to compare film-based radiography to computed radiography. X-ray images were collected using both methods on a number of cracked plates arranged with other non-cracked plates into three different total stack-up thicknesses. Recommendations from MIL-HDBK 1823 for the number of cracked and un-cracked inspection opportunities were observed. The experiment was conducted for each of the computed radiography and film cases with 1650 inspection opportunities, of which, 330 opportunities contained cracks. The POD analysis was conducted for each of these two cases on a total of 246 cracked inspection opportunities by eliminating repeat inspections of cracks and leaving 82 unique cracks for each of the three stack-up thicknesses ($82 \times 3 = 246$). False-call analysis was conducted using all un-cracked inspection opportunities in the experiment – a total of 1290. Raw images were interpreted by eight different operators in a blind test. Results of their hit/miss readings were tabulated and formed the basis for hit-miss POD analysis.

3.6.2 POD Analysis Methods. Results of the operator hit/miss readings formed the basis for hit/miss POD analysis in accordance with MIL-HDBK 1823 and POD Version 3 software. Fit curves were compared with POD results and found to be reasonable. Statistical tests were conducted to show that the POD results from different operators were not statistically different, could be assumed to represent the same NDE capability for a number of different metrics, and could, consequently, be combined for further analysis. Further tests were conducted to show that the POD results from the three stack-up thicknesses represented the same basic NDE capability for three generalized metrics. Based on these positive test results, a "combined" data set was created. To preserve independence in the data set, only one third of the cracks in each stack-up thickness were used in the combined data set, making sure that each crack was included once (and only once) in the final data set. Fit plots and the data were examined and found to reasonable. Additional statistical tests were conducted to show that data from different operators for this combined data set could be aggregated for further analysis.

3.6.3 POD Results Summary. Based on this analysis, the POD results derived from the aggregate over all operators for the various metrics for computed radiography and film-based radiography were compared using a statistical chi-squared test defined in MIL-HDBK 1823. ***There was insufficient data from this experiment to reject the null hypothesis: the POD results for the two methods represent the same NDE capability.*** The two methods appear to have the same basic NDE capability, even though the film-based results are somewhat more conservative (i.e. CR results indicate slightly better detection capability than film, even though statistically they are the same). If no distinction is to be made between film and computed radiography, then the more-conservative film POD results should be quoted. Otherwise, the POD results should be quoted based on results determined for the individual methods.

3.7 Training Materials

As discussed in Section 2.7, training materials were prepared that could be used to transition the guidelines and procedures developed under this program into the field and depot NDI facilities. The training materials include a tutorial on general background information regarding use of CR in crack detection. This text document can be used as the basis of a section within the T.O. 33B-1-1 AF NDI documentation [14].

Additional training materials were developed to be used as part of a classroom program or as an on-line computer-based training program. The training materials consist of PowerPoint slides, with narration included within the notes accompanying the slides. The CR training is designed as a single training module, with four separate parts. Each part focuses on a specific topic area which may be targeted at a specific audience. The four training module parts are titled:

1. Fundamentals of CR
2. System Qualification and Performance Testing
3. Guidelines for Technique Development Using Computed Radiography for Crack Detection
4. Field Guidelines for Crack Detection Technique Execution Using Computed Radiography

Training programs that include both Parts 1 and 2 are necessary for all AF users of CR for crack detection, since these parts discuss the background information on CR and the process of system performance and qualification testing that is the basis of all other guidelines and procedures using CR. In particular, Part 2 discusses the steps involved with the CR System Performance and Qualification Test Procedure discussed in [13] and must be performed on all CR systems to be used in crack detection.

Although the four training module parts build on each other and can be viewed by all users of CR, two modules focus specifically on certain users within the AF. Part 3 is directed toward the ALC or depot-level T.O. writers. This part is intended to provide supplemental training information that can be of benefit when developing new inspection techniques using CR for crack detection. This module is designed to follow the procedures discussed in [11] and provides an example of an actual technique developed for the F-15 Outboard Torque Box Upper Spar. By applying the technique development procedure to a specific application within the training module, additional details regarding processes, such as validation testing, can be more clearly presented than is possible within the actual guidelines.

Field-level operators, on the other hand, are primarily concerned with executing the T.O.s that pertain to the specific weapons systems to which they are assigned. Therefore, Part 4 of the training module focuses on how to adapt the inspection procedures in T.O.s to the local CR systems at their facility. Discussions in Part 4 make use of the background information in Part 1 and the system performance test procedures in Part 2 to describe how the field-level operator can create techniques that are appropriate for the CR system and specific inspection application described by the T.O. Field-level operators do not need the level of detail contained in Part 3 of the training module and, therefore, may be omitted from their training programs.

When taken together, the four training modules provide a comprehensive training program for the use of CR in crack detection. These four training modules were developed and delivered under the CR program to assist with current and future training programs on the use of CR in crack detection.

4.0 CONCLUSIONS

The results of the x-ray CR-film validation study showed that, under some experimental conditions, CR systems may exhibit detection capability for cracks that is equivalent to film. Cracks that were approximately 1 in. in length, in stack-ups ranging from 0.375-1.125 in thick, were detected using several different CR systems with a capability comparable to film. For cracks that were approximately 0.3 in. in length, only one CR system exhibited detection capability comparable to film. CR system performance, measured using image quality standards, was correlated with crack detection capability to identify performance requirements for crack detection capability that is equivalent to film.

Based on the results of system performance testing and crack detection capability determined from laboratory testing, a CR system performance test procedure was developed. This test procedure is based on visual tests that are software- and CR system-independent and, therefore, can be applied to any CR system. When used to compare with the performance of the CR systems that are equivalent to film, the performance test can be used to qualify CR systems for crack detection [13]. To summarize, a system with spatial resolution and image noise of >6.0 lp/mm and <1.19%EPS may be used for the range of materials and applications tested in this program. CR systems with >5.0 lp/mm and <1.33 %EPS may be used for a slightly more limited set of applications, which requires further analysis to establish these limits. Spatial resolution is measured using the existing USAF CRPCS, while image noise is measured with a new test standard that is basically an aluminum version of the ASTM E746-07 Relative Image Quality Indicator.

Based on the results of system performance testing and crack detection capability testing, guidelines were created which can be used to develop optimized techniques for CR systems that can be used in crack detection [11]. These guidelines are based on the individual performance of each CR system as characterized using the procedures in [13].

Inspection procedures for three different high-priority inspection applications were developed for CR systems and tested in the laboratory. Two of the three procedures were validated on-wing at field locations and capability compared with film images of the same structures. The procedures for the three specific structures can be found in [7-9].

Training programs were conducted on three different occasions, to both field- and depot-level AF radiographers. Training materials were developed for the programs and delivered in hard copy and electronic forms. The electronic versions are designed to be used in classrooms or as an online computer-based training program that could be made available through the AF intranet [12].

POD testing was conducted using film and CR images obtained under optimum conditions. Images were evaluated using a representative pool of AF operators and analysis conducted following

guidelines in MIL-HDBK 1823. Results of the POD analysis showed that there was insufficient data from this experiment to reject the null hypothesis: the POD results for the two methods represent the same NDE capability. Therefore, based on the POD study and laboratory testing, CR systems as defined in this document which demonstrate performance equivalent to an image noise measurement of EPS=1.19% and image spatial resolution of 6.0 lp/mm provide crack capability equivalent to film over the detection range: aluminum: 0.375-1.125 inches total stack-up thickness, with crack parameters equal to: crack length 0.3-1.0 inches, crack depth: 0.040-0.375 inches. Laboratory testing indicated that crack detection capability for all CR systems was equivalent to film for steel 0.25 inches thick, containing cracks 0.3-1.0 inches in length, with up to 0.25 inches of additional aluminum in the steel stack-up.

5.0 RECOMMENDATIONS FOR FUTURE WORK

Significant testing and analysis was conducted under this program, but due to the time constraints, was not completed. Continuing the work that was initiated under this program would provide insight into the specific crack detection limitations of CR systems, and provide information on how systems that, perhaps, do not perform optimally as compared to film, may provide sufficient capability for some inspection applications. Recommendations for future work that would provide benefit in this area are discussed below.

5.1 CR System Capability Study

Crack parameters, such as crack length and percentage of crack layer thickness, were varied in the current specimen set. Crack layer percent of total stack-up was varied over a range of 4-100%, but the effect of crack layer thickness was not evaluated under the capability study. Other metrics explored in the POD study could also be applied to the laboratory data to determine the best method for comparing crack detection capability between CR systems. Other factors, such as false calls and image artifacts, were noted and taken into consideration in an overall sense in the development of procedures and guidelines. However, a quantitative assessment of false call rates with different CR systems may provide insight into the relationships between image noise, image spatial resolution, and defect detection. Furthermore, other quantitative image quality metrics (such as signal-to-noise, contrast-to-noise, and defect line profiles), can be used to characterize both images and defects. Additional funding opportunities could make use of the existing CR images to develop more-reliable, automated, methods of system performance testing and defect detection.

Preliminary testing conducted early on in this program was designed to select the most significant test conditions for the capability study. In the interest of efficiency, Type III plates were tested using only a 50 micron scan resolution. Although results of the current study showed that in general, lower noise, higher spatial resolution images were acquired when using Type III plates and a 50 micron scan resolution, under some conditions when using Type II plates crack detection capability was slightly better when using 100 micron scan resolution rather than 50 micron. Recommendations for future work would include additional testing using Type III plates with a 100 micron scan resolution so that the effect on crack detection can be assessed. In addition, future crack studies should consider specimen design that allows orientation variations within the same image (i.e. square specimens that can be rotated by 90 degrees).

5.1.1 CR System Qualification Testing. All qualification and performance testing conducted under this program was performed using a single set of EPS plaques and absorber plates. Commercially available plaques and plates were purchased under the program to assess differences in system performance that might be attributed to differences in EPS plaques or absorber plate response. Limited testing was performed using the second set of plaques, but a comparison of EPS readings of other commercially available plaques versus those used in the study was not completed. Additional EPS evaluations to support guidelines for technique development are also recommended that include absorber plates of various thicknesses and performance testing using steel plaques. Furthermore, day-to-day variability of CR systems could contribute to the system performance. An assessment of the changes in system performance with time was initiated but could not be completed under this program. Differences in EPS readings due to both differences in commercially available standards and system performance variability with time should be evaluated to determine if the EPS criteria needs to be adjusted prior to fully implementing the recommended performance test procedures. Recommendations for follow-on programs would include development of qualification and acceptance procedures for the EPS plaques and absorber plates, as well as analysis of the variability in system performance measurements due to standards, and day-to-day variability.

The effect of beam angle on crack detection is known to be a factor, thus, the current study maintained no more than a 7.5 degree angle between the main beam and the crack face. However, for some crack profiles, the effect of beam angle may be more significant than for others. Under the current program, test matrices were created and images acquired that could be used to evaluate the effect of beam angle on CR crack images. However, time constraints did not allow for a full analysis of that data. These results, combined with an evaluation of un-sharpness data, could be used to further identify CR systems that could be used in less-demanding crack detection applications.

Angle beam crack specimens were created under this program that contain cracks which initiated in the radius and then grew into the web portion. Although fatigue crack grow testing of these "L"-shaped panels showed that actual structures could be simulated using flat panel stack-ups, these structures could be used in other tests to evaluate the effects of scatter and interference of other structures on crack detection capability. Further testing using these "L"-shaped crack specimens could provide insight into the effect of beam angle on the detection of cracks within actual structures as well.

The effect of CR scanner pre-processing (i.e. Fuji CR systems) of imaging data was evaluated on a very limited basis. Although system qualification testing could be performed on the CR system with image pre-processing, two different pre-processing schemes were required for acquisition of the image noise and spatial resolution images. Limited testing using TM2 showed that crack detection capability for this system was consistent with other CR systems with similar performance. Therefore the results of limited testing showed that there are no specific implementation issues with CR systems that impose image pre-processing, but these systems should be further evaluated and guidelines developed to optimize their use in crack detection applications. The use of pre- or post- processing filters is not recommended for crack detection at this time. However, improvements in software applications may show that some pre- or post- processing features do provide

additional capability that is not anticipated at this time. Re-evaluation of CR system hardware and software capability is recommended on a regular basis.

Results of the POD and laboratory studies showed that, for some CR systems, crack detection capability is comparable to film. However, there are many metrics that can be used to evaluate detection capability that could be explored with the existing data. Furthermore, with all NDE systems, there is variability that can be attributed to randomized measurements or can be due to real factors. Some analysis of the variability due to statistical randomness was initiated under this program, but could not be completed. A recommended follow-on program would allow for the completion of the variability analysis and development of additional qualification criteria.

However, there are many factors that influence operator efficiency and reliability in image evaluation, including training programs. A continued CR training program is recommended that would include application-specific training using actual CR images acquired on laboratory crack specimens that operators could use to practice imaging and recognizing cracks in the structures. There are many examples of CR images that were generated on this program that could be used to develop a hands-on training or additional POD testing.

6.0 REFERENCES

1. MIL-HDBK 1823, ASC/ENOI, 2530 Loop Road W., Wright-Patterson AFB 45433-7101.
2. "Computed Radiography – Film-Based X-Ray Comparative Study –Phase 1 Final Report", UDRI Technical Report Number: UDR-TR-2009-00015, Contract Number: FA8601-06-D-0013.
3. ASTM E-746-07, ASTM International, 100 Barr Harbor Drive, P.O. Box C700, West Conshohocken, PA 19428-2959, United States.
4. Radiography Process Control, SWP 106-01, T.O. 33B-1-2.
5. Website: http://rsbweb.nih.gov/ij/docs/install/windows.html.
6. "POD Analysis Report for Computed Radiography Program", Wally Hoppe and Victoria Kramb, UDRI TR 2011-71.
7. "Specific Application Radiographic Inspection Procedure – F15 Outboard Torque Box Upper Spar", UDRI TR-2011-72.
8. "Specific Application Radiographic Inspection Procedure – B-52 Flap Track", UDRI TR-2011-67.
9. "Specific Application Radiographic Inspection Procedure – C-5 Fuselage Upper Lobe Splice Plate", UDRI TR-2011-66.
10. ASTM E-2002, ASTM International, 100 Barr Harbor Drive, P.O. Box C700, West Conshohocken, PA 19428-2959, United States.
11. "Computed Radiography for Crack Detection Guidelines for Technique Development", Victoria Kramb, UDR-TR-2011-68.
12. "Computed Radiography Training Materials", Victoria Kramb, Greg Mohr, and Ollie Scott, UDRI TR-2011-70.
13. "Computed Radiography Qualification (Performance) Test Procedure for Crack Detection Systems", Victoria Kramb UDRI TR-2011-73.
14. Nondestructive Inspection Methods, Basic Theory, Chapter 6: Radiographic Inspection Method Sections 4-8, T.O. 33B-1-1.

Appendix A

Computed Radiography Crack Detection Validation Study Test Plan

This document summarizes the Computed Radiography Crack Detection Validation Study test plan as discussed during the kickoff meeting held on September 17, 2009. The goal of this study was to conduct a validation assessment of the fatigue crack detection capability of commercial "off-the-shelf" Computed Radiography systems, and transition the capability to the USAF. A summary of the deliverables generated as a result of the program are shown in Table A1 below.

Table A1. Deliverables Summary

Deliverable	Scope	Data Acquired	Specimens Used	AF Interaction Required
System Performance Testing	Evaluate various tests for measuring system performance and establishing optimum techniques	System performance data *CR and film data*	Line pairs, EPS plaques, hole-type penetrameter, wire IQIs, (others?)	Data acquisition and evaluation at AFRL
Technique Guidelines	Develop hardware setup and viewing protocol	Crack detection and image quality *CR and film data*	Standard image quality indicators, crack panels	Data acquisition and protocol development at *AFRL*
Technique Validation Protocol	Process to verify CR techniques used in TOs	Crack detection *CR and film data*	Crack panels, engineered components	Data acquisition and protocol development at *AFRL, validation at AF Bases*
CR System Qualification Protocol	Rate CR System crack detection capability based on prior tests and establish qualification criteria	Images acquired using standards and crack specimens, *CR and film data*	Standards and crack specimens	Protocol development at *AFRL*, testing at *AF Bases*
POD Analysis Report	Comparison of crack detection capability for film and CR in terms of POD	Optimized film and CR images of representative structures analyzed by AF inspectors	Actual aircraft structures, scrap or on-wing, with crack panels	Data acquisition at AFRL and AF Bases, image analysis by *AF Inspectors*
CR Training Materials	CR training conducted at 2 locations, material delivered includes supplements to 33B-1-1	Standard and crack specimens used for demonstration purposes only	Standards used in CR Qualification Protocol and Technique Validation	Preliminary training scheduled for NDI WGM Feb. 2010. 2nd session TBD

A1.0 DELIVERABLES DEFINITIONS

A1.1 System Performance Testing

System Performance Testing will establish a method to measure the performance of various CR or film systems. The intent is to "categorize" CR systems much like film types are categorized today. This data would then be compared to crack detection data developed in other planned tests and used to develop System Qualification criteria. The System Performance Tests will also evaluate technique parameters which will feed into the *Technique Guideline* task.

A1.2 Technique Guidelines

Technique Guidelines are rules used to develop new x-ray inspection procedures or to convert existing film inspection procedures for use with CR imaging technologies. Technique guidelines describe settings for the x-ray tube, generic CR scanner, and viewing software that are recommended for inspection of crack specimens or components satisfying specific inspection criteria (stack-up, source-to-film distance, etc). The technique guidelines also include generic procedures for viewing CR images and the criteria by which image quality is assessed. The guidelines should be written using generic terminology, such that the recommended procedures are independent of CR scanner manufacturer, software application, and imaging plate (IP) used.

A1.3 Technique Validation Protocol

A Technique Validation Protocol describes tests used to validate that an x-ray inspection procedure generated using the above Technique Guidelines adequately interrogates a region of interest and satisfies ***specific inspection*** detection requirements. The validation procedure for CR-based x-ray inspections includes a specific image quality assessment procedure that is used to insure that images obtained are adequate for crack detection within the region of interest.

A1.4 CR System Qualification Protocol

The CR System Qualification Protocol describes the data acquisition and analysis procedures that are used to qualify a "CR System" for use in crack detection. The protocol describes image characteristics based on standardized targets to rate system performance for crack detection. The "CR System" as defined within the protocol includes: 1) the x-ray tube with specific focal spot, 2) CR Scanner with a specified scan resolution, 3) Imaging Plate (IP) model, 4) Data acquisition and analysis software application and version number, and 5) viewing monitor.

A1.5 POD Analysis Report

Probability of Detection (POD) analysis methods will be applied to x-ray inspection data acquired under the CR Crack Detection Validation Study. A comparison of the crack detection capability of film and CR will be discussed in terms of POD. Analysis of the POD data will be used as the basis for validation of the viewing protocol developed under this program.

A1.6 CR Training Materials

CR Training will be conducted for AF personnel for the use of CR in crack detection. Training will be directed toward three areas: 1) Background in CR Systems, 2) use of the Technique Guidelines and Technique Validation Protocol, and 3) Maintenance, Calibration and Process Control of CR Systems used in crack detection.

A2.0 TASK DESCRIPTIONS

A2.1 System Performance Testing

The *System Performance Testing* is based on a set of standards taken from the USAF CR Process Controls and a draft version of ASTM E2033 "Standard Practice for Computed Radiography". System Performance Test data of each "system" will be compared to their crack-detection performance in the tests outlined in Sections A2.2. and A2.3 to establish the CR System Qualification Protocol outlined in Section A2.4.

For purposes of these tests, a CR "system" is defined as any combination of hardware/software as described in Table A2 below.

Table A2. CR System Details

Tube Head (Focal Spot)	CR Scanner	CR Scanner Resolution	Imaging Plate	Viewing Monitor	Software
0.4mm	Scanner A	50 μm	Type II (standard resolution)	Monitor A (3MP)	Software A
1.5mm (Lorad)	Scanner B	100 μm	Type III (high resolution)	Monitor B(3MP)	Software B
3.0mm	Scanner C		Type I (coarse grain)		
	Others as available	Others as available (<50 μm)	Others as available Type IV (ultra-high resolution)	Others as available (5MP?)	Others as available

The minimum set of tests is listed in Table A3. Tests will include visual and/or measurable evaluation of significant image quality metrics.

Table A3. System Performance Tests

Test Device	Test Parameters	Metric	Evaluation Method
Line pair gauges from CRPCS	SDD = 48 in ODD = 0 to 20 in	Spatial resolution (x and y directions)	Visual and line profile tool*
Wire IQIs	Exposure range from ~5 to ~95% MPV**	Equivalent Penetrameter Sensitivity (EPS)	Visual only
Hole-type penetrameters	Exposure range from ~5 to ~95% MPV**	T-hole visibility CNR of 4T hole	Visual and pixel statistics tool*
E746 Relative Quality Image Indicator (a.k.a EPS plaques)	Exposure range from ~5 to ~95% MPV**	Equivalent Penetrameter Sensitivity (EPS)	Visual only

**Use and availability of specific software tools are dependent on each manufacturer's software.*

*** Maximum Pixel Value (MPV) is dependent on CR system (e.g. 16-bit systems have 65504 MPV)*

A2.2 Technique Guidelines

Technique Guidelines will be developed based on analysis of x-ray inspection results obtained from crack specimens tested in a laboratory environment. The *Technique Guidelines* will be developed to include a range of test conditions based on information contained in the TOs listed in Table A8. Table A4 below lists the variables that will be considered in the creation of the test matrix.

Table A4. Inspection Variables Considered in Technique Guideline Creation

Crack Specimen	Inspection Setup	CR Scanner	IP	Exposure Parameters
Stack-Up Thickness	Source-to-film distance	Scanner type/ Model	Type (resolution)	kV, mA, time
Crack Length	X-ray beam angle	Scan resolution	Orientation	Object-to-detector (ODD) distance
Crack Opening	Tube/spot size			Source-to-detector (SDD) distance
Crack Panel Thickness	Use of lead screens			

The effect that each inspection variable in Table A2 has on CR imaging will be considered and a test matrix will be developed to examine the effect on crack detection. The need for lead screens and the effect of kV range on scatter will be addressed as an outcome of the planned testing. The range of each specimen and test parameter to be included in creation of the *Technique Guidelines* is listed in Tables A5 through A7.

Table A5. Crack Specimen Parameter Range

Aircraft Component Geometry	Crack Specimen Geometry	Specimen Parameters	Dimension Range (inches)
Cracks from Fastener Holes	Flat panels with fatigue-cracked center notch	Crack panel thickness	0.040-0.289
		Stack-up thickness	0.100-2.0 (estimate)*
		Crack length	0.125-2.00
		Crack opening	Closed (<0.001), or Open (>0.001)
Cracks in Rib/Spar Flange	Curved sections with radii and web containing fatigue cracks	Specimen shape	"L" and "T"
		Crack location	In radius and in web
		Crack panel thickness at radius	0.063-0.200
		Crack type	Partial and thru crack

** Maximum stack-up thickness limit for crack detection will be determined empirically.*

Table A6. Inspection Setup

Crack Specimen	Inspection Setup Variable	Dimension Range (inches or degrees)
Flat Panel	Source-to-film distance	48*
	X-ray beam angle	0, 5, 10
	Specimen-to-film/IP distance	0.050-12"
Radius	Source-to-film distance	48*
	X-ray beam angle	0, 5, 10

**Unsharpness performance of other source to film distances will be extrapolated from CR Performance testing detailed in the following section.*

Table A7. CR Systems

CR Scanner			Scan Resolution	Imaging Plate	X-Ray Tube/" Focal Spot
	Lab	Field*			
Scanner A	AFRL	TBD	50 µm, 100 µm	Type II, Type III	Phillips: 0.4mm, 3.0mm, Lorad 1.5mm
Scanner B	AFRL	TBD	50 µm, 100 µm	Type II, Type III	Phillips: 0.4mm, 3.0mm, Lorad 1.5mm
Scanner C	AFRL	TBD	TBD	TBD	Phillips: 0.4mm, 3.0mm, Lorad 1.5mm
Other systems *	TBD	TBD	TBD	TBD	TBD

**Field systems to be used for testing will be determined by schedule and availability and will use Lorad x-ray tubes exclusively. Other CR systems will be tested using the qualification protocol and crack specimen set as they become available.*

Not all combinations of test parameters shown in Tables A4-A7 will be used in development of the test matrix. Testing will proceed in the most efficient manner possible to characterize CR inspection performance while minimizing test time and the number of crack specimens needed to develop the guidelines. Recommendations for technique development which lies outside the range of specimen parameters and inspection variables examined will be included in the protocol.

Inspection data acquired during execution of the above test matrix will be compared with the results of the CR System Performance assessment described below. Correlation of the crack inspection data with the system performance based on standardized qualification tests will be used to create a CR image viewing protocol for use in crack detection that will be included in the Technique Guidelines.

A2.3 Technique Validation Protocol

A protocol for validating the inspection procedures created using the CR Technique Guidelines discussed above will be developed for use in the transition of existing film inspection procedures to CR. CR inspection procedures will be created for 3 high-priority structural inspections using the Technique Guidelines. Crack detection capability for these inspections will be validated through comparison of the CR detection capability to that of film for the same structures. Specimens used for the validation testing will include engineered crack specimens representative of the aircraft structure. Representative structures will be created using fatigue crack specimens generated in the laboratory, with total stack-up and standoff distances (crack-to-detector distances) representative of those encountered in the actual inspections. All testing and image quality assessments will follow the Technique Guidelines discussed in Section A2.1.

A2.4 CR System Qualification Protocol

A CR System Qualification Protocol will be developed based on the results of the CR System Performance Testing and Technique Guidelines testing. Correlation of the CR system performance based on standardized imaging tests with crack detection conditions will provide a baseline for classifying CR System performance for specific limits of crack detection. The protocol will be applied to CR systems currently used in the field to identify current capability. In addition, the protocol will be applied to new CR systems and technology.

A2.5 POD Analysis Report

POD testing will be conducted using both film and CR images acquired on structures containing features which represent actual inspections as closely as possible. Field- or depot-level AF inspectors will be used for the POD testing and selection of the inspector pool will be coordinated with the NDI program managers. Images provided to the inspectors for examination will represent TOs with which he/she is familiar. CR images will be viewed and analyzed using the software application for which the inspector has been previously trained. The region of interest within each image may or may not contain cracks. Crack parameters for those included in the images will be varied in order to provide POD type test results. All images used in the study will be optimized such that image quality criteria established by the Technique Guidelines are satisfied prior

to examination by the AF Operators. Analysis of the POD data will be used as the basis for validation of the viewing protocol developed under this program.

A2.6 CR Training Materials

CR training will be conducted for AF personnel for the use of CR in crack detection. Training will be directed toward three areas: 1) Background in CR Scanners and IP Technology, 2) Use of the Technique Guidelines and Technique Validation Protocol, and 3) Maintenance, Calibration and Process Control of CR systems used in crack detection. Training materials that can be used to further train AF inspectors will be delivered. One outcome of the training materials will be a supplement to the 33B-1-1 Technical Manual, Chapter 6 on Radiographic Inspection Methods. Training materials will be available and coordinated with the NDI Functional Managers and the Training Managers at Sheppard AFB through the Utilization and Training Workshop.

A3.0 SCHEDULE

A3.1 Technique Guidelines

Development of the *Technique Guidelines* requires extensive laboratory testing with ASTM standards, analysis, and processing of x-ray data using multiple CR scanner systems. In addition, crack test specimens will need to be created and characterized prior to x-ray testing. X-ray tests will then be conducted on the crack specimens over the range of test parameters with multiple CR scanner system configurations. Data analysis and correlation with the results of CR system performance testing will result in the creation of the Technique Guidelines. Further progress on other program tasks is dependent upon creation of the Technique Guidelines. Estimated time for completion: 7 months, March 2010.

A3.2 Technique Validation Protocol

A protocol for validating the inspection procedures created using the CR Technique Guidelines can be developed in parallel with the Technique Guidelines. As specimens are created and tested using the guidelines, procedures for validating detection capability will be developed as well. Final validation of the procedure will be performed using engineered crack specimens representing the high-priority aircraft structures and will, therefore, be limited to completion of the test specimens needed for the validation testing. Estimated time to completion: 8 months, April 2010.

A3.3 CR System Qualification Protocol

A CR System Qualification Protocol will be developed based on the results of the CR System Performance Testing and Technique Guidelines testing. A draft of the protocol will be developed as testing progresses. Assessment of the applicability of the protocol to characterize CR systems for x-ray detection will be conducted at the AF bases and on new CR systems made available to the study. The final CR System Qualification Protocol will not be completed until after testing has been conducted on the CR systems of interest to the AF. Estimated time to completion: 6 months, February 2010.

A3.4 POD Analysis Report

POD testing will require creation of x-ray film and CR images representative of actual inspections and, therefore, is dependent upon creation of crack specimens and representative structures. In addition, conducting the POD testing will require scheduling with AF bases so that actual inspectors can be dedicated to the image analysis necessary to conduct the POD testing. Based on these requirements for completion of the POD testing and analysis, an estimated time to completion is 10 months, June 2010.

A3.5 CR Training Materials

CR training will be conducted for AF personnel for the use of CR in crack detection at locations and times to be determined. A preliminary training session will be scheduled during the NDI WGM in February 2010 (Second training site – TBD). At that time, a draft of the Technique Guidelines and Technique Validation Protocol should be available for review and will be presented to the audience. CR technology, as well as Maintenance, Calibration, and Process Control of CR systems used in crack detection will also be covered during the training session. Documentation and training materials cannot be finalized until completion of the other tasks, therefore, estimated time to completion is 10 months, June 2010.

Table A8. Air Force Film-Based X-Ray Inspection Parameters Summary

	X-ray System Setup						Relevant Crack Specimen Parameters					
Component	tube voltage (kV)	filament current (mA)	exposure time (sec)	tube-part angle (degrees)	source to target distance (FFD) (inches)	film/IP-target distance (inches)	mat'l	geometry (crack initiation)	no. layers, source to crack	thickness crack to film/CR (inches)	approx. fastener hole diameter (inches)	crack length (inches)
C5A T.O 1C-5A-36												
Upper Lobe Truss Splice, Fuselage Station 1383	140-150	4.5	720	0	24, 80		Al	cracks from fastener hole	4		5/16 (?)	
Horizontal Stabilizer Chordwise Skin Splice-*Upper Splice Plate*	105-135	4.5	120	±5	varies-tube on part surface≈20		Al	cracks from fastener hole	4		3/8-1/4 (?)	
Horizontal Stabilizer Chordwise Skin Splice-Lower *Splice Plate*	110-125	4.5	120	±5	varies-tube on part surface≈20		Al	cracks from fastener hole	4		3/8-1/4 (?)	
B52 T.O. 1B-52H-36												
Trailing Edge Flap Track--WS 303, 398, 491, 586-left	90	4.5	55	0	17		steel	cracks from fastener hole	3 or 4	0.354		
Trailing Edge Flap Track--WS 586-right	90	4.5	55	0	15		steel	cracks from fastener hole	3 or 4	0.354		
Trailing Edge Flap Track--WS 766	90	4.5	55	0	17		steel	cracks from fastener hole	3 or 4	0.292		
Trailing Edge Flap Track--WS 855	90	4.5	55	0	17		steel	cracks from fastener hole	3 or 4	0.292		
Trailing Edge Flap Track--WS 944	90	4.5	55	30	17		steel	cracks from fastener hole	3 or 4	0.292		
F15A T.O. 1F-15A-36												
Outboard Torque Box, Main Spar, Upper Flange	120	4	150	0, 15	ground to wing		Al	cracks in flange radius	?			
Wing Tip Closure Rib	80-95	3	150	0, 5	45		Al	cracks in flange radius	4			
Wing Tip Forward Spar	120	4	90	24	ground to wing (90)		Al	cracks in flange radius	4			
Outboard Trailing Edge Ribs	130	4.5	120	22	97		Al	cracks in flange radius	3 or 4			
Outboard Torque Box Ribs, Cracks in Upper Flange	120	4	150	0, 15	90		Al	cracks in flange radius and fastener hole area	?			
Outboard Torque Box Ribs Notch Areas	120	4	150	53	60		Al	cracks in flange radius and fastener hole area				
C130A T.O.1C-130A-36												
Fuselage Frames at FUS Sta 212, 228, WL195	130	3	30	37-WRT part	48			cracks in flange radius	4			

Appendix B

Flat Panel Fatigue Crack Specimen Characterization

Flat panel fatigue crack specimens were manufactured from 2024 and 7075 T3 aluminum alloys and 304 stainless steel. Cyclic fatigue loading at 10Hz was used to initiate and grow the cracks from a centrally located electro-machine discharge (EDM) notch. After fatigue loading to achieve the desired crack length, some of the crack specimens were intentionally overloaded, or subjected to pin-loading, to encourage a more "open" crack profile. All fatigue cracks grew through the thickness of the specimen, which varied from 0.040 in to 0.375 in. After achieving the desired crack profile, the specimens were machined to create a center cracked specimen with nominal dimensions 3.85 in wide by 2.0 in tall. The excess material machined from the fatigue specimen was used to make uncracked blank specimens or spacers that could be used with the crack specimens to create a variety of total stack-up thicknesses. These flat panel fatigue crack specimens were used in the laboratory and field x-ray testing discussed in this final report.

The following pages show a micrograph of each flat panel crack specimen at the crack mouth, near the center notch. The micrographs provide a visual indication of the amount of crack opening for each fatigue crack. Since the crack grew symmetrically from the center notch, two cracks are described by the "right" and „left" side of the notch. Specimen thickness, crack length measurements for each crack, and an approximate measure of crack opening is also shown with the micrographs. The micrographs were taken at a magnification of 10× unless otherwise noted.

Table B1. Complete Listing of All Flat Panel Aluminum Crack Specimens

Specimen Number	Nominal Thickness (in)	Nominal Width (in)	Left Crack Length (in)	Right Crack Length (in)	Material	Crack Opening
Al-040-1	0.040	3.85	0.320	0.318	2024	Closed
Al-040-2	0.040	3.85	1.028	0.940	2024	Closed
Al-040-3	0.040	3.85	1.121	1.123	2024	Open
Al-050-1	0.050	3.85	0.308	0.312	7075	Closed
Al-050-2	0.050	3.85	0.987	0.926	7075	Closed
Al-050-3	0.050	3.85	Fractured	Right Side Only	7075	**Fractured**
Al-050-4	0.050	3.85	0.522	0.492	7075	Closed
Al-050-5	0.050	3.85	0.621	0.609	7075	Closed
Al-063-1	0.063	3.85	0.65	0.7200	2024	Closed
Al-063-2	0.063	3.85	0.49	0.4700	2024	Closed
Al-063-3	0.063	3.85	0.78	0.7300	2024	Closed
Al-100-1	0.100	3.85	0.320	0.300	2024	Closed
Al-100-2	0.100	3.85	0.969	0.932	2024	Closed
Al-100-3	0.100	3.85	0.234	0.222	2024	Pin-Loaded
Al-100-4	0.100	3.85	0.573	0.542	2024	Closed
Al-100-5	0.100	3.85	0.524	0.507	2024	Closed
Al-125-1	0.125	3.85	0.309	0.298	7075	Closed
Al-125-2	0.125	3.85	0.968	0.945	7075	Closed
Al-125-3	0.125	3.85	Fractured		7075	**Fractured**
Al-125-4	0.125	3.85	0.532	0.514	7075	Closed
Al-125-5	0.125	3.85	0.554	0.550	7075	Closed
Al-125-1-1	0.125	3.85	0.320	0.320	7075	Closed
Al-125-2-1	0.125	3.85	0.670	0.750	7075	Closed
Al-125-3-1	0.125	3.85	1.090	0.950	7075	Closed
Al-189-1	0.189	3.85	0.293	0.308	2024	Closed
Al-189-2	0.189	3.85	1.009	0.899	2024	Closed
Al-189-3	0.189	3.85	1.063	1.017	2024	Open
Al-189-4	0.189	3.85	0.308	0.301	7075	Closed
Al-189-5	0.189	3.85	0.974	0.958	7075	Closed
Al-189-6	0.189	3.85	0.310	0.299	7075	Closed
Al-189-4-1	0.189	3.85	0.318	0.323	7075	Closed
Al-189-5-1	0.189	3.85	0.671	0.680	7075	Closed
Al-189-6-1	0.189	3.85	1.046	1.016	7075	Closed
Al-250-1	0.250	3.85	0.308	0.300	2024	Closed
Al-250-2	0.250	3.85	0.953	0.950	2024	Closed
Al-250-3	0.250	3.85	1.185	1.122	2024	Open
Al-250-4	0.250	3.85	0.305	0.305	7075	Closed
Al-250-5	0.250	3.85	0.947	0.934	7075	Closed
Al-250-6	0.250	3.85	0.315	0.293	7075	Closed
Al-375-1	0.375	3.85	0.328	0.336	2024	Closed
Al-375-2	0.375	3.85	1.081	0.977	2024	Closed
Al-375-3	0.375	3.85	0.261	0.245	2024	**Pin-Loaded**
Al-375-4	0.375	3.85	0.296	0.299	7075	Closed
Al-375-5	0.375	3.85	0.974	0.940	7075	Closed
Al-375-6	0.375	3.85	Fractured		7075	**Fractured**

Table B2. Complete Listing of All Flat Panel Steel Crack Specimens

Specimen Number	Nominal Thickness (in)	Nominal Width (in)	Left Crack Length (in)	Right Crack Length (in)	Material	Crack Opening
ST-050-1	0.050	3.85	0.299	0.302	304 SS	Closed
ST-050-2	0.050	3.85	0.946	0.803	304 SS	Closed
ST-050-3	0.050	3.85	0.896	0.917	304 SS	Open
ST-063-1	0.063	3.85	0.318	0.193	304 SS	Closed
ST-063-2	0.063	3.85	0.608	0.585	304 SS	Closed
ST-063-3	0.063	3.85	0.886	1.014	304 SS	Closed
ST-125-4	0.125	3.85	0.109	0.093	304 SS	Closed
ST-125-5	0.125	3.85	0.238	0.305	304 SS	Closed
ST-125-6	0.125	3.85	0.83	0.5819	304 SS	Closed
ST-250-1	0.250	3.85	0.30	0.3077	304 SS	Closed
ST-250-2	0.250	3.85	0.85	0.8830	304 SS	Open
ST-250-3	0.250	3.85	0.148	0.151	304 SS	Closed
ST-250-4	0.250	3.85	0.307	0.299	304 SS	Closed
ST-250-5	0.250	3.85	0.942	0.941	304 SS	Closed
ST-250-6	0.250	3.85	0.149	0.143	304 SS	Closed
ST-350-1	0.350	3.85	0.303	0.302	304 SS	Closed
ST-350-2	0.350	3.85	0.958	0.957	304 SS	Closed
ST-350-3	0.350	3.85	0.150	0.152	304 SS	Closed
ST-350-4	0.350	3.85	0.305	0.303	304 SS	Closed
ST-350-5	0.350	3.85	0.951	0.947	304 SS	Open
ST-350-6	0.350	3.85	0.151	0.150	304 SS	Closed

AL-040-1a

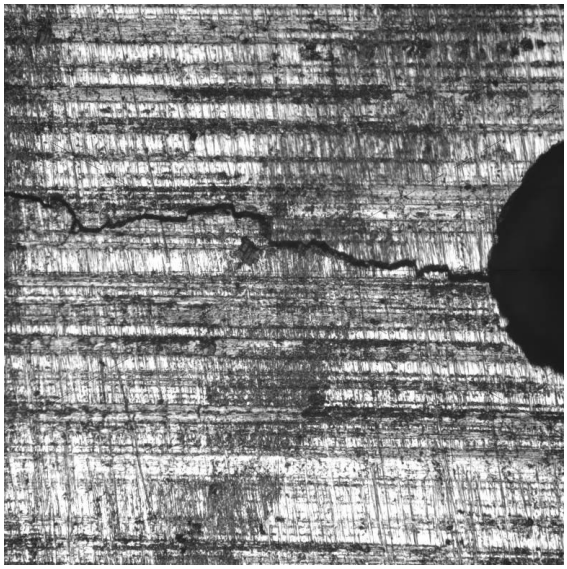

AL-040-1b

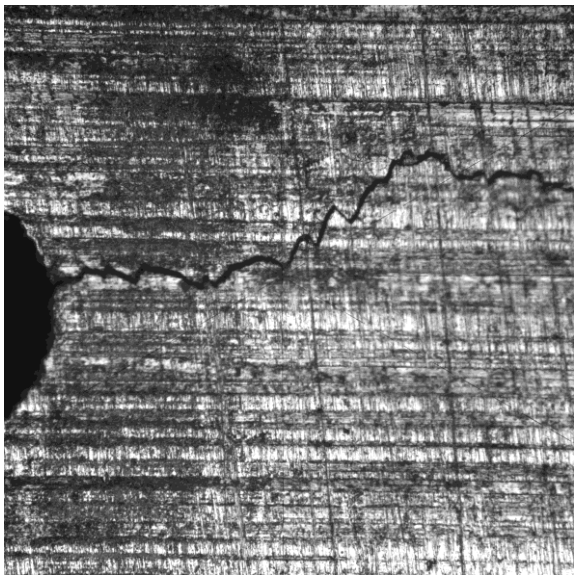

Specimen Number	Nominal Thickness (in)	Left Crack Length (in)	Right Crack Length (in)	Average Crack Opening (x1000 in)	Material
Al-040-1	0.040	0.320	0.318	0	2024

AL-040-2a

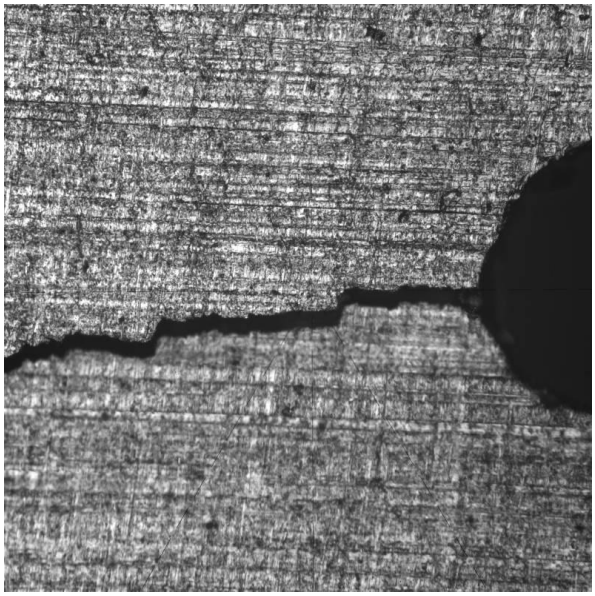

AL-040-2b

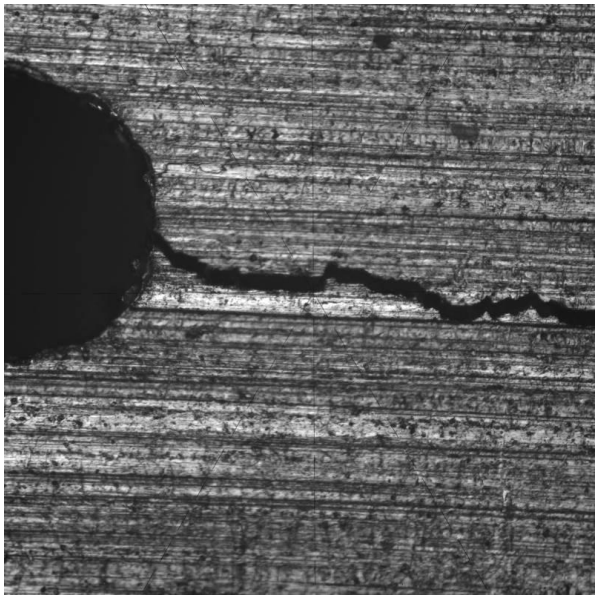

Specimen Number	Nominal Thickness (in)	Left Crack Length (in)	Right Crack Length (in)	Average Crack Opening (x1000 in)	Material
Al-040-2	0.040	1.028	0.940	1	2024

AL-040-3a

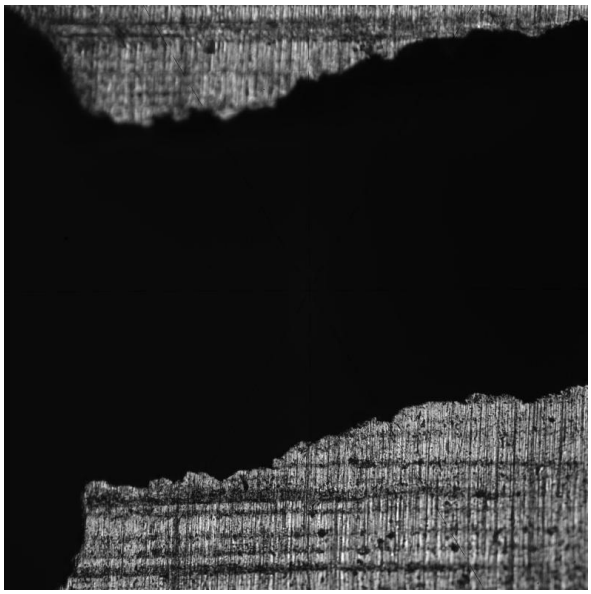

AL-040-3b

Specimen Number	Nominal Thickness (in)	Left Crack Length (in)	Right Crack Length (in)	Average Crack Opening (x1000 in)	Material
Al-040-3	0.040	1.121	1.123	30	2024

AL-050-1a

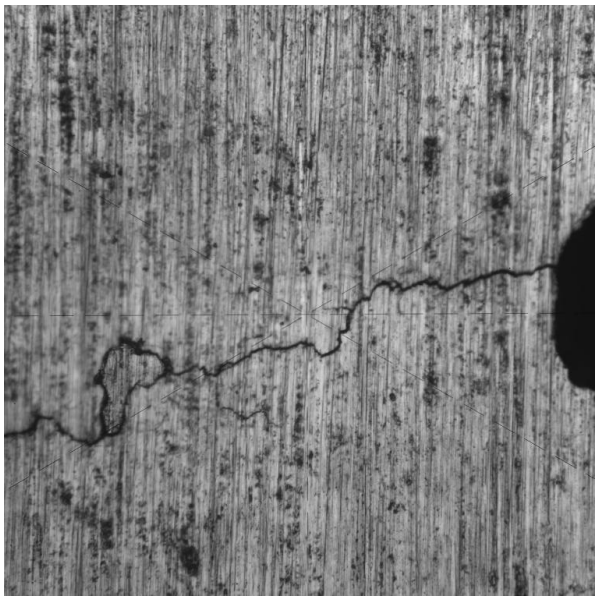

AL-050-1b

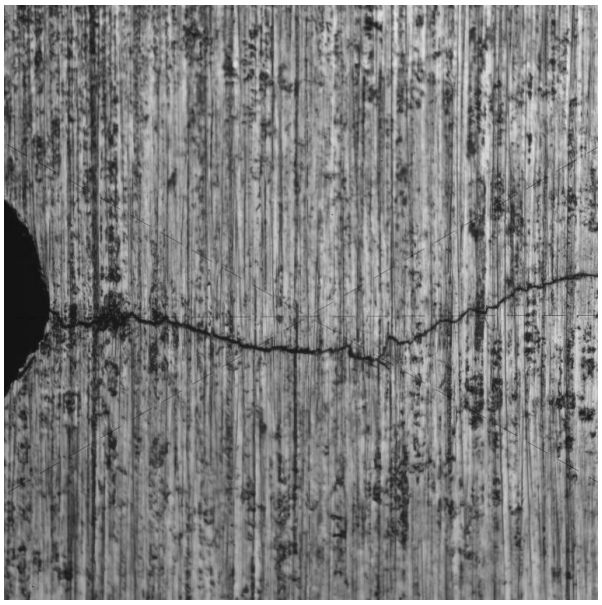

Specimen Number	Nominal Thickness (in)	Left Crack Length (in)	Right Crack Length (in)	Average Crack Opening (x1000 in)	Material
Al-050-1	0.050	0.308	0.312	0	7075

AL-050-2a

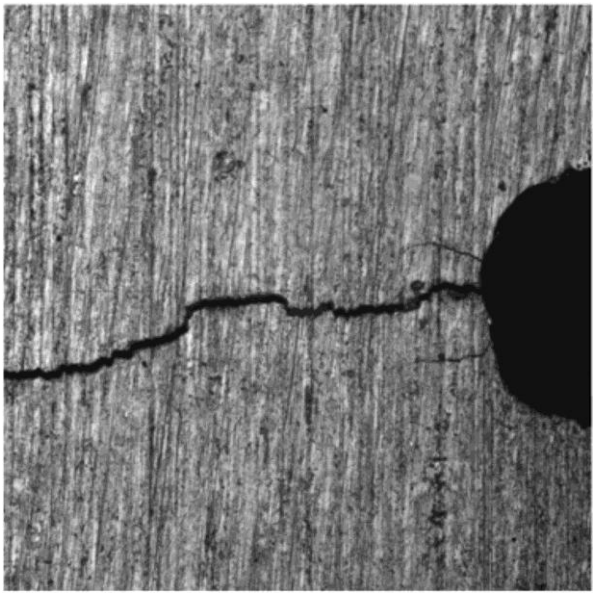

AL-050-2b

Specimen Number	Nominal Thickness (in)	Left Crack Length (in)	Right Crack Length (in)	Average Crack Opening (x1000 in)	Material
Al-050-2	0.050	0.987	0.926	0	7075

AL-050-3a (10x)

AL-050-3b (10x)

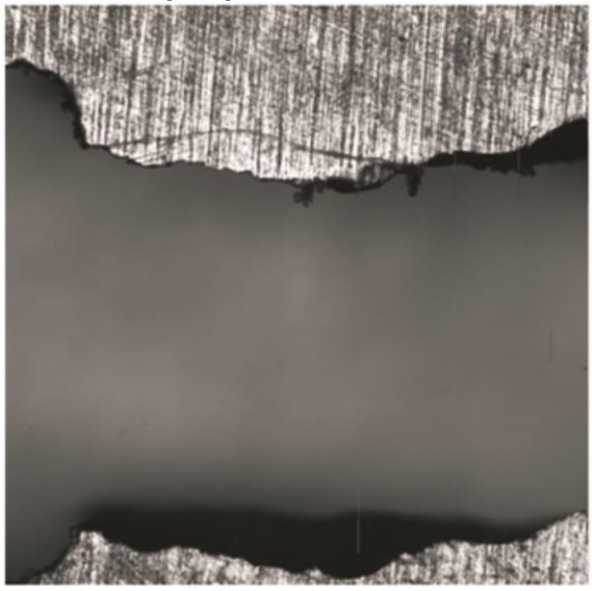

Specimen Number	Nominal Thickness (in)	Left Crack Length (in)	Right Crack Length (in)	Average Crack Opening (x1000 in)	Material
Al-050-3	0.050	1.270	1.880	34	7075

AL-050-4a

AL-050-4b

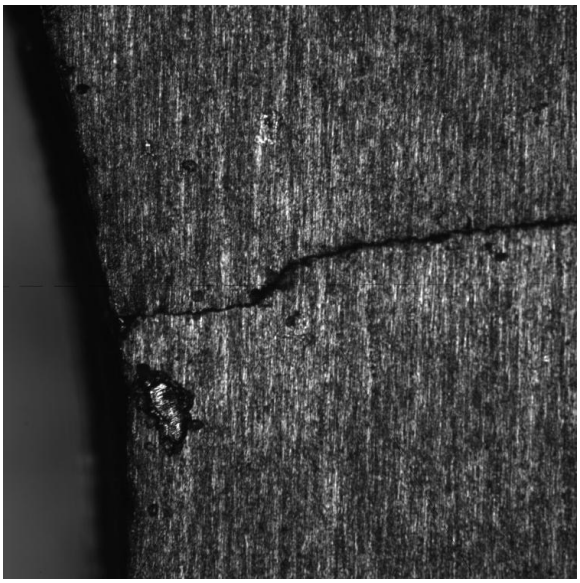

Specimen Number	Nominal Thickness (in)	Left Crack Length (in)	Right Crack Length (in)	Average Crack Opening (x1000 in)	Material
Al-050-4	0.050	0.522	0.492	0	7075

AL-050-5a

AL-050-5b

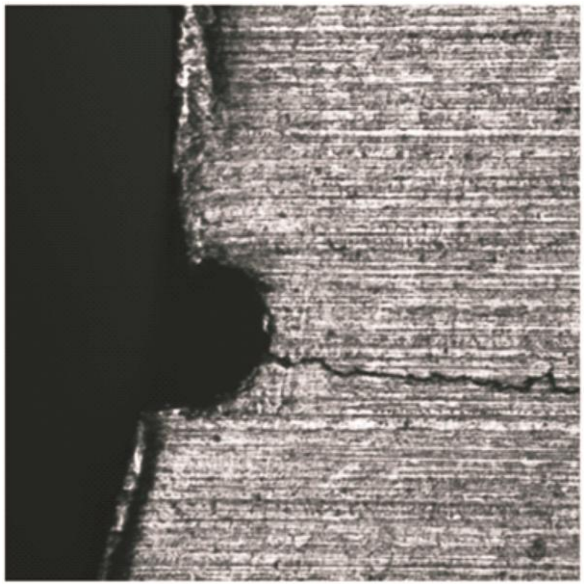

Specimen Number	Nominal Thickness (in)	Left Crack Length (in)	Right Crack Length (in)	Average Crack Opening (x1000 in)	Material
Al-050-5	0.050	0.621	0.609	1	7075

AL-063-1a

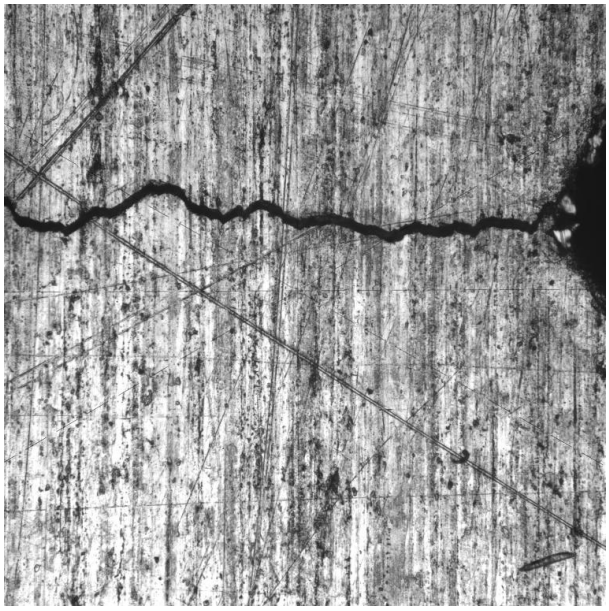

AL-063-1b

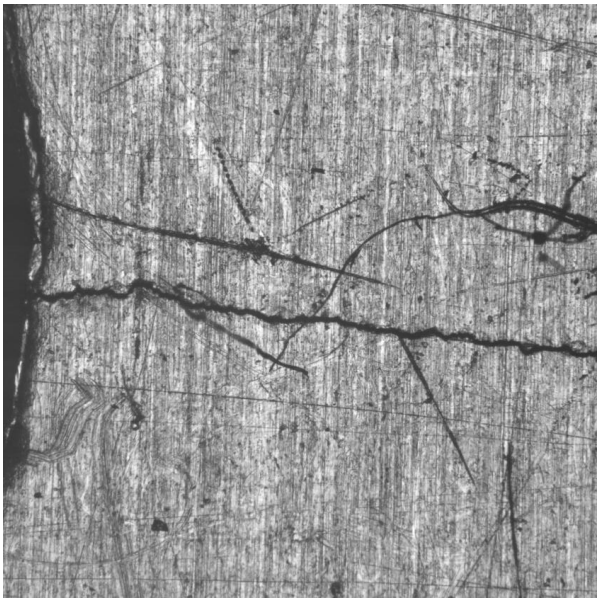

Specimen Number	Nominal Thickness (in)	Left Crack Length (in)	Right Crack Length (in)	Average Crack Opening (x1000 in)	Material
Al-063-1	0.063	0.65	0.720	1	2024

AL-063-2a

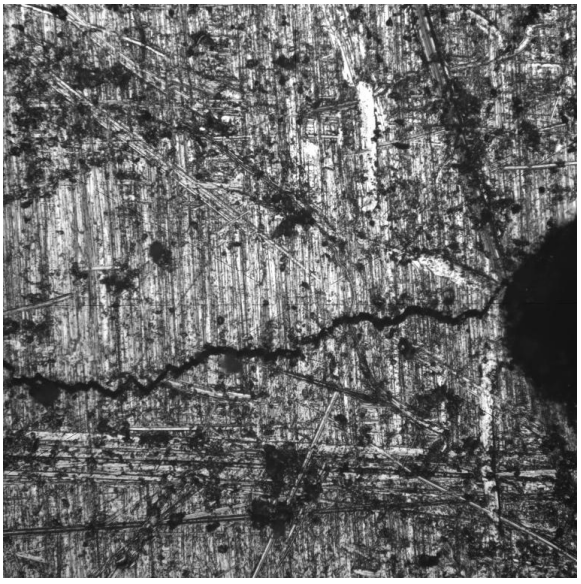

AL-063-2b

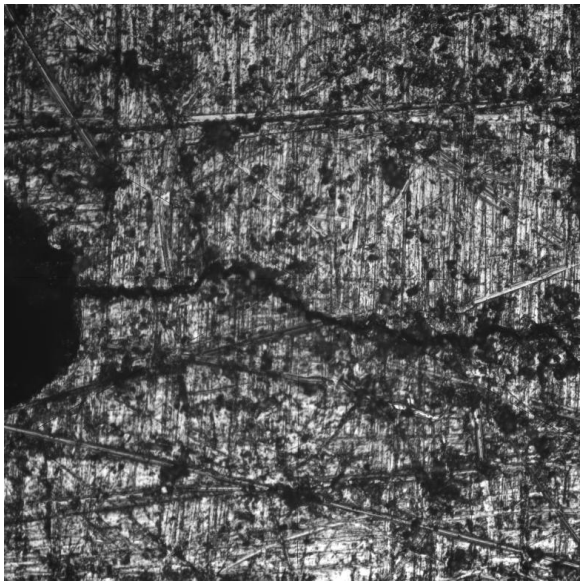

Specimen Number	Nominal Thickness (in)	Left Crack Length (in)	Right Crack Length (in)	Average Crack Opening (x1000 in)	Material
Al-063-2	0.063	0.49	0.470	1	2024

AL-063-3a

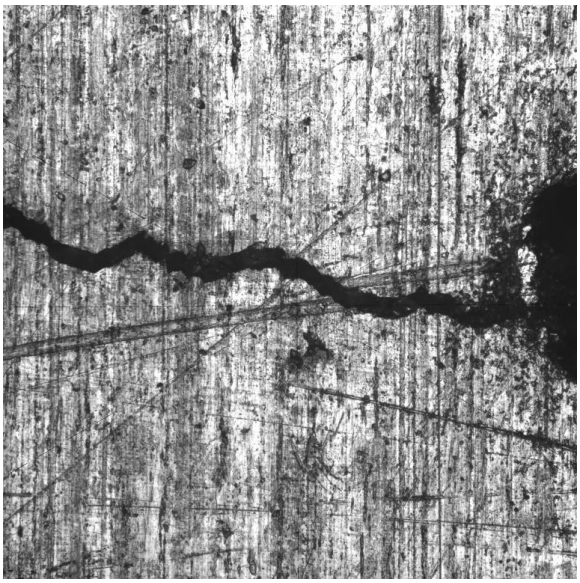

AL-063-3b

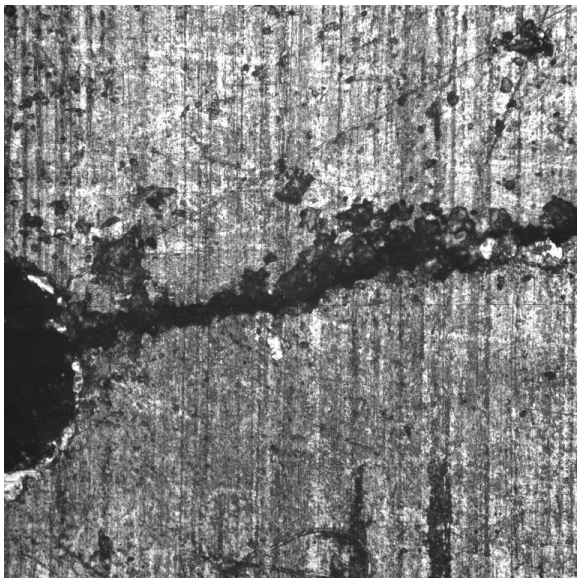

Specimen Number	Nominal Thickness (in)	Left Crack Length (in)	Right Crack Length (in)	Average Crack Opening (x1000 in)	Material
Al-063-3	0.063	0.78	0.730	1	2024

AL-100-1a

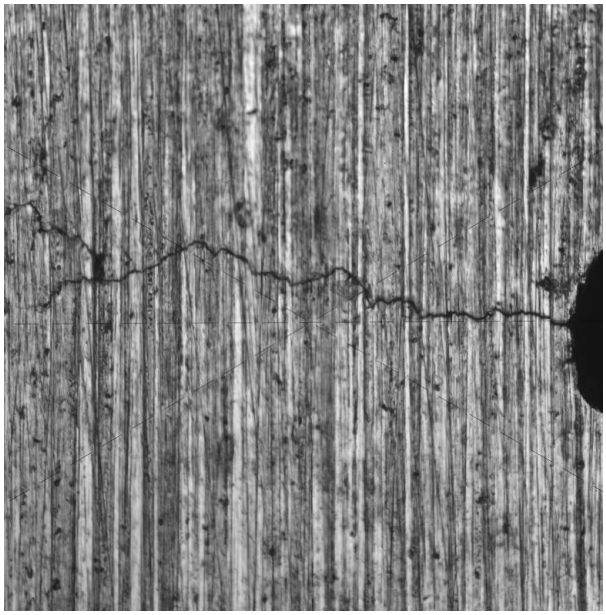

AL-100-1b

Specimen Number	Nominal Thickness (in)	Left Crack Length (in)	Right Crack Length (in)	Average Crack Opening (x1000 in)	Material
Al-100-1	0.100	0.320	0.300	1	2024

AL-100-2a

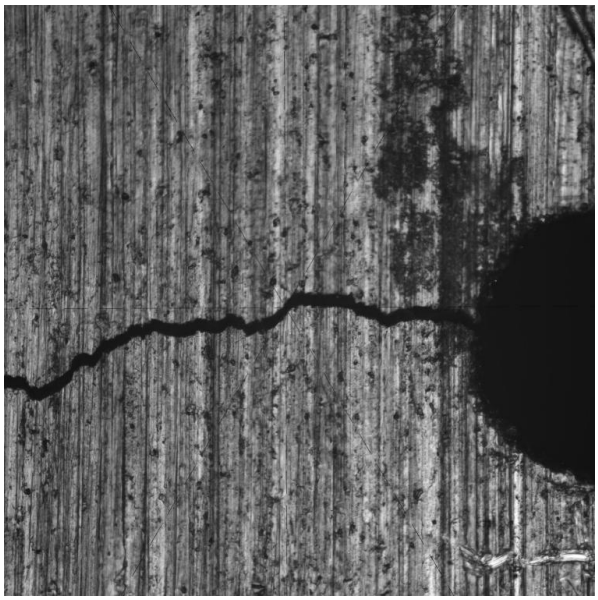

AL-100-2b

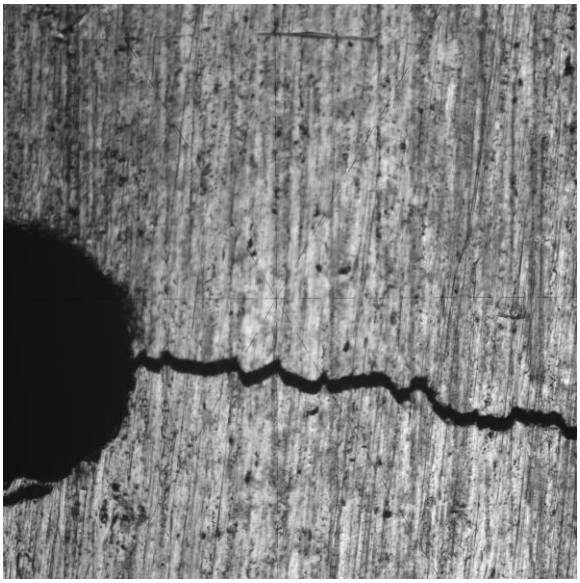

Specimen Number	Nominal Thickness (in)	Left Crack Length (in)	Right Crack Length (in)	Average Crack Opening (x1000 in)	Material
Al-100-2	0.100	0.969	0.932	1	2024

AL-100-3a

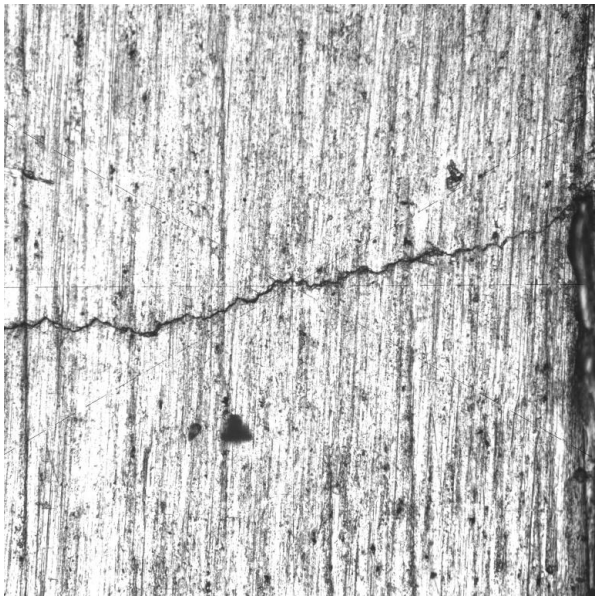

AL-100-3b

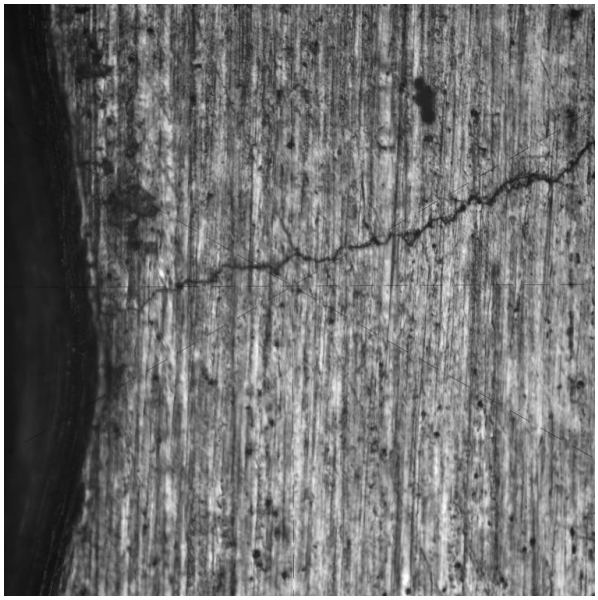

Specimen Number	Nominal Thickness (in)	Left Crack Length (in)	Right Crack Length (in)	Average Crack Opening (x1000 in)	Material
Al-100-3	0.100	0.234	0.222	1	2024

AL-100-4a

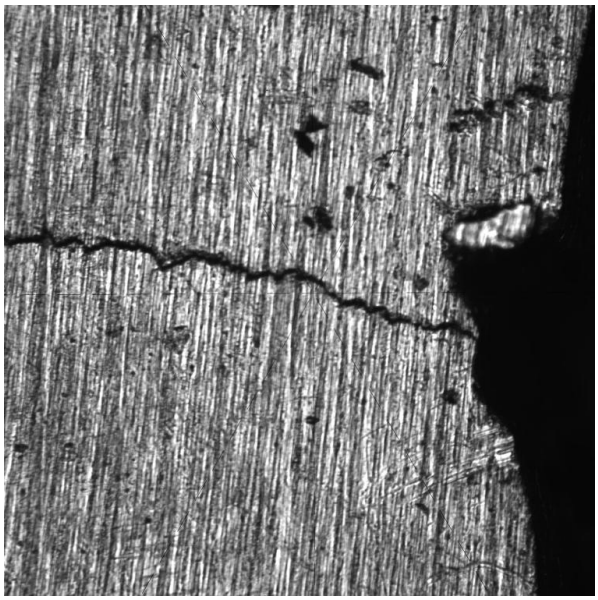

AL-100-4b

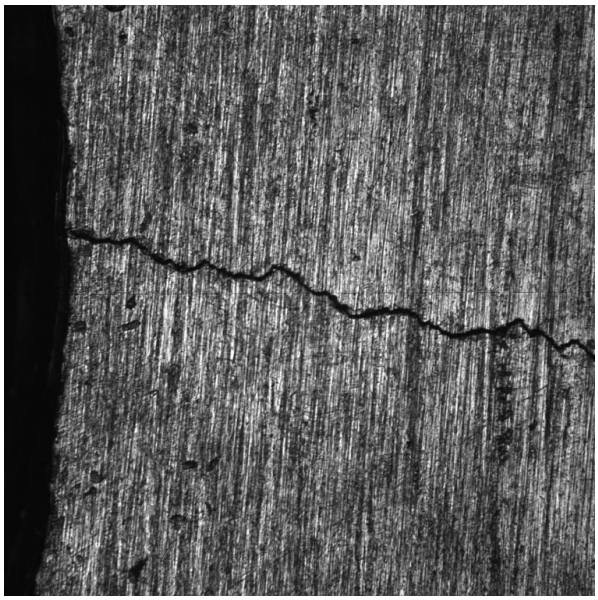

Specimen Number	Nominal Thickness (in)	Left Crack Length (in)	Right Crack Length (in)	Average Crack Opening (x1000 in)	Material
Al-100-4	0.100	0.573	0.542	0	2024

AL-100-5a

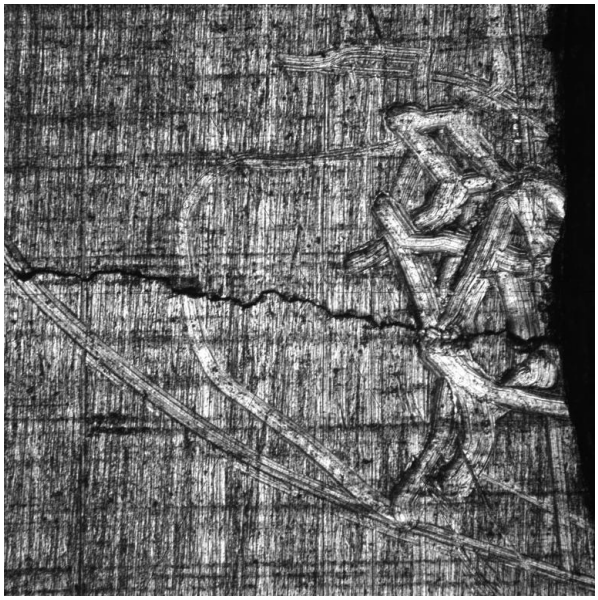

AL-100-5b

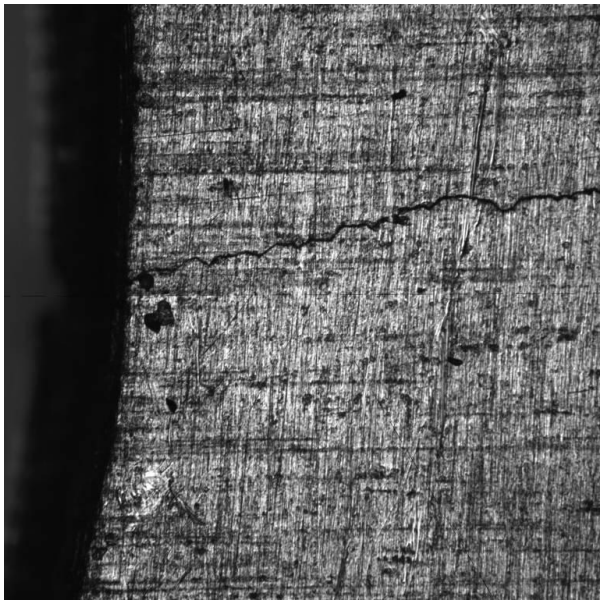

Specimen Number	Nominal Thickness (in)	Left Crack Length (in)	Right Crack Length (in)	Average Crack Opening (x1000 in)	Material
Al-100-5	0.100	0.524	0.507	0	2024

AL-125-1a

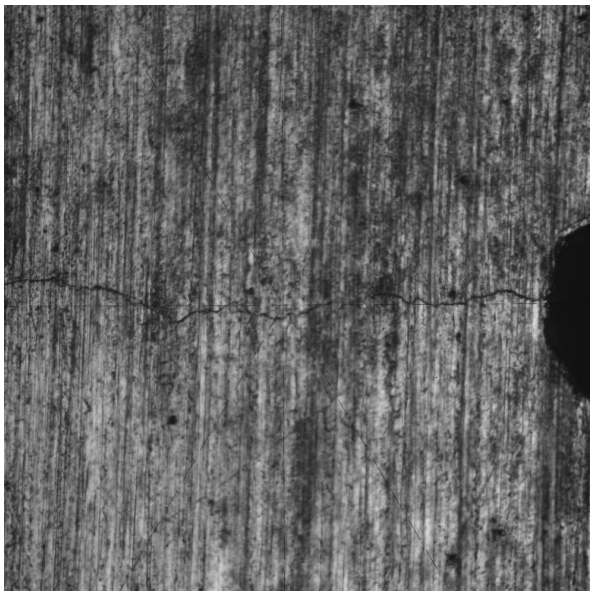

AL-125-1b

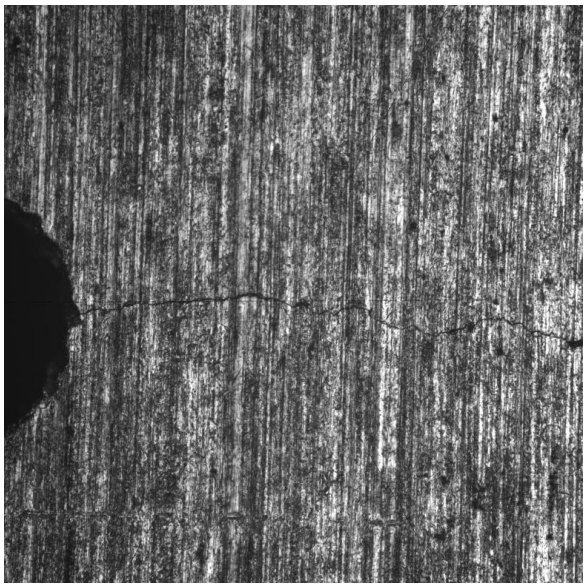

Specimen Number	Nominal Thickness (in)	Left Crack Length (in)	Right Crack Length (in)	Average Crack Opening (x1000 in)	Material
Al-125-1	0.125	0.309	0.298	0	7075

AL-125-2a

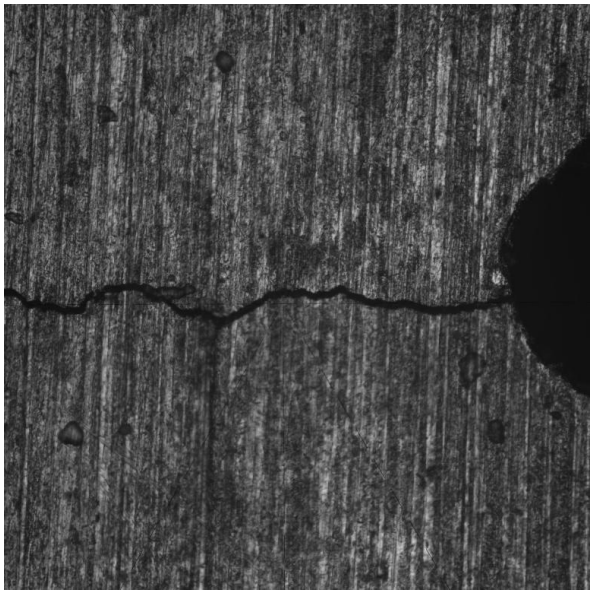

AL-125-2b

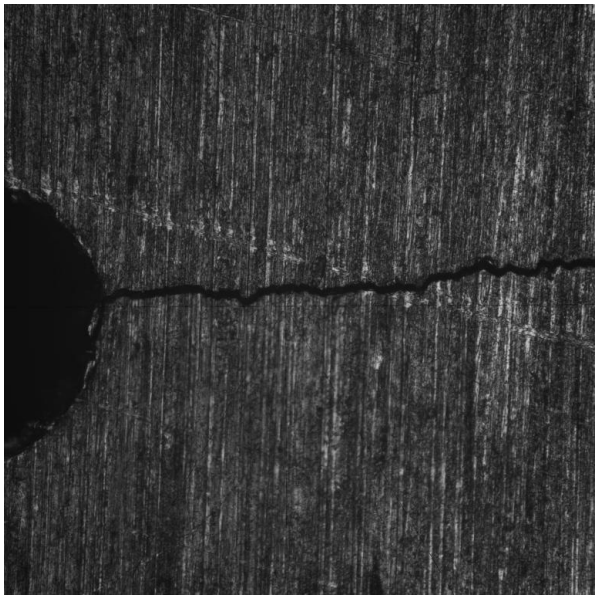

Specimen Number	Nominal Thickness (in)	Left Crack Length (in)	Right Crack Length (in)	Average Crack Opening (x1000 in)	Material
Al-125-2	0.125	0.968	0.945	0	7075

AL-125-4a

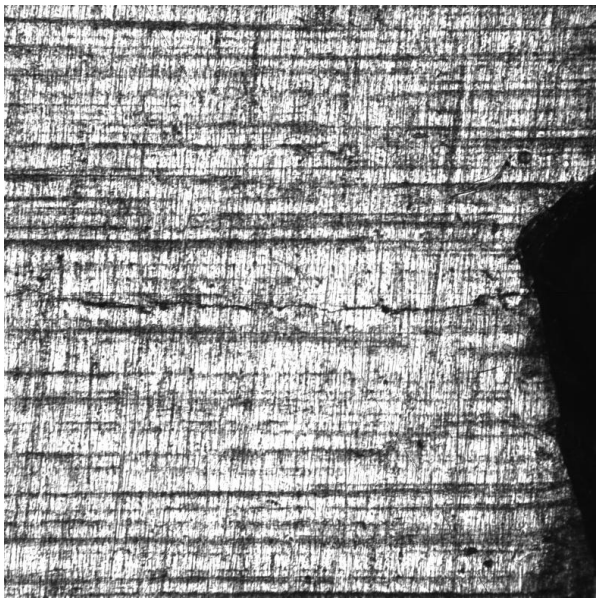

AL-125-4b

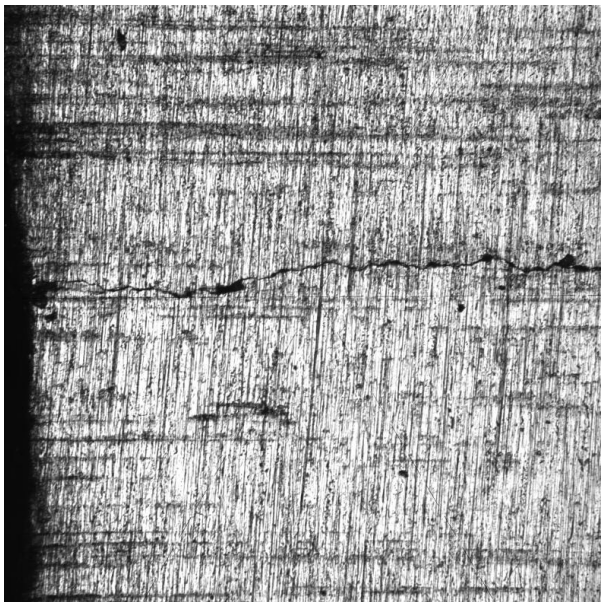

Specimen Number	Nominal Thickness (in)	Left Crack Length (in)	Right Crack Length (in)	Average Crack Opening (x1000 in)	Material
Al-125-4	0.125	0.532	0.514	0	7075

AL-125-5a

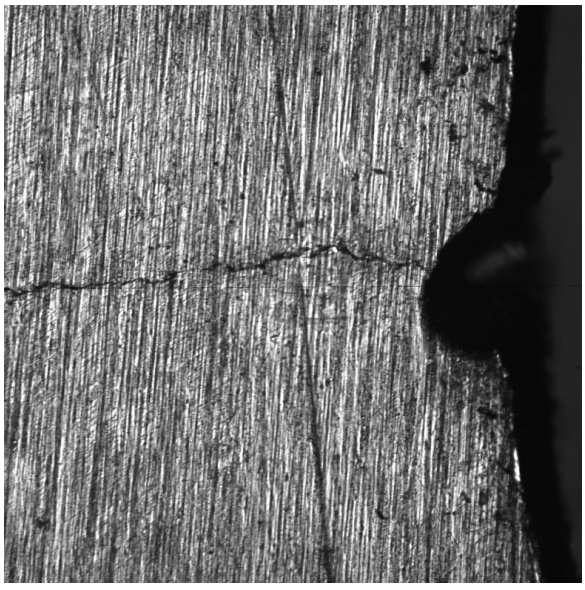

AL-125-5b

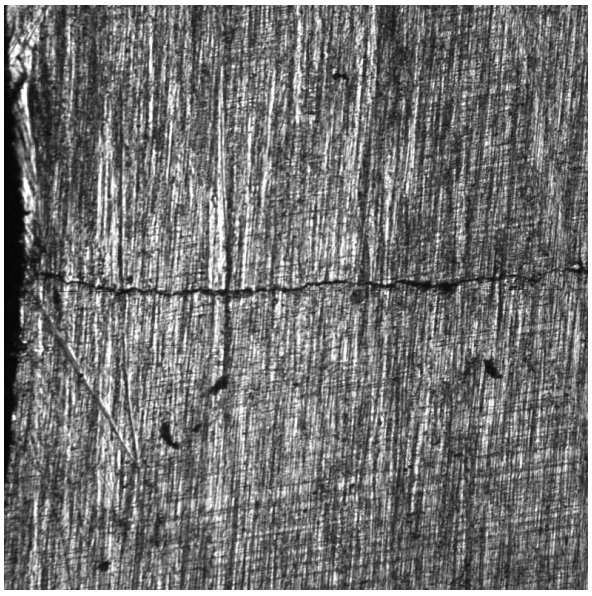

Specimen Number	Nominal Thickness (in)	Left Crack Length (in)	Right Crack Length (in)	Average Crack Opening (x1000 in)	Material
Al-125-5	0.125	0.554	0.550	0	7075

AL-125-1-1a

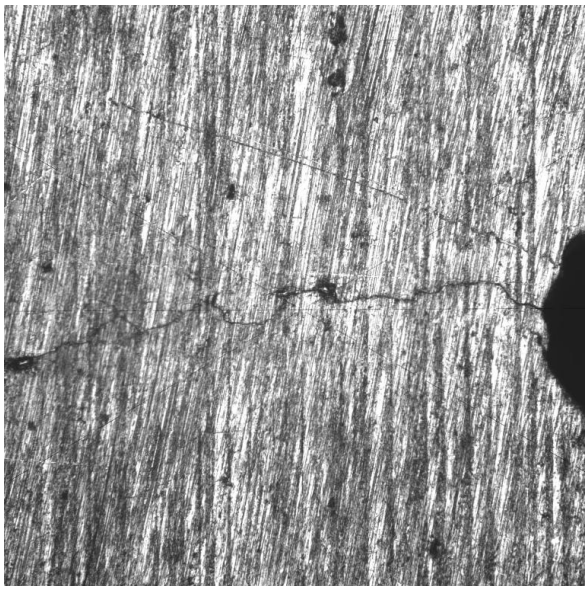

AL-125-1-1b

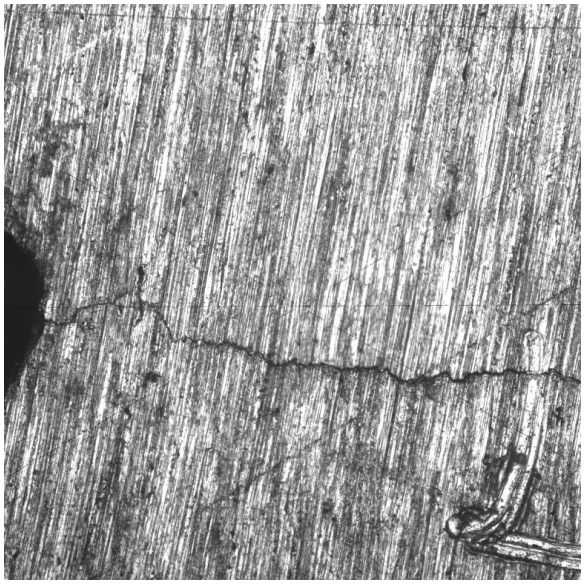

Specimen Number	Nominal Thickness (in)	Left Crack Length (in)	Right Crack Length (in)	Average Crack Opening (x1000 in)	Material
Al-125-1-1	0.125	0.320	0.320	0	7075

AL-125-2-1a

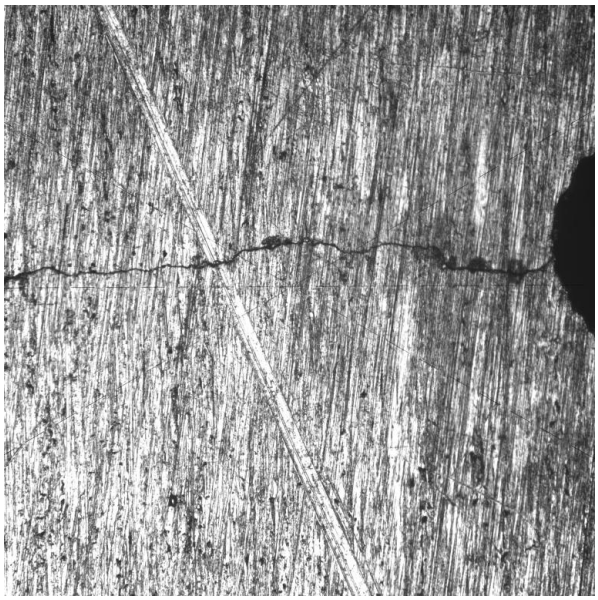

AL-125-2-1b

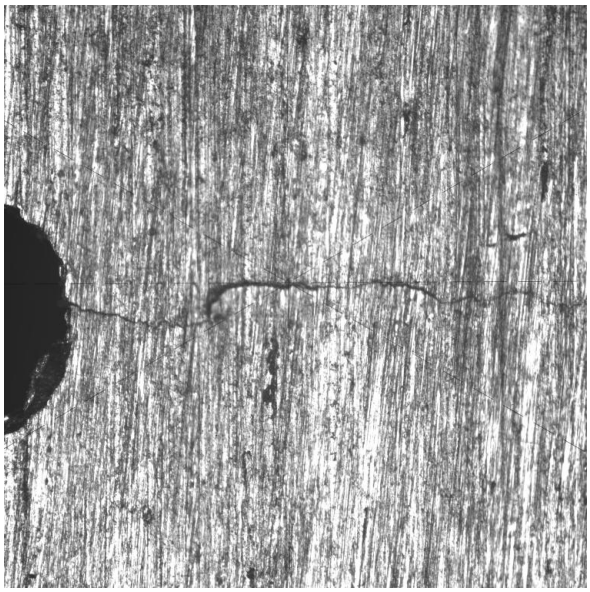

Specimen Number	Nominal Thickness (in)	Left Crack Length (in)	Right Crack Length (in)	Average Crack Opening (x1000 in)	Material
Al-125-2-1	0.125	0.670	0.750	0	7075

AL-125-3-1a

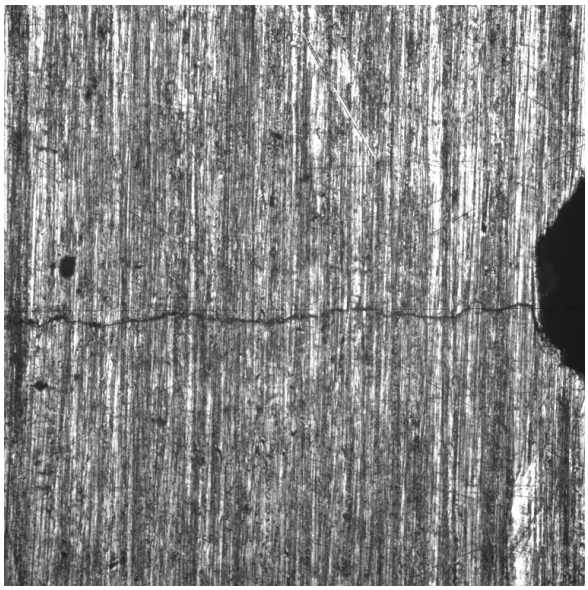

AL-125-3-1b

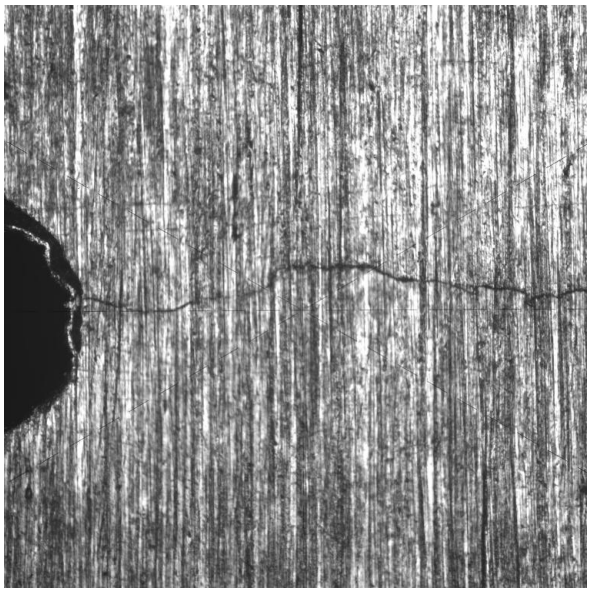

Specimen Number	Nominal Thickness (in)	Left Crack Length (in)	Right Crack Length (in)	Average Crack Opening (x1000 in)	Material
Al-125-3-1	0.125	1.090	0.950	0	7075

AL-189-1a

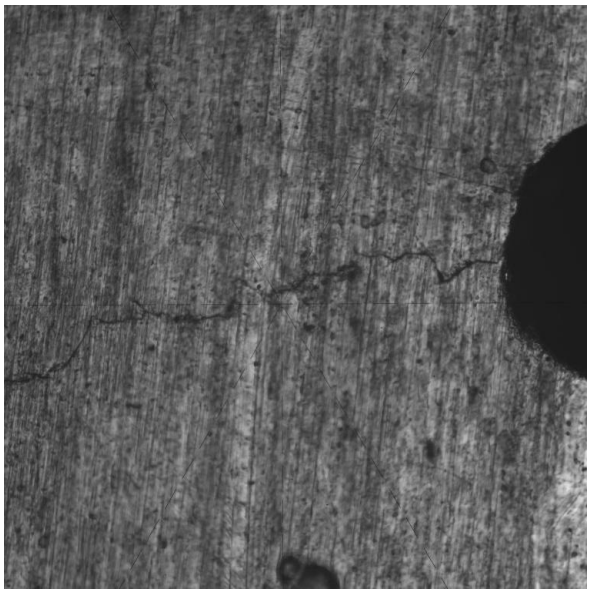

AL-189-1b

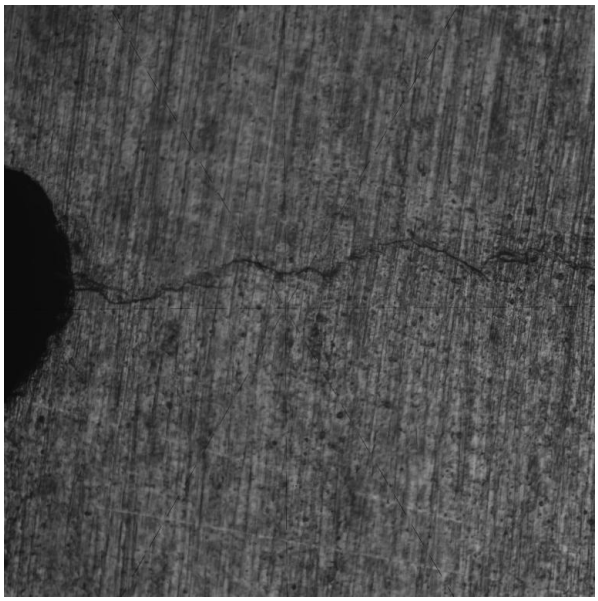

Specimen Number	Nominal Thickness (in)	Left Crack Length (in)	Right Crack Length (in)	Average Crack Opening (x1000 in)	Material
Al-189-1	0.189	0.293	0.308	0	2024

AL-189-2a

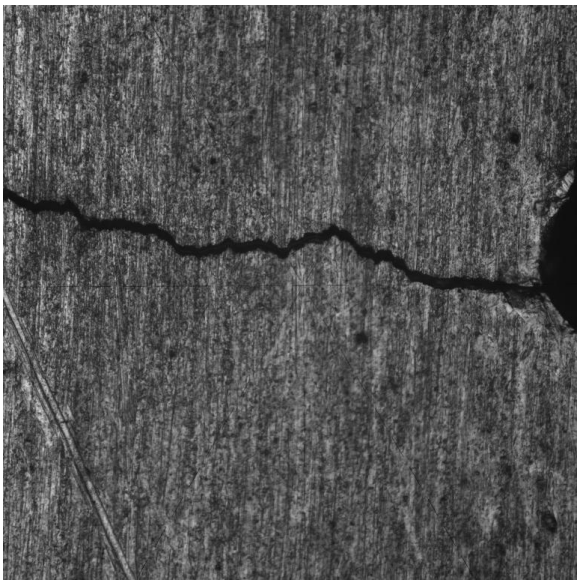

AL-189-2b

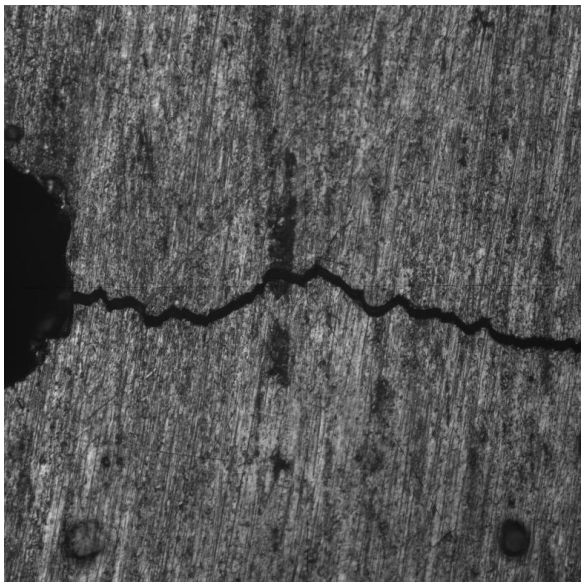

Specimen Number	Nominal Thickness (in)	Left Crack Length (in)	Right Crack Length (in)	Average Crack Opening (x1000 in)	Material
Al-189-2	0.189	1.009	0.899	1	2024

AL-189-3a

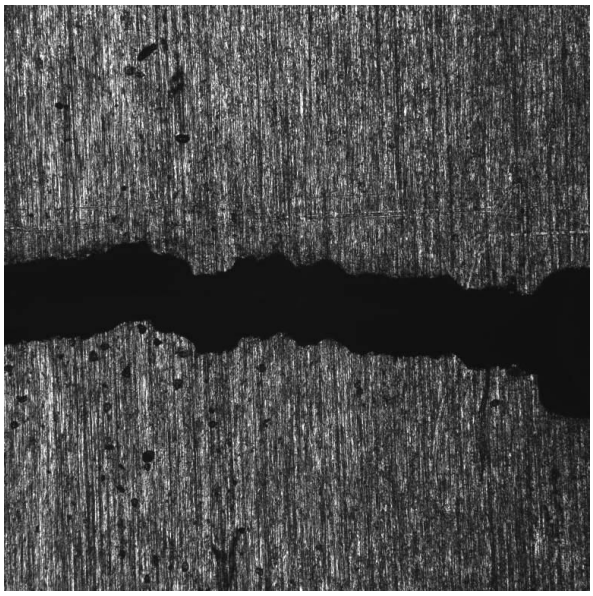

AL-189-3b

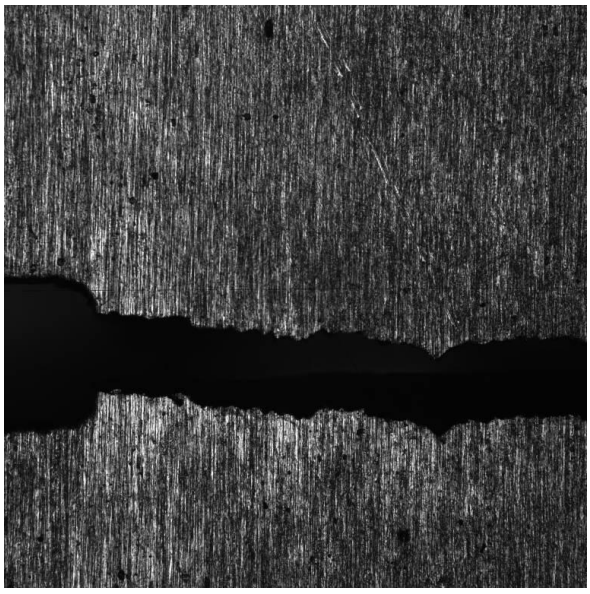

Specimen Number	Nominal Thickness (in)	Left Crack Length (in)	Right Crack Length (in)	Average Crack Opening (x1000 in)	Material
Al-189-3	0.189	1.063	1.017	13	2024

AL-189-4a

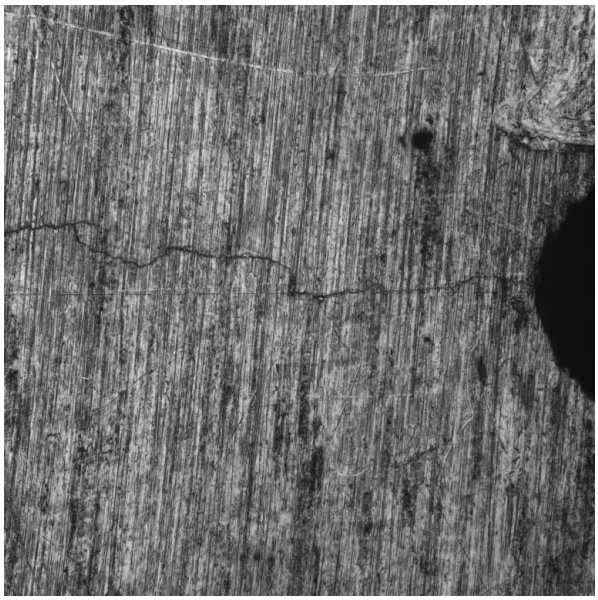

AL-189-4b

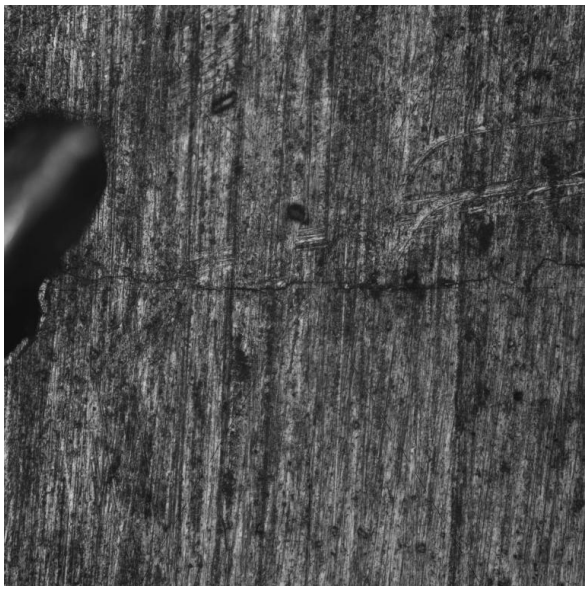

Specimen Number	Nominal Thickness (in)	Left Crack Length (in)	Right Crack Length (in)	Average Crack Opening (x1000 in)	Material
Al-189-4	0.189	0.308	0.301	0	7075

AL-189-5a

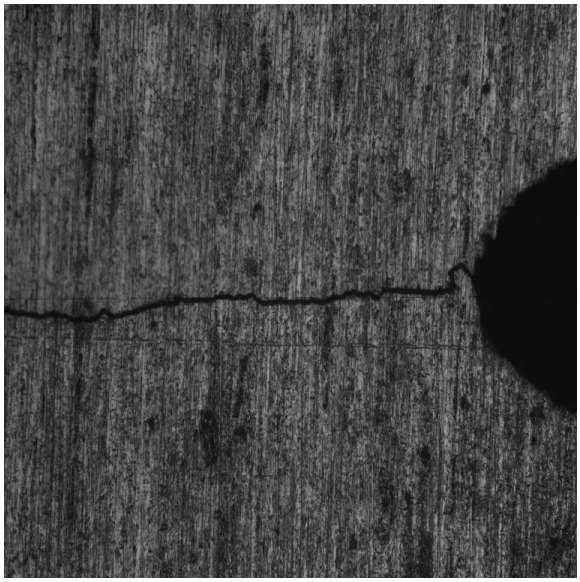

AL-189-5b

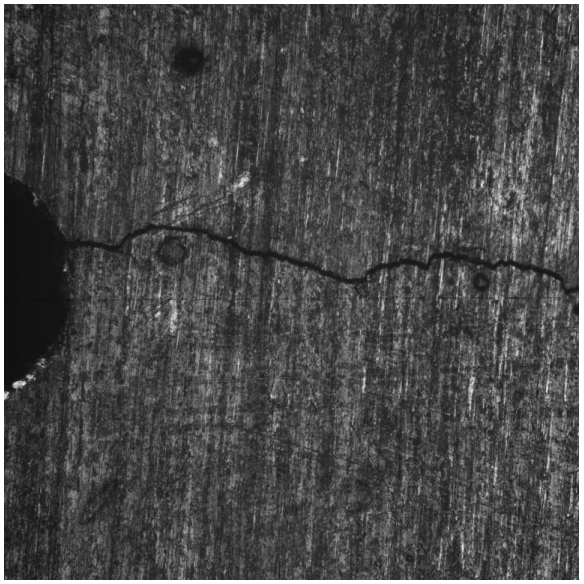

Specimen Number	Nominal Thickness (in)	Left Crack Length (in)	Right Crack Length (in)	Average Crack Opening (x1000 in)	Material
Al-189-5	0.189	0.974	0.958	0	7075

AL-189-6a

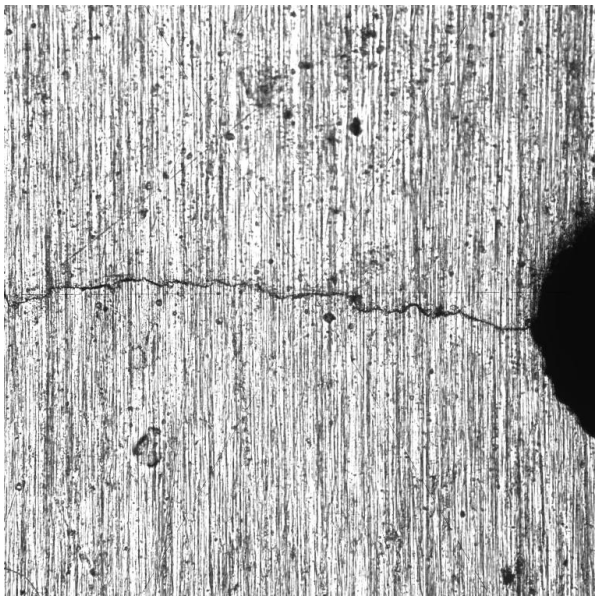

AL-189-6b

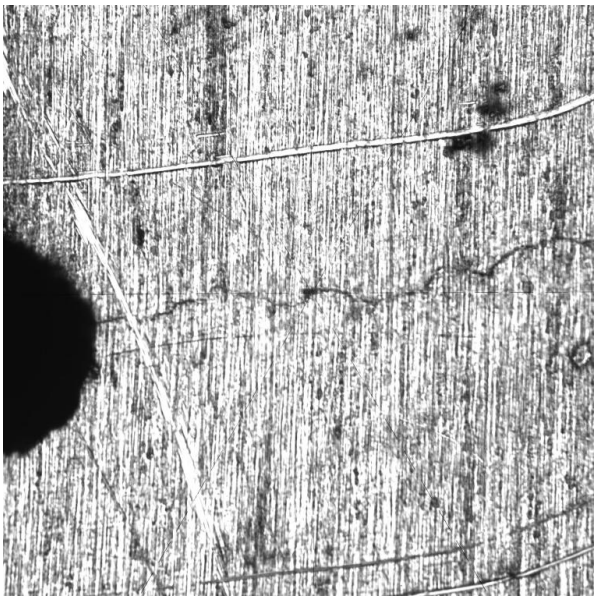

Specimen Number	Nominal Thickness (in)	Left Crack Length (in)	Right Crack Length (in)	Average Crack Opening (x1000 in)	Material
Al-189-6	0.189	0.299	0.307	0	7075

AL-189-4a-1

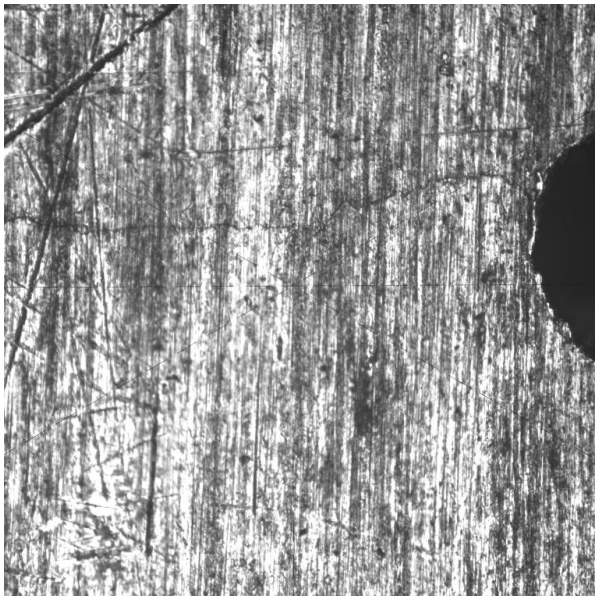

AL-189-4b-1

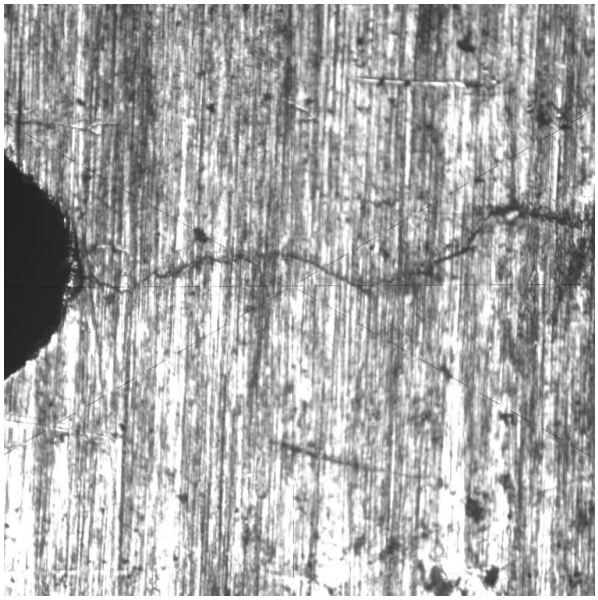

Specimen Number	Nominal Thickness (in)	Left Crack Length (in)	Right Crack Length (in)	Average Crack Opening (x1000 in)	Material
Al-189-4-1	0.189	0.318	0.323	0	7075

AL-189-5a-1

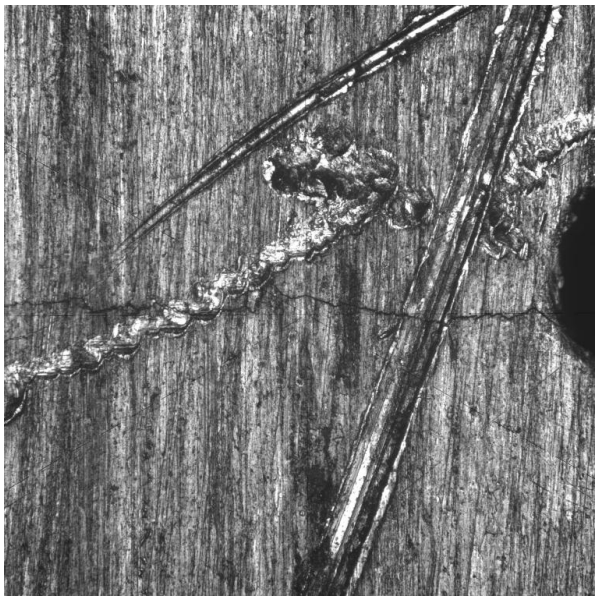

AL-189-5b-1

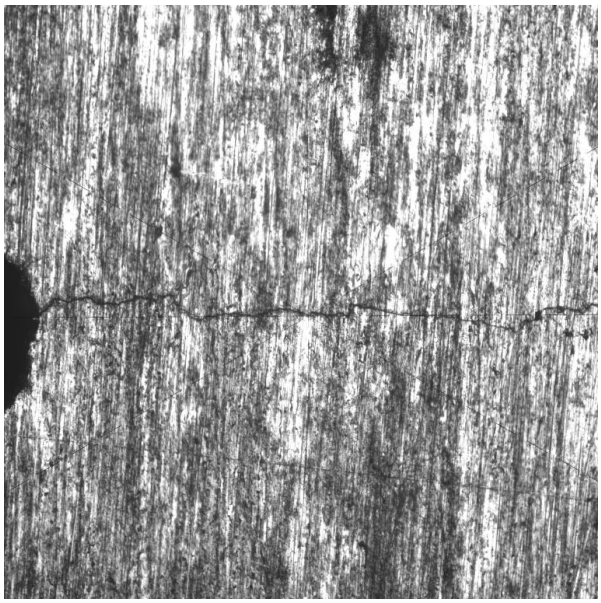

Specimen Number	Nominal Thickness (in)	Left Crack Length (in)	Right Crack Length (in)	Average Crack Opening (x1000 in)	Material
Al-189-5-1	0.189	0.671	0.680	0	7075

AL-189-6a-1

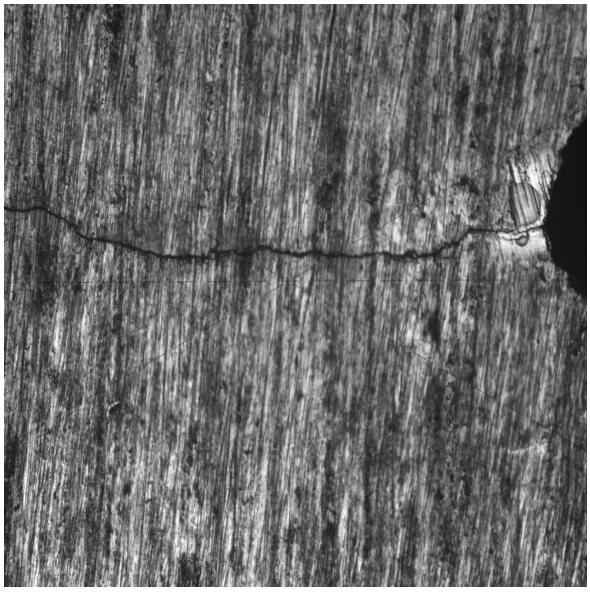

AL-189-6b-1

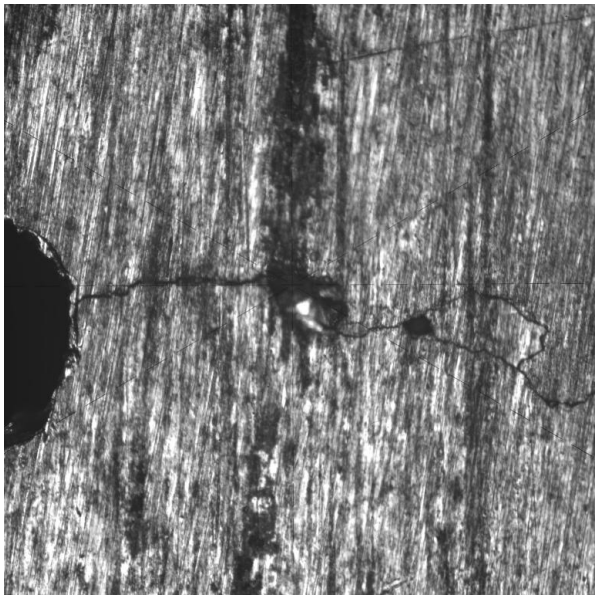

Specimen Number	Nominal Thickness (in)	Left Crack Length (in)	Right Crack Length (in)	Average Crack Opening (x1000 in)	Material
Al-189-6-1	0.189	1.046	1.016	0	7075

AL-189-1a

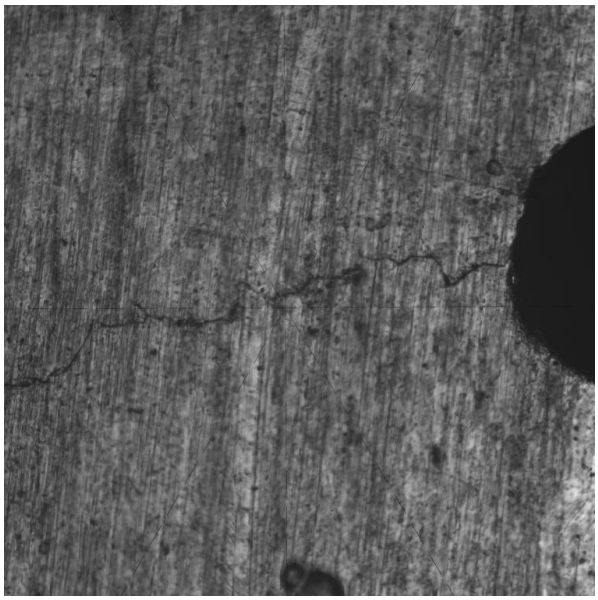

AL-189-1b

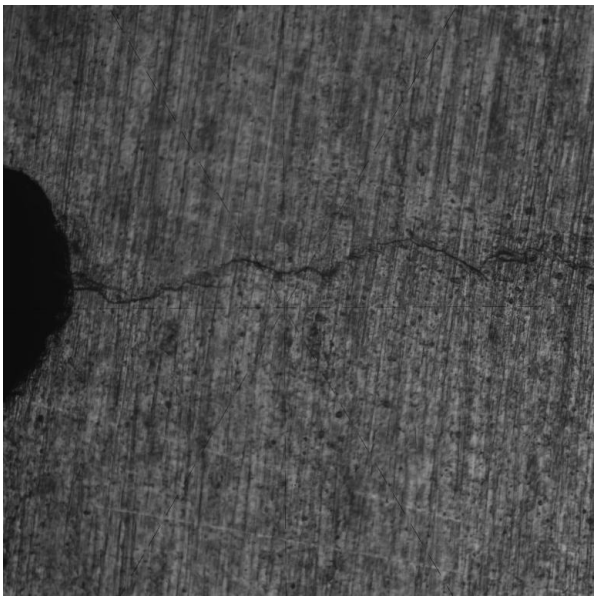

Specimen Number	Nominal Thickness (in)	Left Crack Length (in)	Right Crack Length (in)	Average Crack Opening (x1000 in)	Material
Al-189-1	0.189	0.293	0.308	0	2024

AL-189-2a

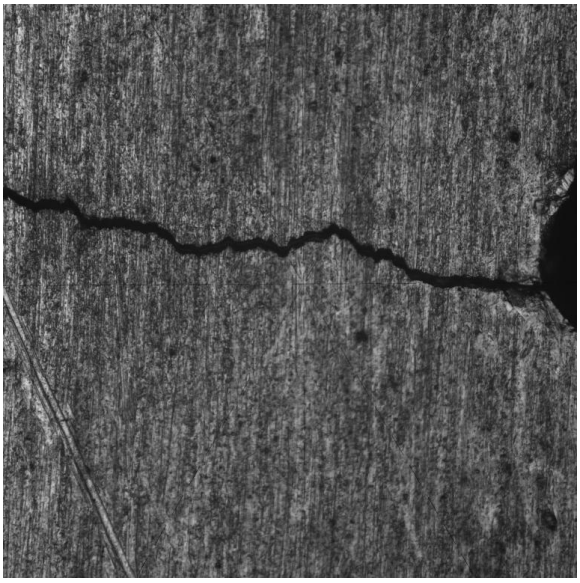

AL-189-2b

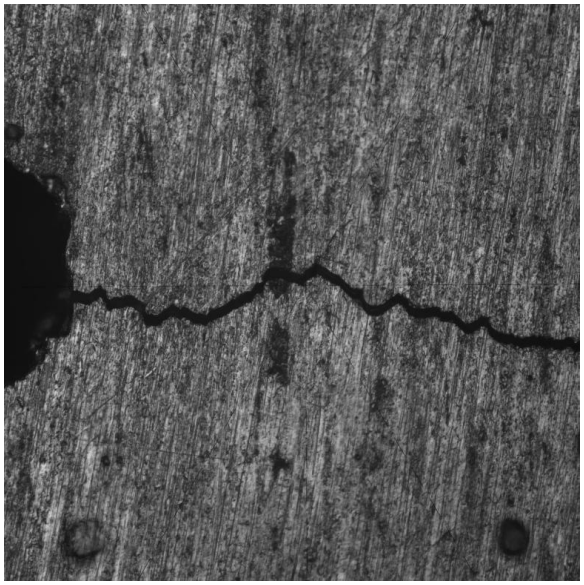

Specimen Number	Nominal Thickness (in)	Left Crack Length (in)	Right Crack Length (in)	Average Crack Opening (x1000 in)	Material
Al-189-2	0.189	1.009	0.899	1	2024

AL-189-3a

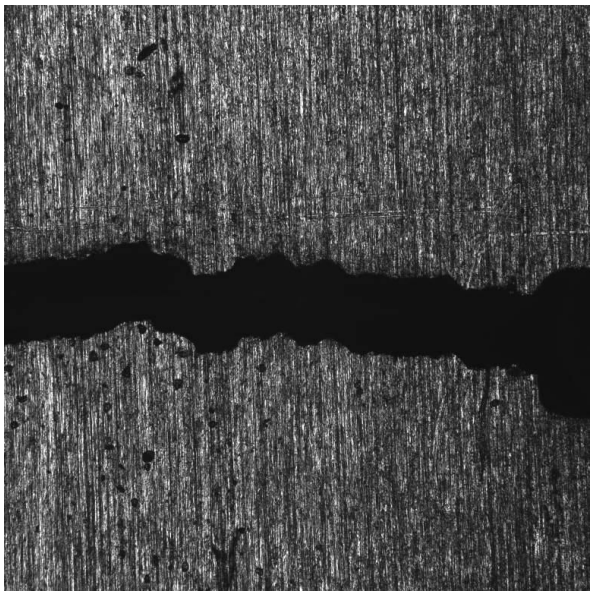

AL-189-3b

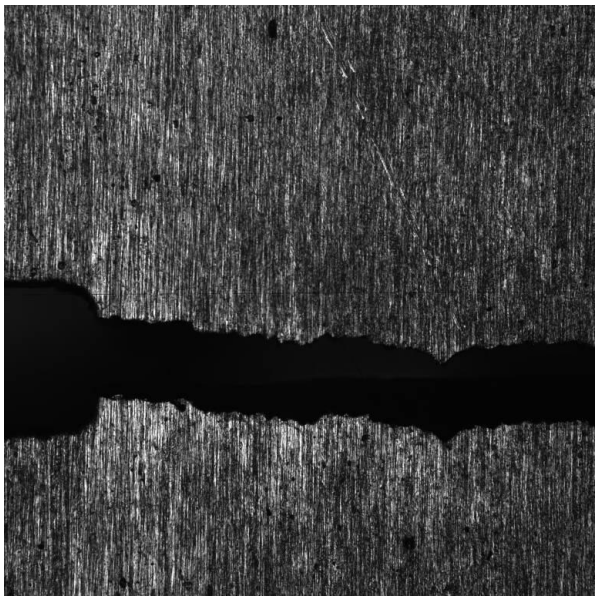

Specimen Number	Nominal Thickness (in)	Left Crack Length (in)	Right Crack Length (in)	Average Crack Opening (x1000 in)	Material
Al-189-3	0.189	1.063	1.017	13	2024

AL-189-4a

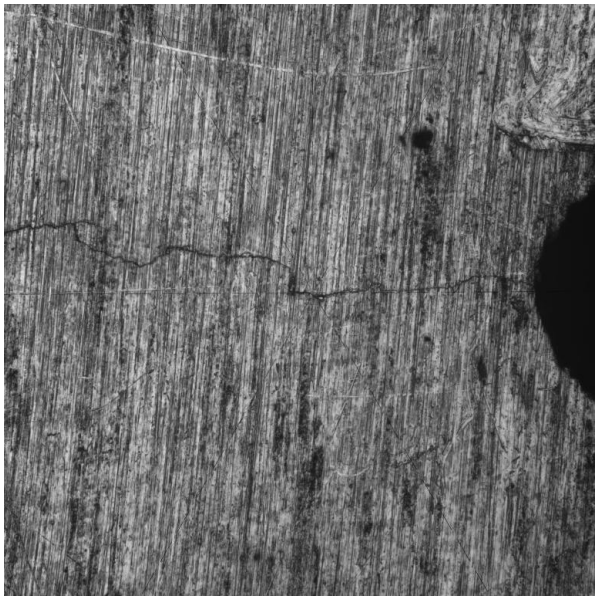

AL-189-4b

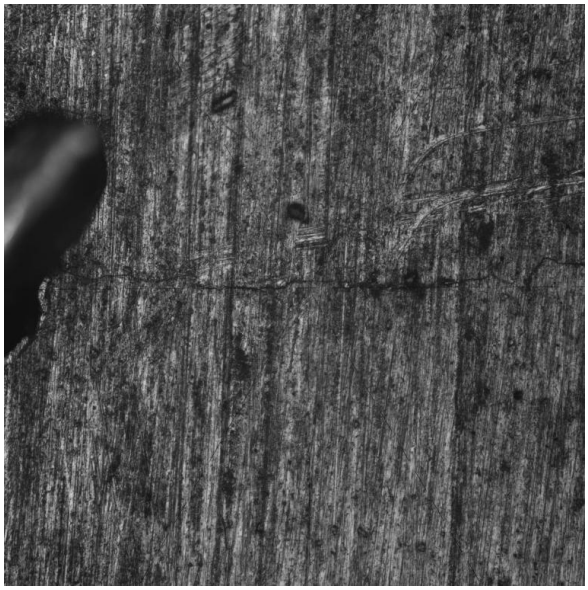

Specimen Number	Nominal Thickness (in)	Left Crack Length (in)	Right Crack Length (in)	Average Crack Opening (x1000 in)	Material
Al-189-4	0.189	0.308	0.301	0	7075

AL-189-5a

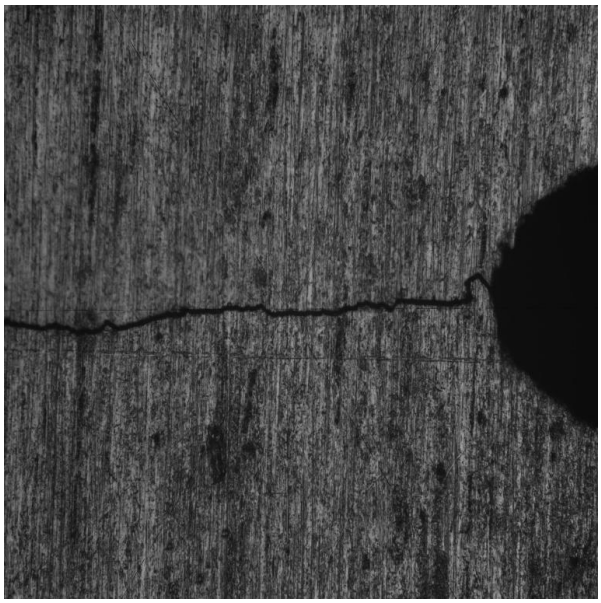

AL-189-5b

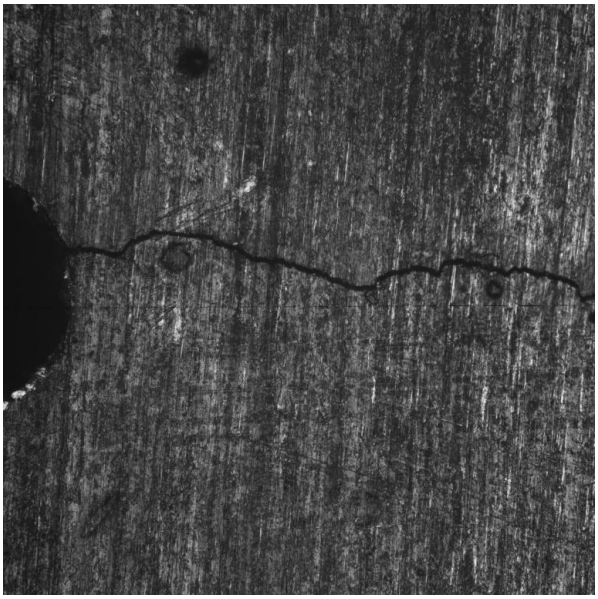

Specimen Number	Nominal Thickness (in)	Left Crack Length (in)	Right Crack Length (in)	Average Crack Opening (x1000 in)	Material
Al-189-5	0.189	0.974	0.958	0	7075

AL-189-6a

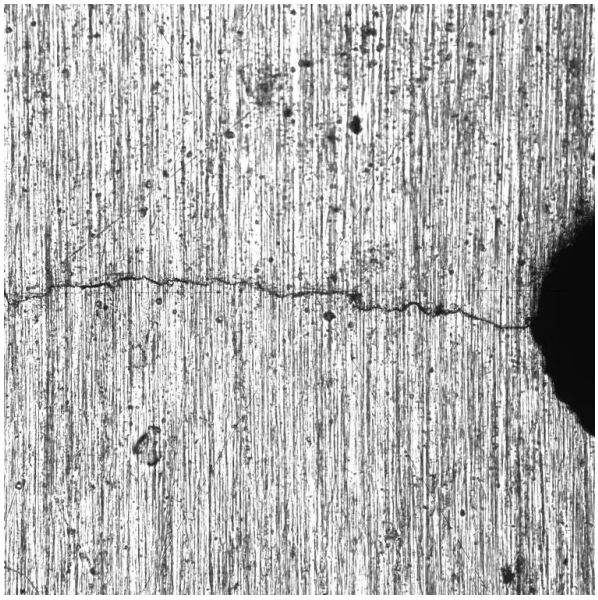

AL-189-6b

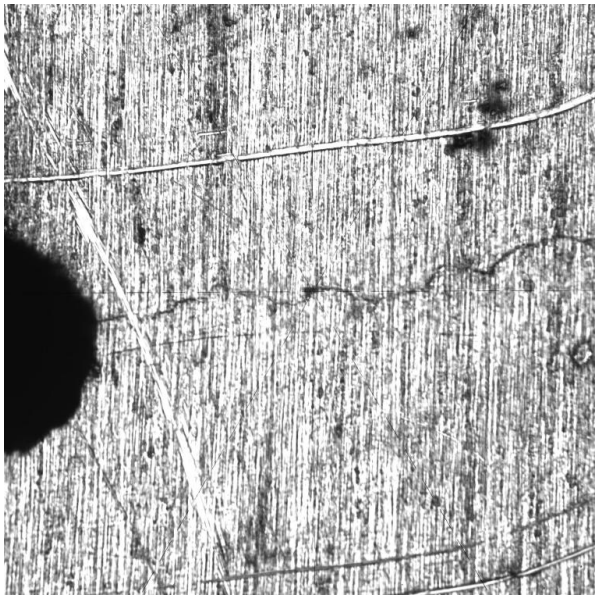

Specimen Number	Nominal Thickness (in)	Left Crack Length (in)	Right Crack Length (in)	Average Crack Opening (x1000 in)	Material
Al-189-6	0.189	0.299	0.307	0	7075

AL-189-4a-1

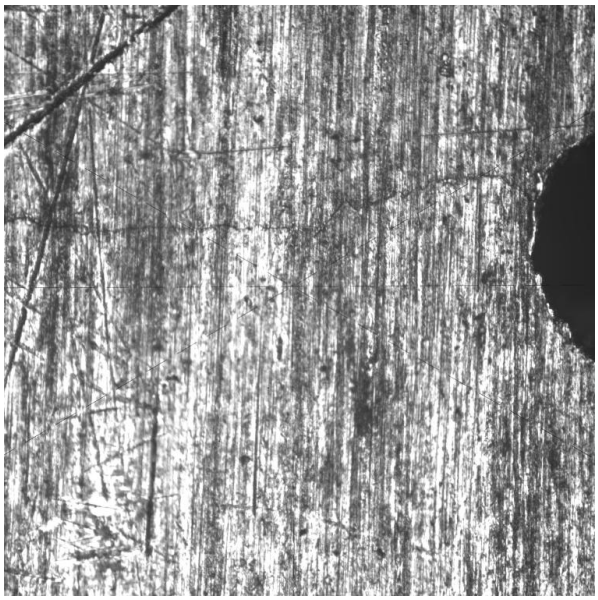

AL-189-4b-1

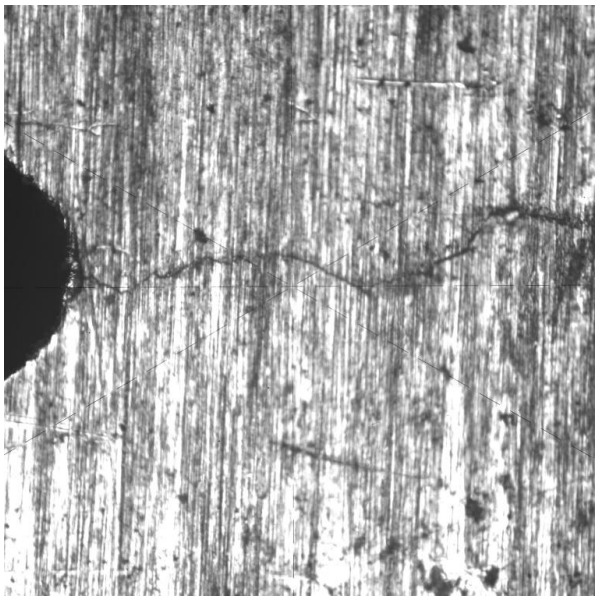

Specimen Number	Nominal Thickness (in)	Left Crack Length (in)	Right Crack Length (in)	Average Crack Opening (x1000 in)	Material
Al-189-4-1	0.189	0.318	0.323	0	7075

AL-189-5a-1

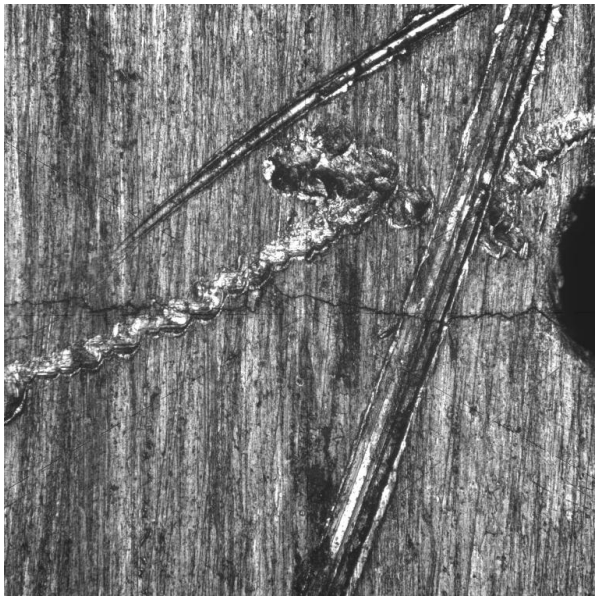

AL-189-5b-1

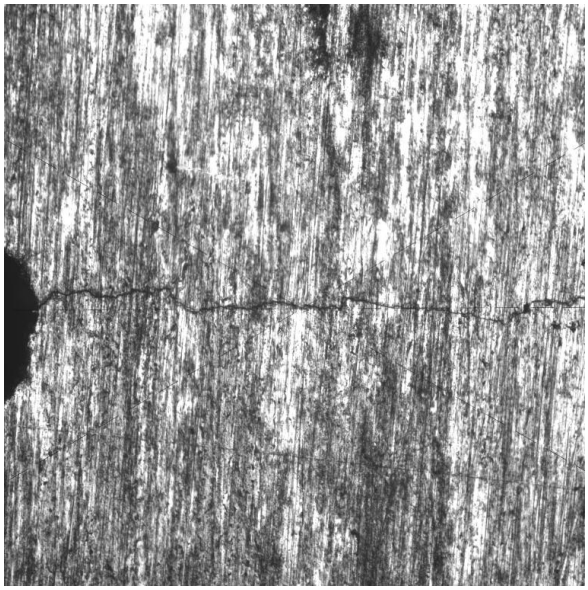

Specimen Number	Nominal Thickness (in)	Left Crack Length (in)	Right Crack Length (in)	Average Crack Opening (x1000 in)	Material
Al-189-5-1	0.189	0.671	0.680	0	7075

AL-189-6a-1

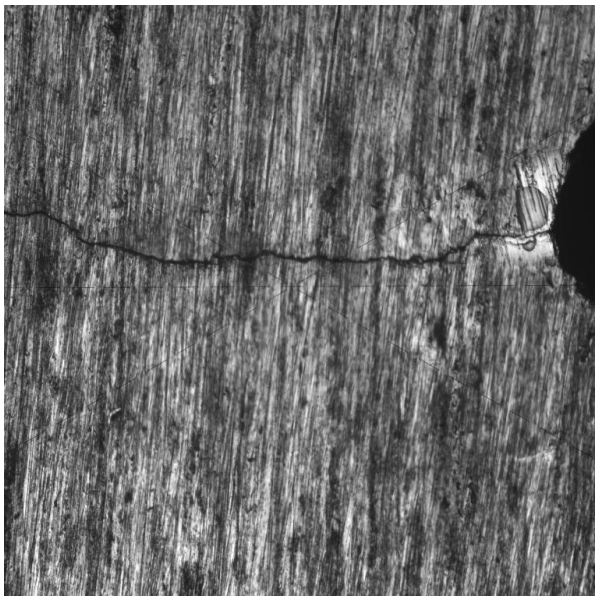

AL-189-6b-1

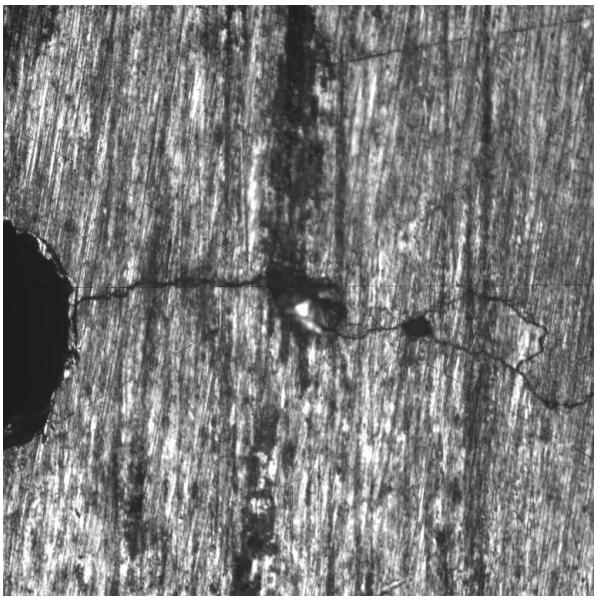

Specimen Number	Nominal Thickness (in)	Left Crack Length (in)	Right Crack Length (in)	Average Crack Opening (x1000 in)	Material
Al-189-6-1	0.189	1.046	1.016	0	7075

AL-250-1a

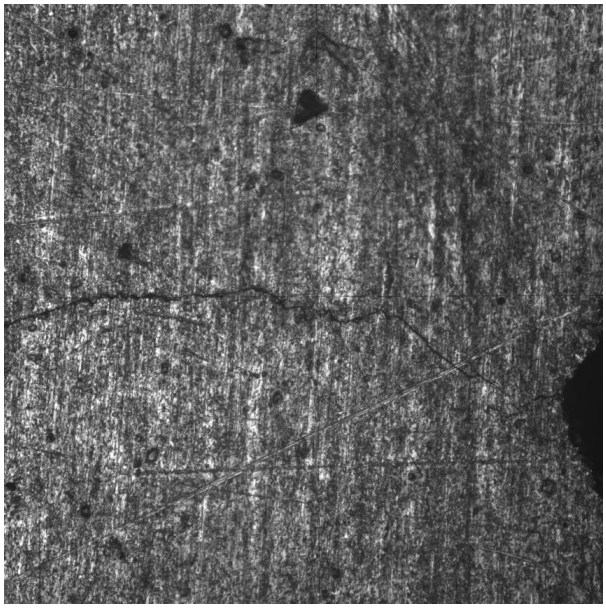

AL-250-1b

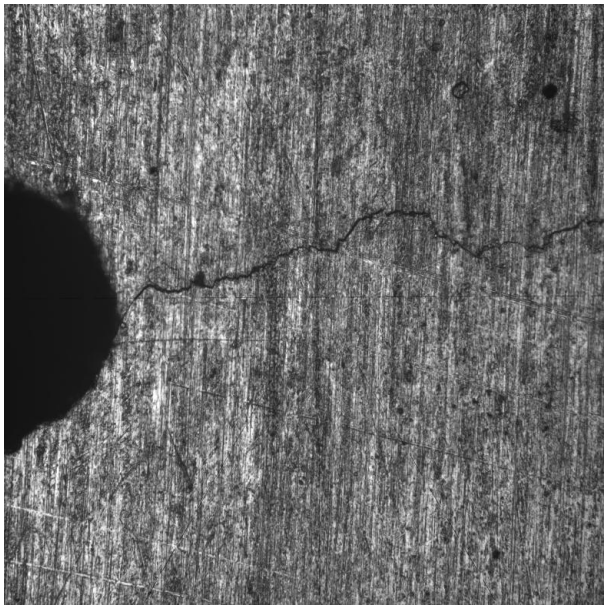

Specimen Number	Nominal Thickness (in)	Left Crack Length (in)	Right Crack Length (in)	Average Crack Opening (x1000 in)	Material
Al-250-1	0.250	0.308	0.300	0	2024

AL-250-2a

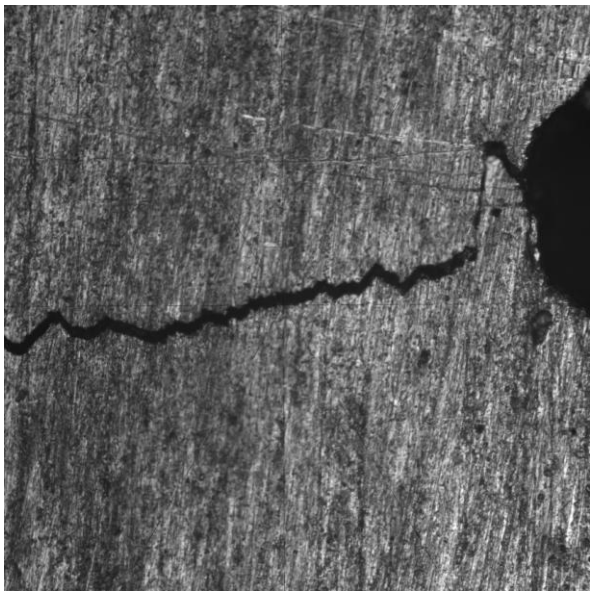

AL-250-2b

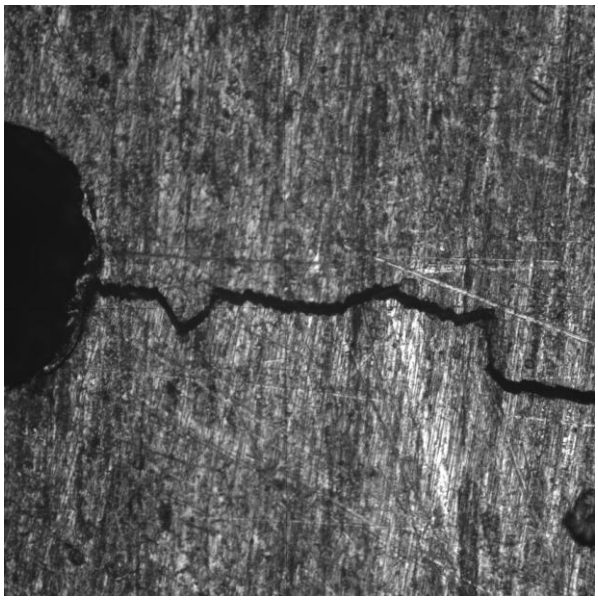

Specimen Number	Nominal Thickness (in)	Left Crack Length (in)	Right Crack Length (in)	Average Crack Opening (x1000 in)	Material
Al-250-2	0.250	0.953	0.950	1	2024

AL-250-3a

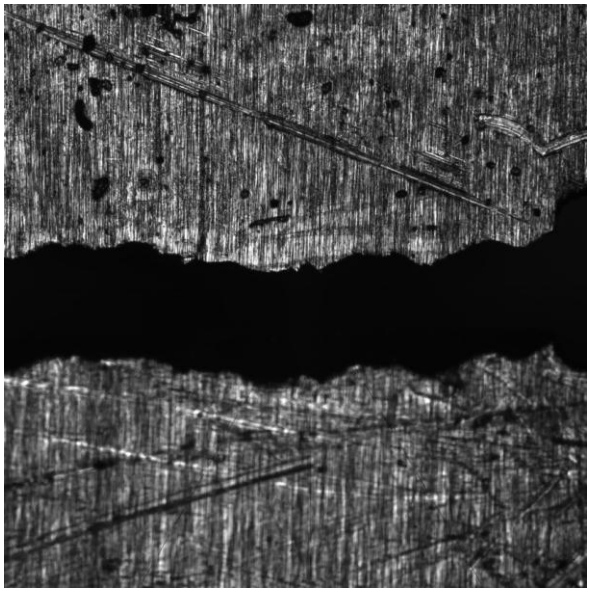

AL-250-3b (10x)

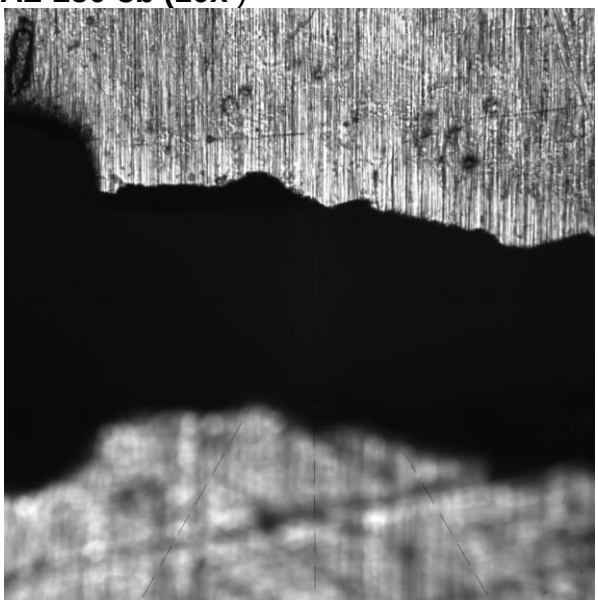

Specimen Number	Nominal Thickness (in)	Left Crack Length (in)	Right Crack Length (in)	Average Crack Opening (x1000 in)	Material
Al-250-3	0.250	1.185	1.122	20	2024

AL-250-4a

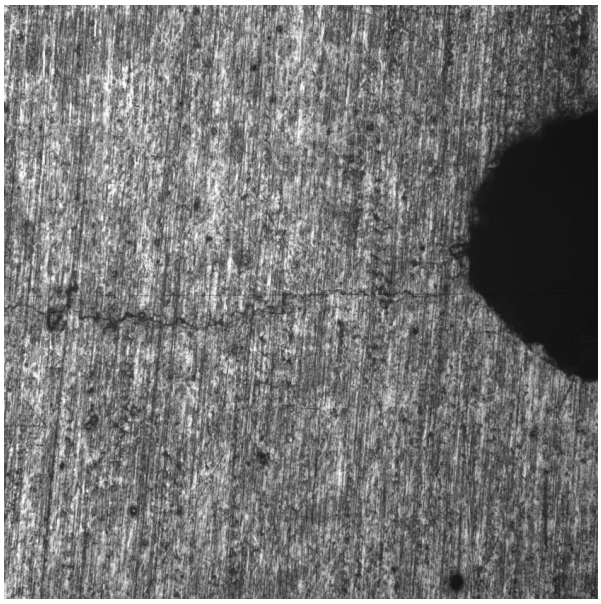

AL-250-4b

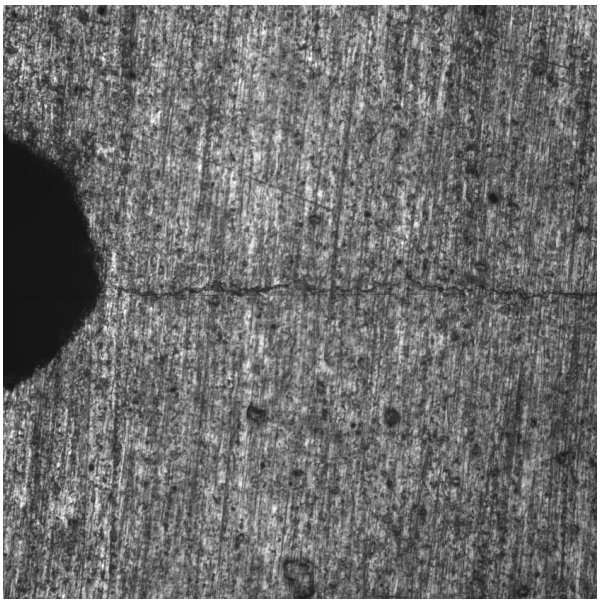

Specimen Number	Nominal Thickness (in)	Left Crack Length (in)	Right Crack Length (in)	Average Crack Opening (x1000 in)	Material
Al-250-4	0.250	0.305	0.305	1	7075

AL-250-5a

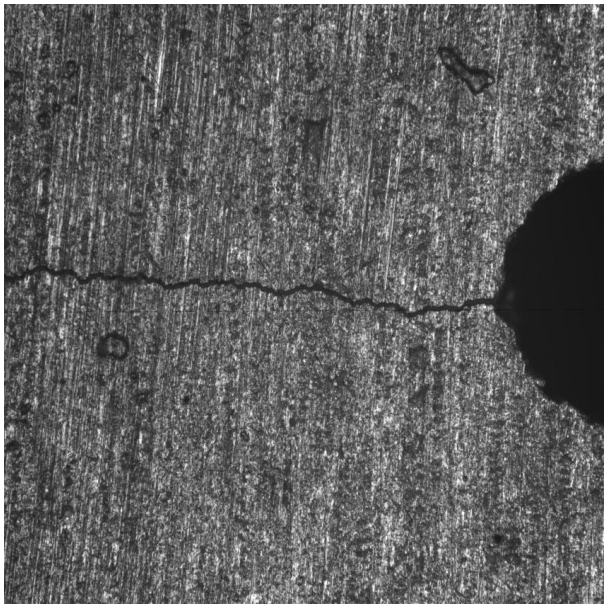

AL-250-5b

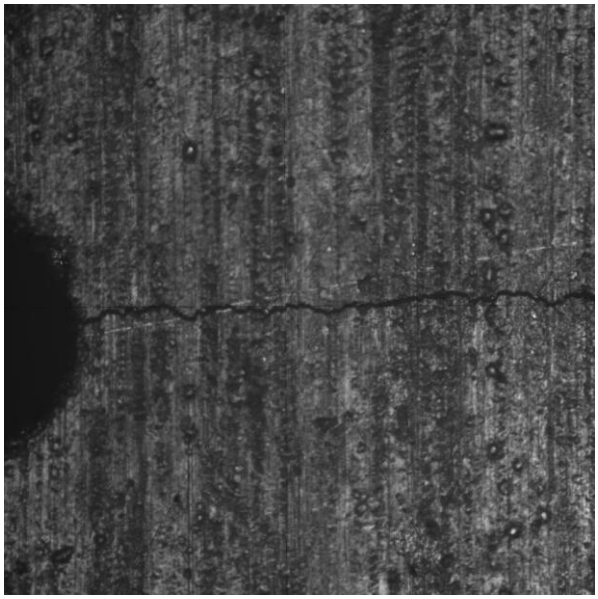

Specimen Number	Nominal Thickness (in)	Left Crack Length (in)	Right Crack Length (in)	Average Crack Opening (x1000 in)	Material
Al-250-5	0.250	0.947	0.934	6	7075

AL-250-6a

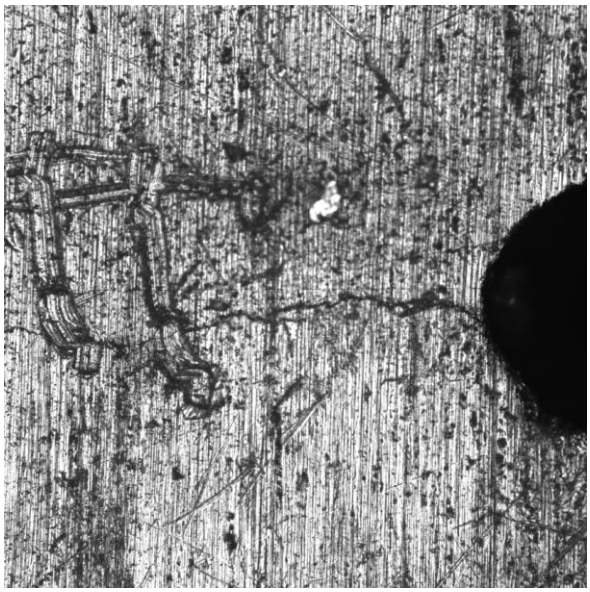

AL-250-6b

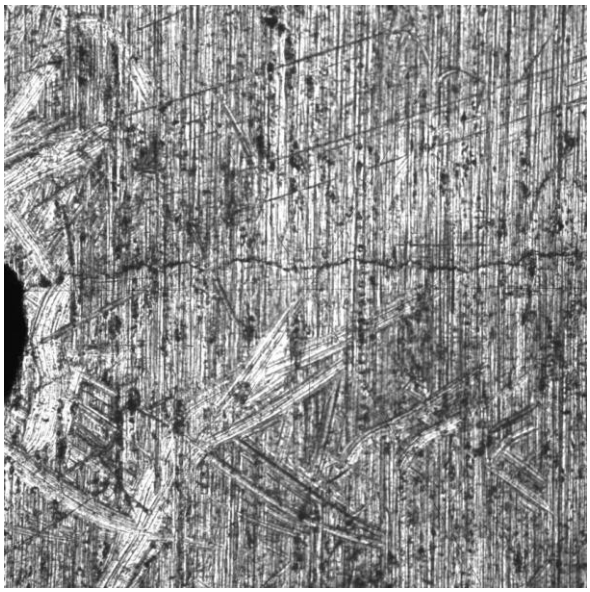

Specimen Number	Nominal Thickness (in)	Left Crack Length (in)	Right Crack Length (in)	Average Crack Opening (x1000 in)	Material
Al-250-6	0.250	0.315	0.293	0	7075

AL-375-1a

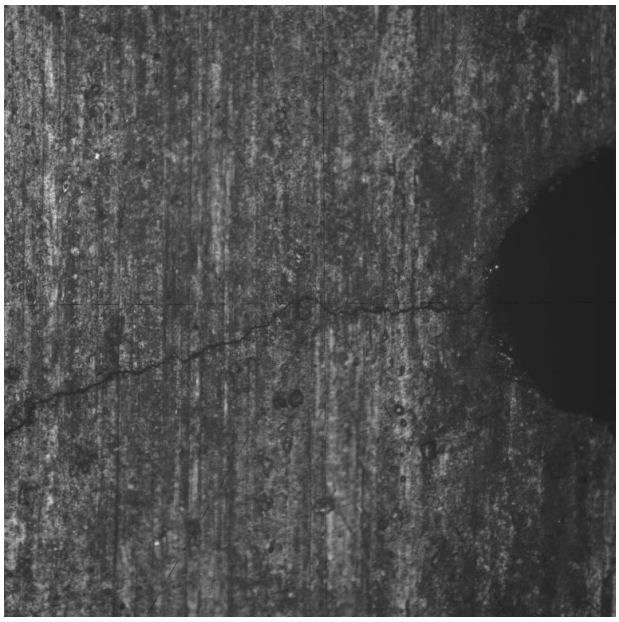

AL-375-1b

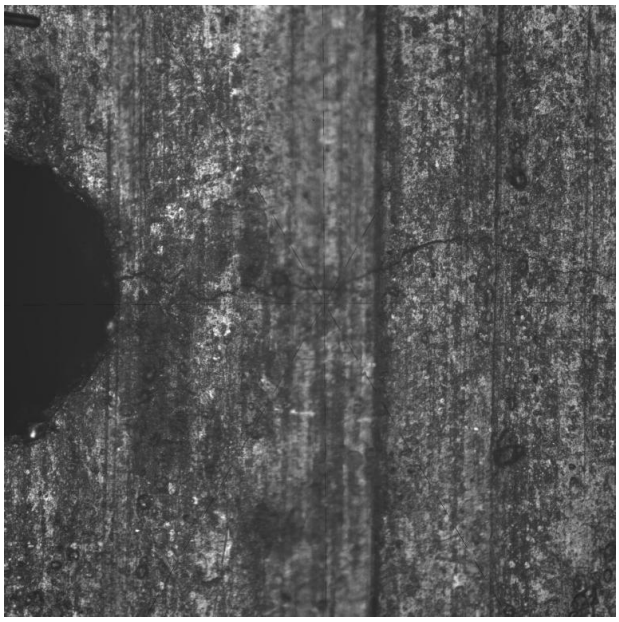

Specimen Number	Nominal Thickness (in)	Left Crack Length (in)	Right Crack Length (in)	Average Crack Opening (x1000 in)	Material
Al-375-1	0.375	0.328	0.336	0	2024

AL-375-2a

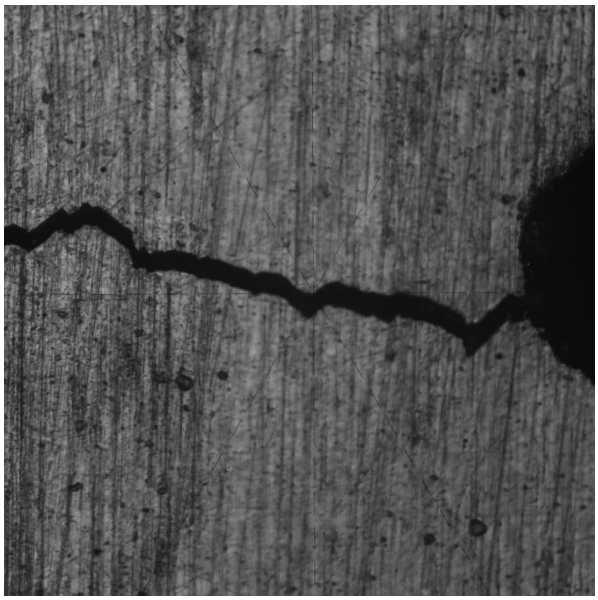

AL-375-2b

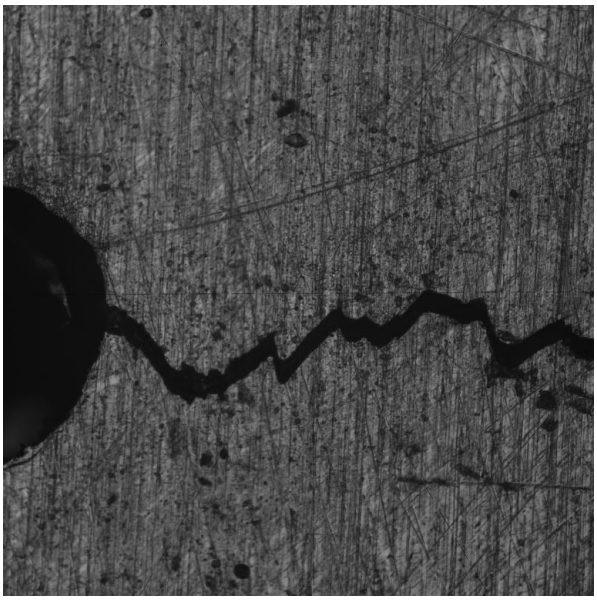

Specimen Number	Nominal Thickness (in)	Left Crack Length (in)	Right Crack Length (in)	Average Crack Opening (x1000 in)	Material
Al-375-2	0.375	1.081	0.977	1	2024

AL-375-3a

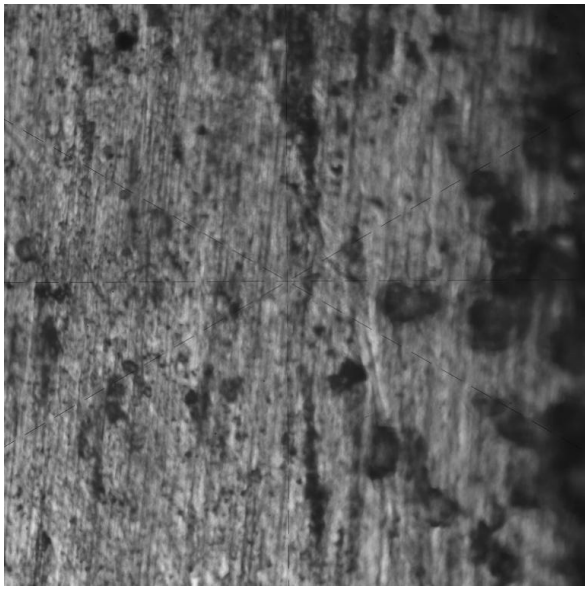

AL-375-3b

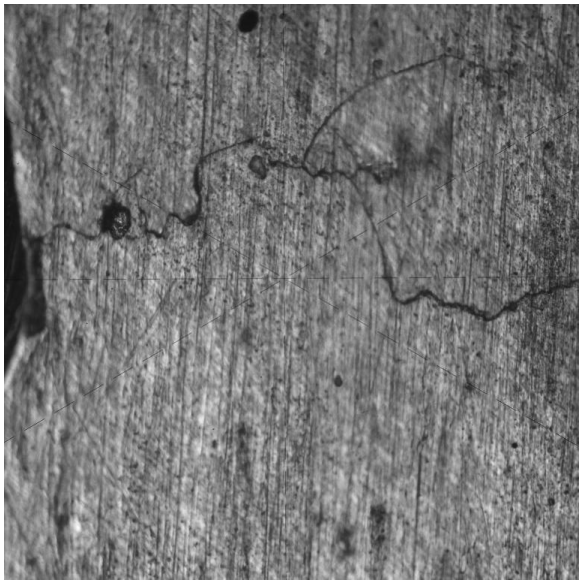

Specimen Number	Nominal Thickness (in)	Left Crack Length (in)	Right Crack Length (in)	Average Crack Opening (x1000 in)	Material
Al-375-3	0.375	not used	not used	not used	2024

AL-375-4a

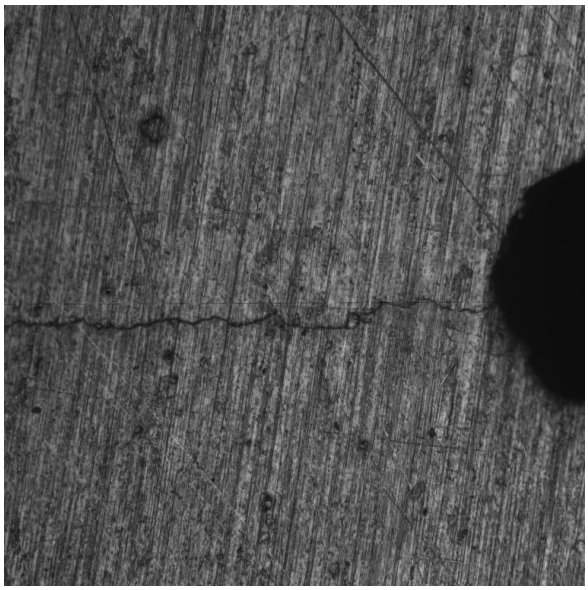

AL-375-4b

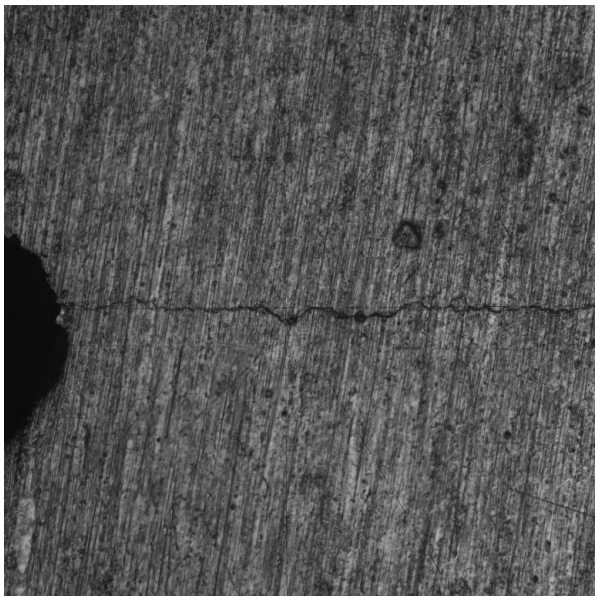

Specimen Number	Nominal Thickness (in)	Left Crack Length (in)	Right Crack Length (in)	Average Crack Opening (x1000 in)	Material
Al-375-4	0.375	0.296	0.299	0	7075

AL-375-5a

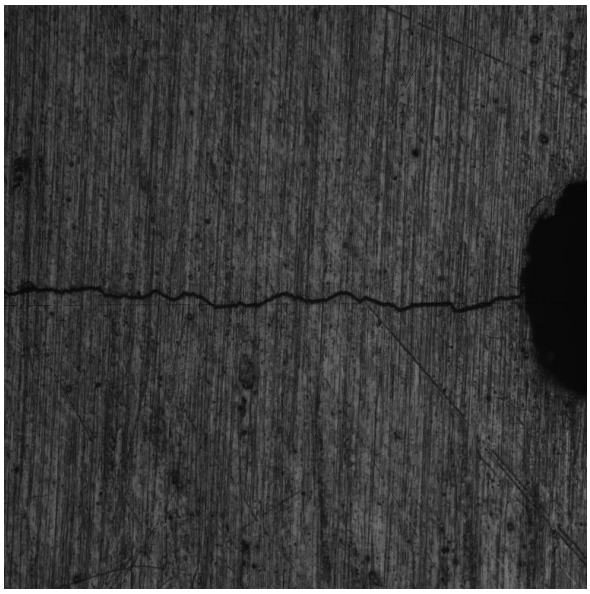

AL-375-5b

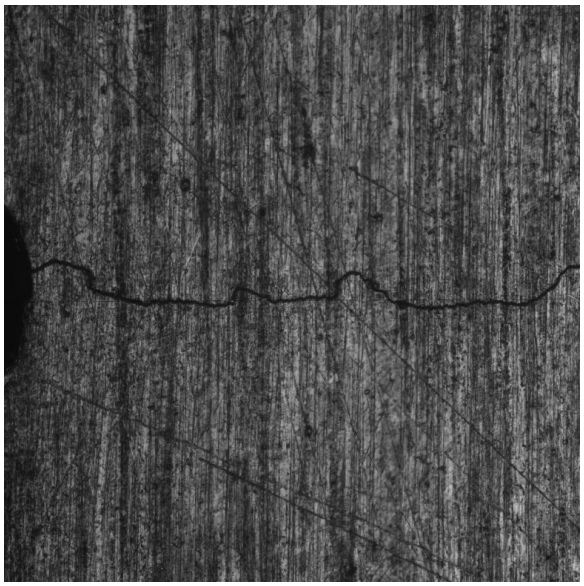

Specimen Number	Nominal Thickness (in)	Left Crack Length (in)	Right Crack Length (in)	Average Crack Opening (x1000 in)	Material
Al-375-5	0.375	0.974	0.940	0	7075

ST-050-1a

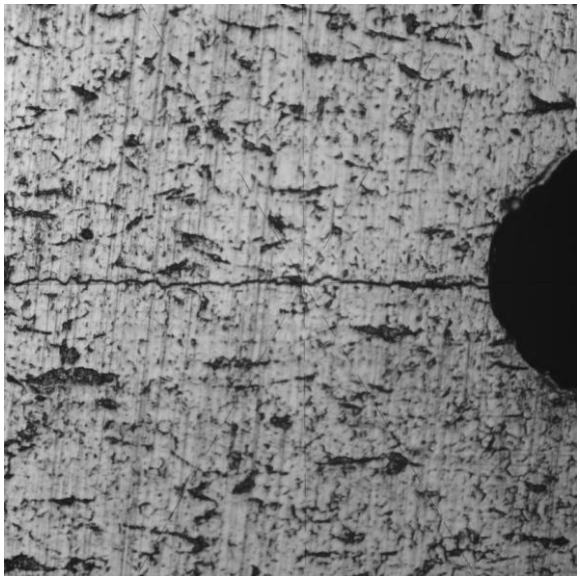

ST-050-1b

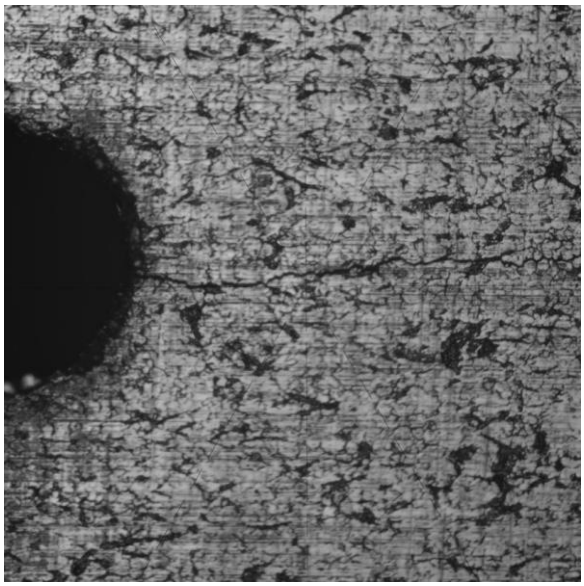

Specimen Number	Nominal Thickness (in)	Left Crack Length (in)	Right Crack Length (in)	Average Crack Opening (x1000 in)	Material
ST-050-1	0.050	0.299	0.302	0	304 SS

ST-050-2a

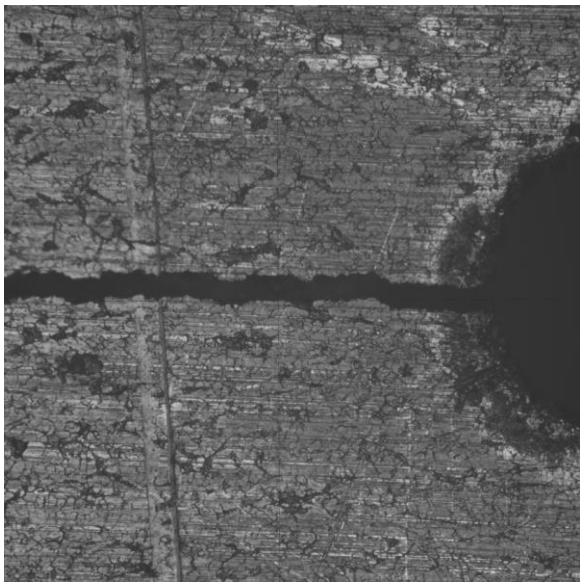

ST-050-2b

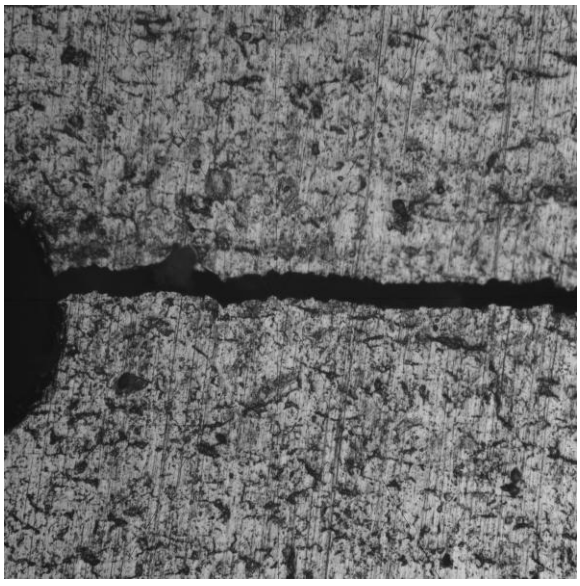

Specimen Number	Nominal Thickness (in)	Left Crack Length (in)	Right Crack Length (in)	Average Crack Opening (x1000 in)	Material
ST-050-2	0.050	0.946	0.803	1	304 SS

ST-050-3a

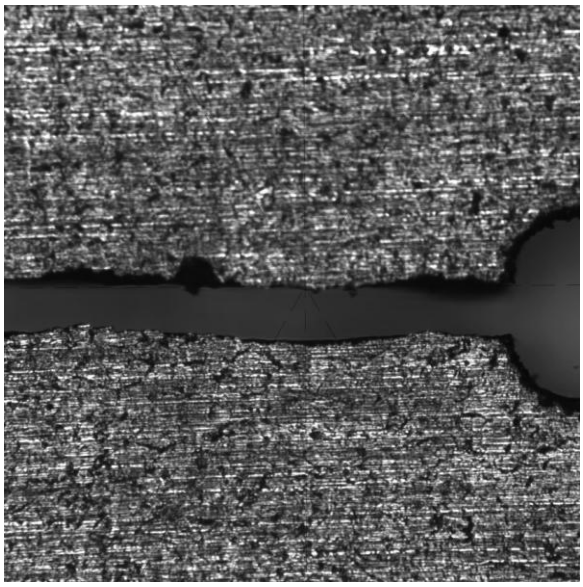

ST-050-3b (20x)

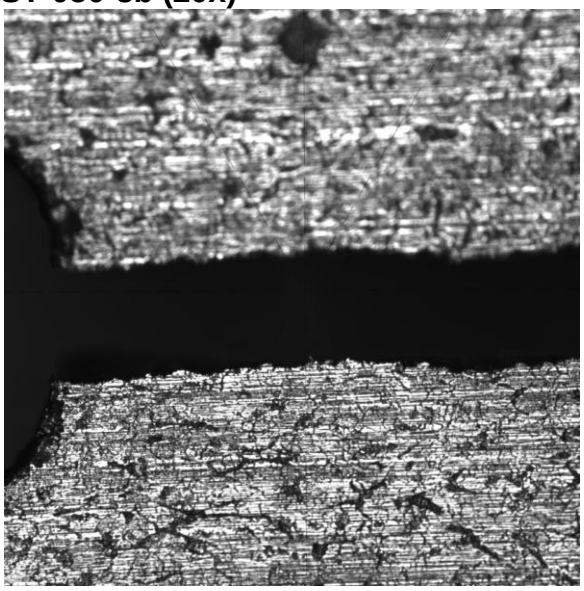

Specimen Number	Nominal Thickness (in)	Left Crack Length (in)	Right Crack Length (in)	Average Crack Opening (x1000 in)	Material
ST-050-3	0.050	0.896	0.917	5	304 SS

ST-063-1a

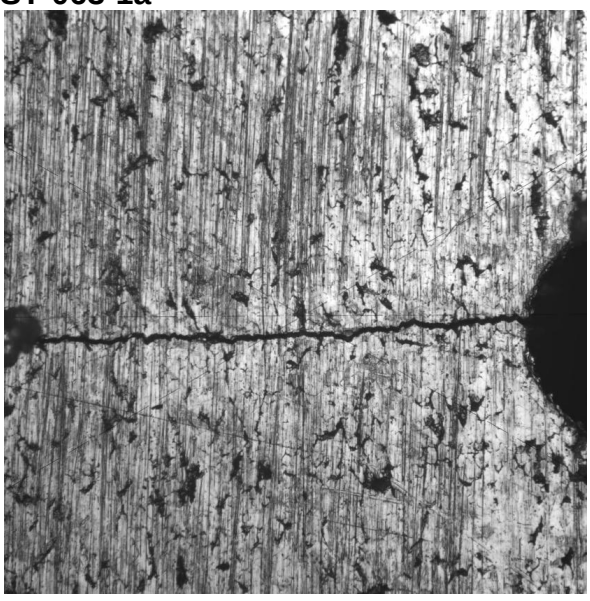

ST-063-1b

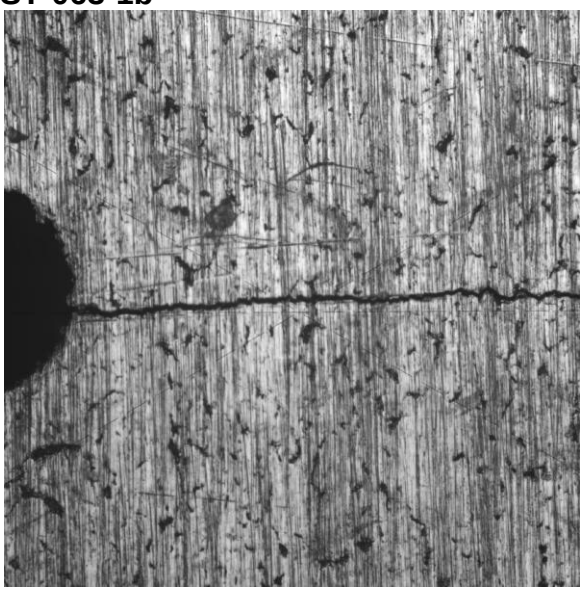

Specimen Number	Nominal Thickness (in)	Left Crack Length (in)	Right Crack Length (in)	Average Crack Opening (x1000 in)	Material
ST-063-1	0.063	0.318	0.193	0	304 SS

ST-063-2a

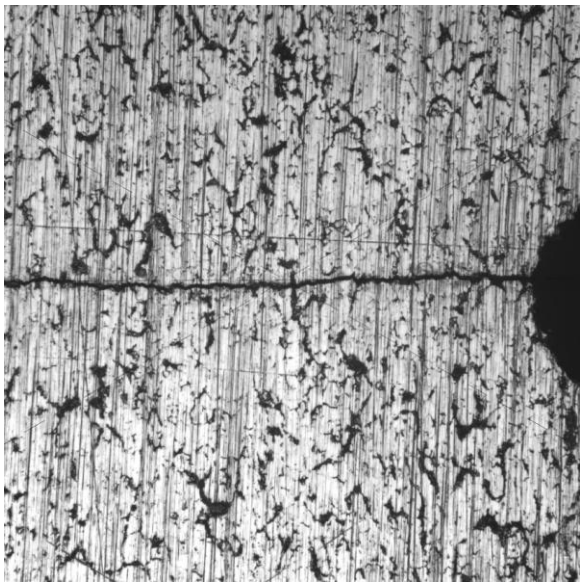

ST-063-2b

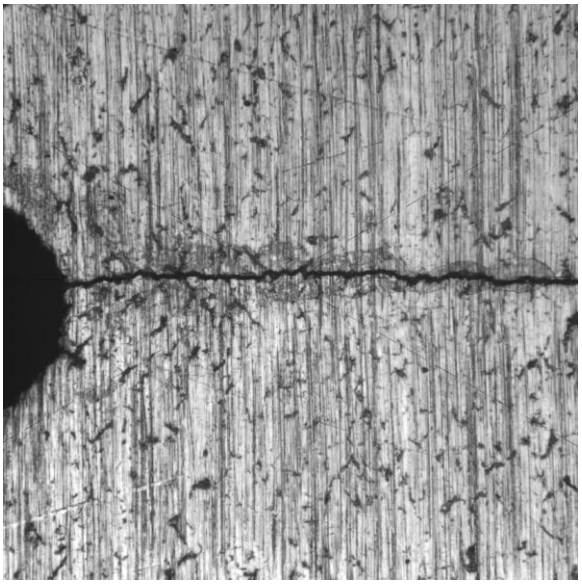

Specimen Number	Nominal Thickness (in)	Left Crack Length (in)	Right Crack Length (in)	Average Crack Opening (x1000 in)	Material
ST-063-2	0.063	0.608	0.585	0	304 SS

ST-063-3a

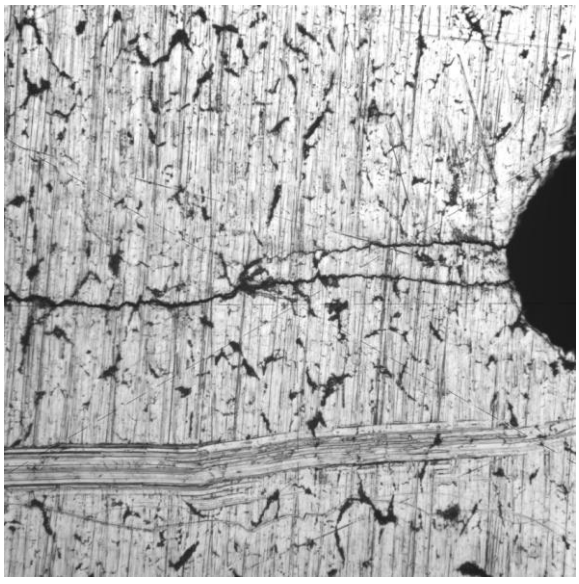

ST-063-3b

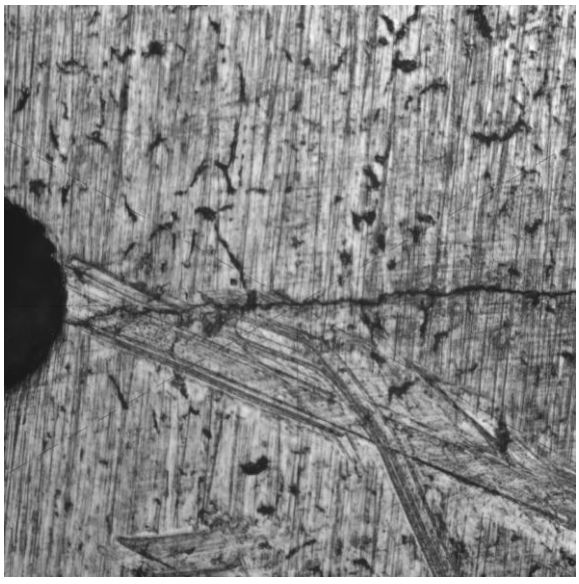

Specimen Number	Nominal Thickness (in)	Left Crack Length (in)	Right Crack Length (in)	Average Crack Opening (x1000 in)	Material
ST-063-3	0.063	0.886	1.014	0	304 SS

ST-125-4a

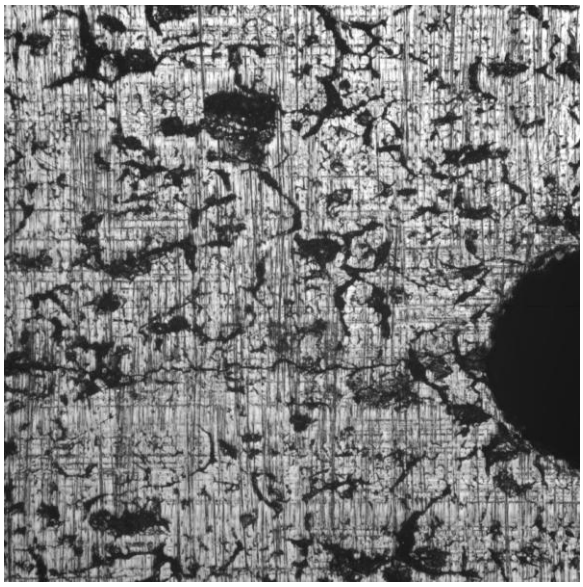

ST-125-4b

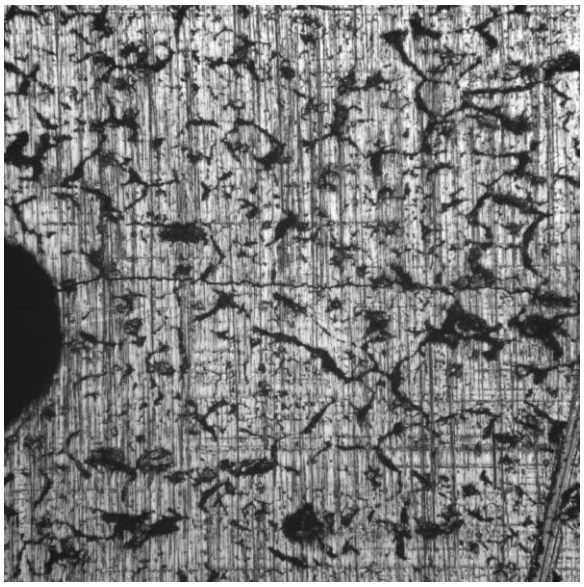

Specimen Number	Nominal Thickness (in)	Left Crack Length (in)	Right Crack Length (in)	Average Crack Opening (x1000 in)	Material
ST-125-4	0.125	0.109	0.093	0	304 SS

ST-125-5a

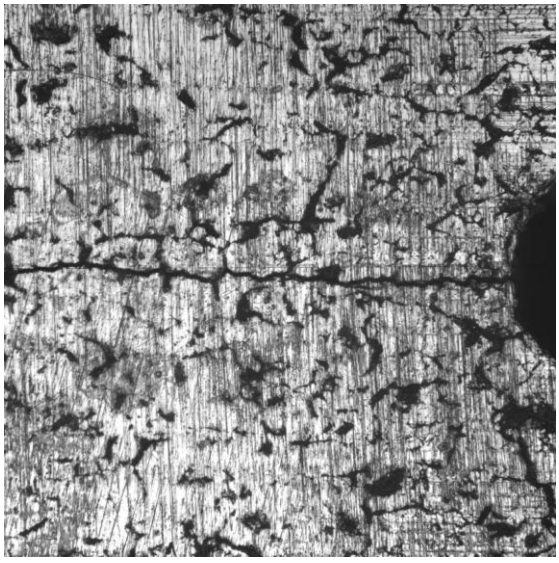

ST-125-5b

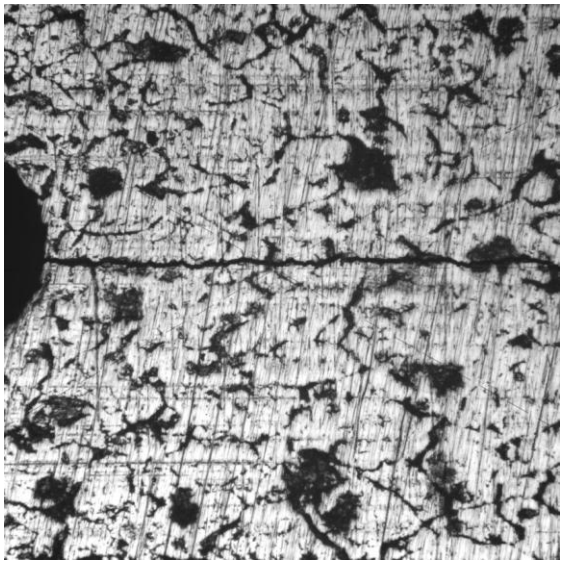

Specimen Number	Nominal Thickness (in)	Left Crack Length (in)	Right Crack Length (in)	Average Crack Opening (x1000 in)	Material
ST-125-5	0.125	0.238	0.305	0	304 SS

ST-125-6a

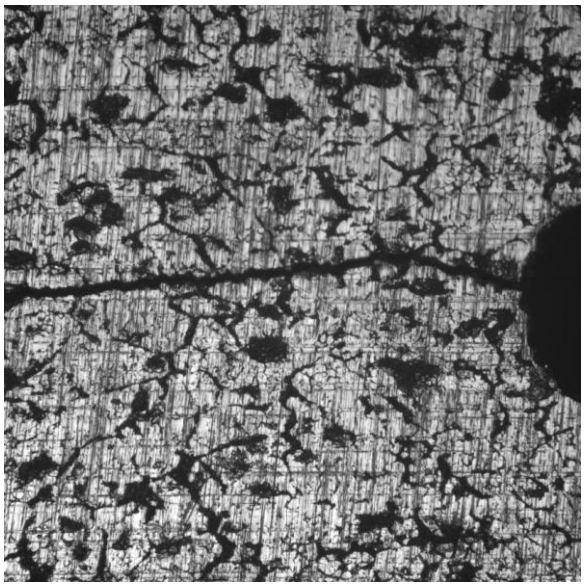

ST-125-6b

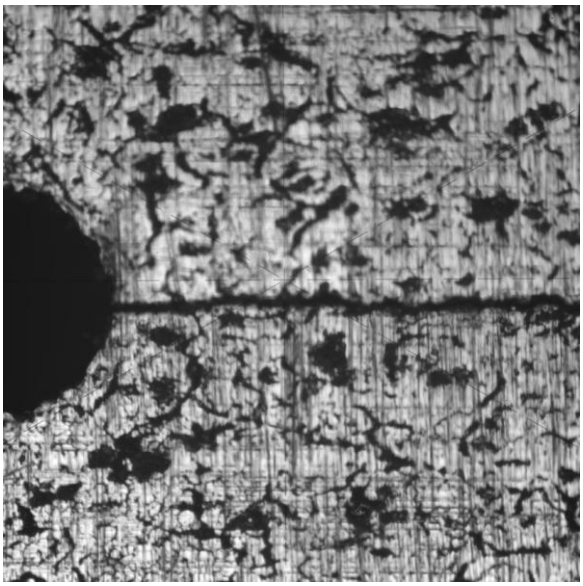

Specimen Number	Nominal Thickness (in)	Left Crack Length (in)	Right Crack Length (in)	Average Crack Opening (x1000 in)	Material
ST-125-6	0.125	0.830	0.582	0	304 SS

ST-250-1a

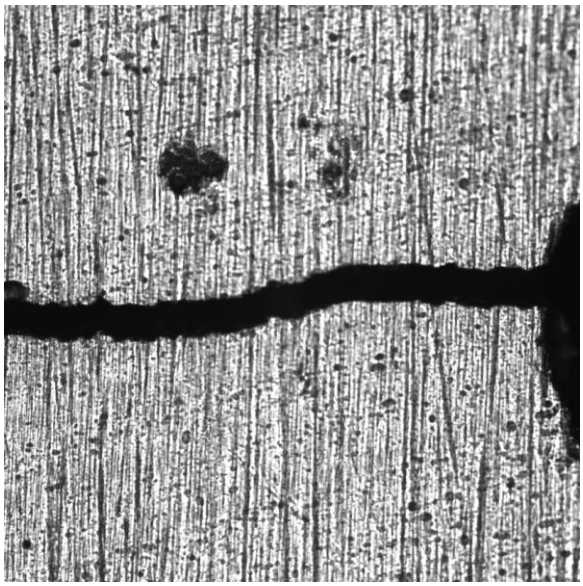

ST-250-1b

Specimen Number	Nominal Thickness (in)	Left Crack Length (in)	Right Crack Length (in)	Average Crack Opening (x1000 in)	Material
ST-250-1	0.250	0.300	0.3087	1	304 SS

ST-250-2a

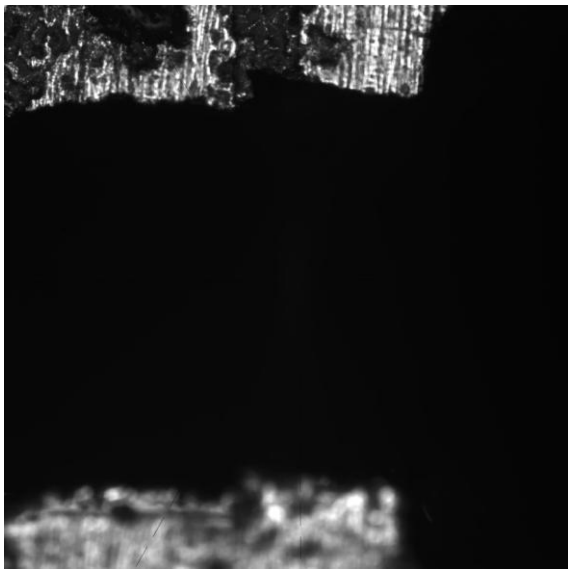

ST-250-2b

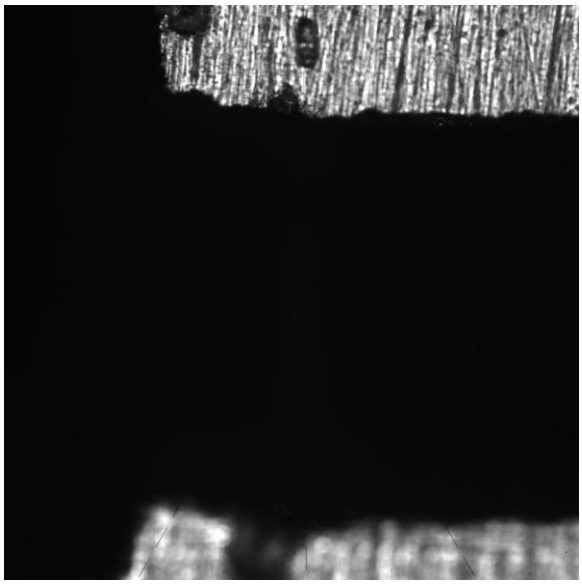

Specimen Number	Nominal Thickness (in)	Left Crack Length (in)	Right Crack Length (in)	Average Crack Opening (x1000 in)	Material
ST-250-2	0.250	0.850	0.883	18	304 SS

ST-250-3a

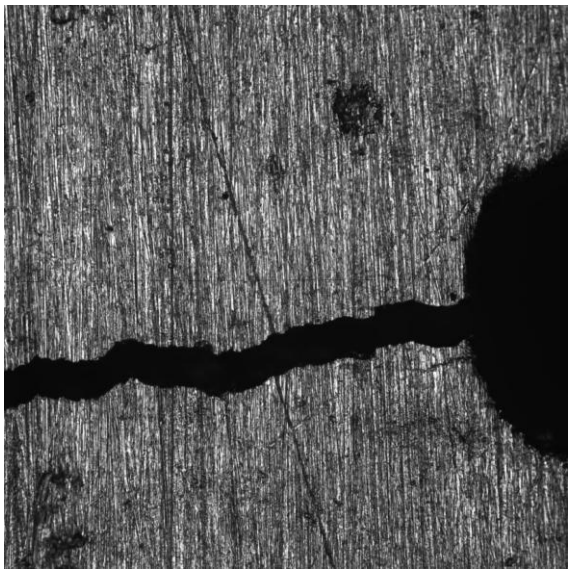

ST-250-3b

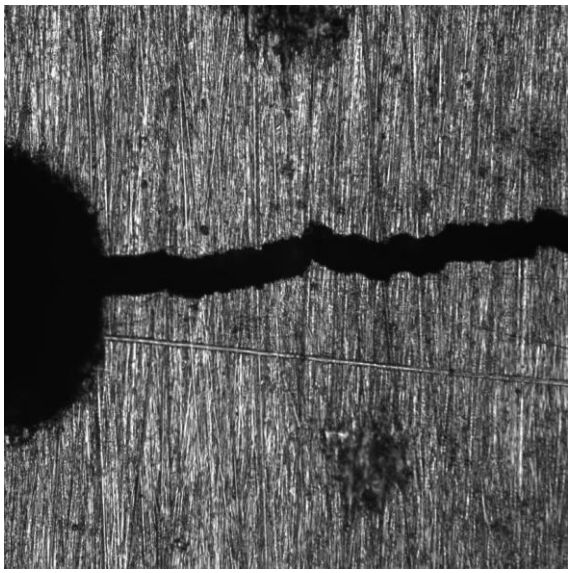

Specimen Number	Nominal Thickness (in)	Left Crack Length (in)	Right Crack Length (in)	Average Crack Opening (x1000 in)	Material
ST-250-3	0.250	0.148	0.151	2	304 SS

ST-250-4a

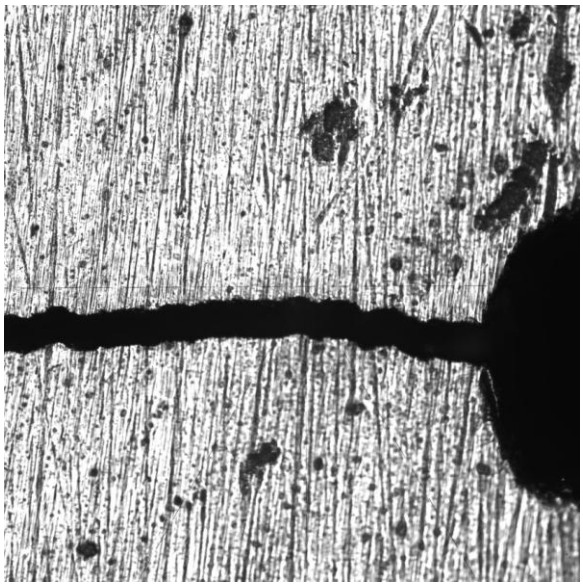

ST-250-4b

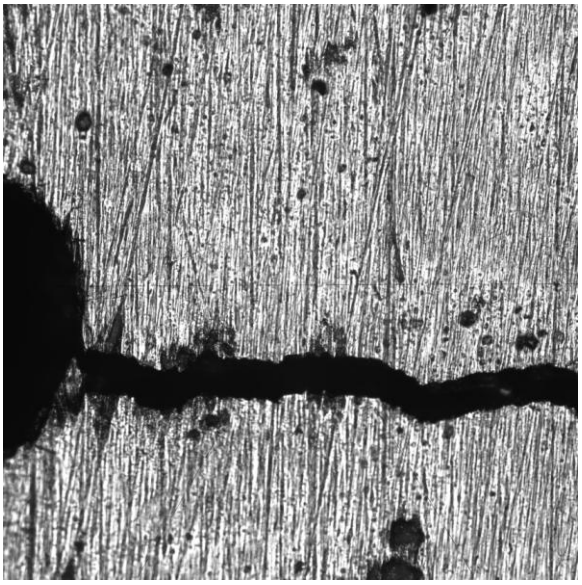

Specimen Number	Nominal Thickness (in)	Left Crack Length (in)	Right Crack Length (in)	Average Crack Opening (x1000 in)	Material
ST-250-4	0.250	0.307	0.299	1	304 SS

ST-250-5a

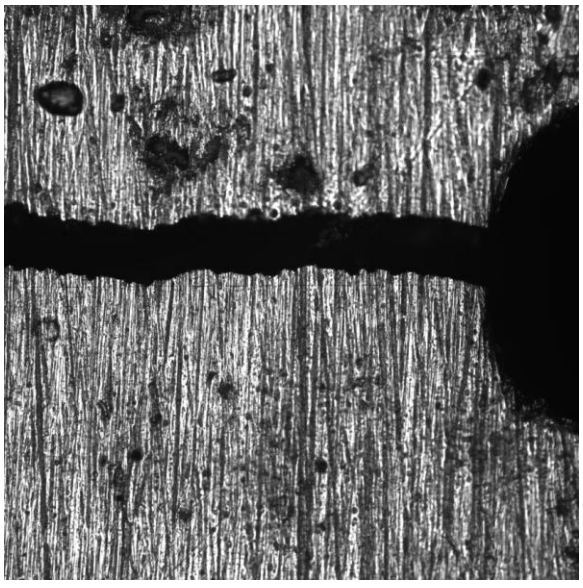

ST-250-5b

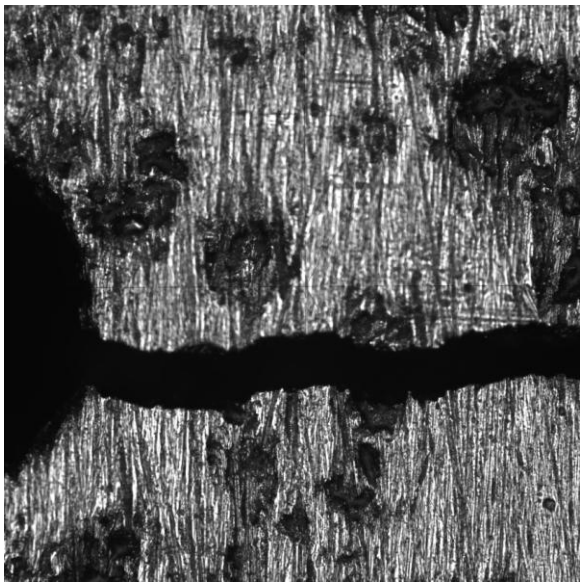

Specimen Number	Nominal Thickness (in)	Left Crack Length (in)	Right Crack Length (in)	Average Crack Opening (x1000 in)	Material
ST-250-5	0.250	0.942	0.941	2	304 SS

ST-250-6a

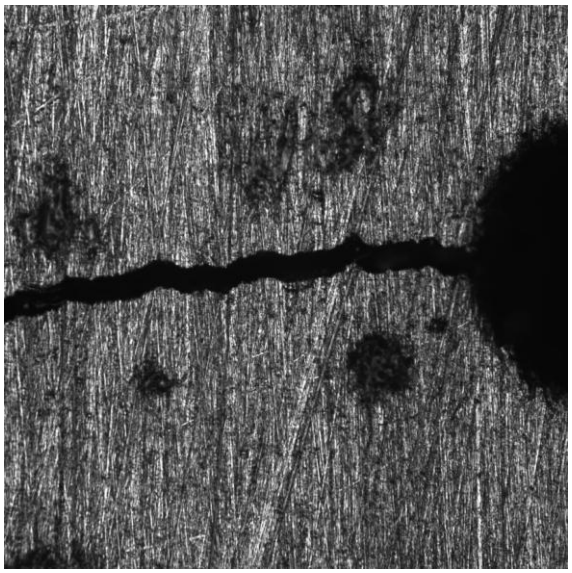

ST-250-6b

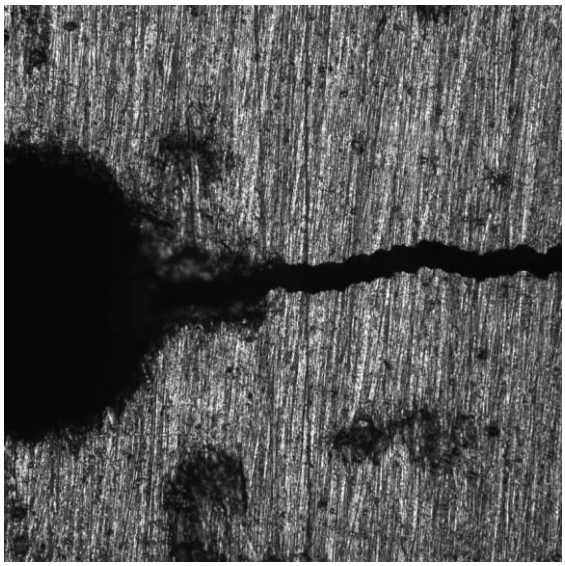

Specimen Number	Nominal Thickness (in)	Left Crack Length (in)	Right Crack Length (in)	Average Crack Opening (x1000 in)	Material
ST-250-6	0.250	0.149	0.143	1	304 SS

ST-350-1a

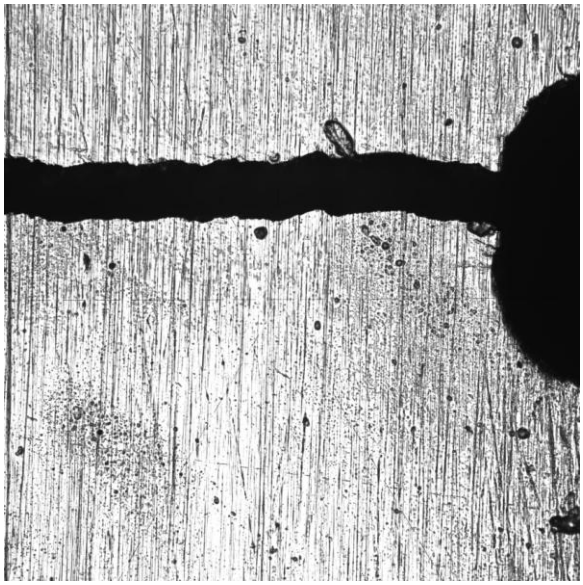

ST-350-1b

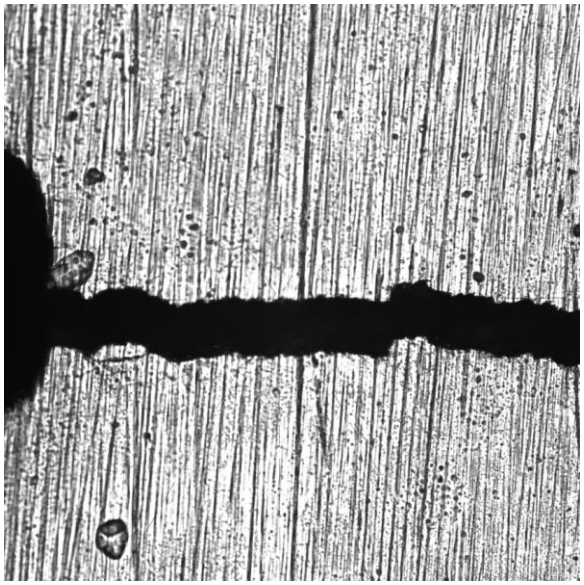

Specimen Number	Nominal Thickness (in)	Left Crack Length (in)	Right Crack Length (in)	Average Crack Opening (x1000 in)	Material
ST-350-1	0.350	0.303	0.302	1	304 SS

ST-350-2a

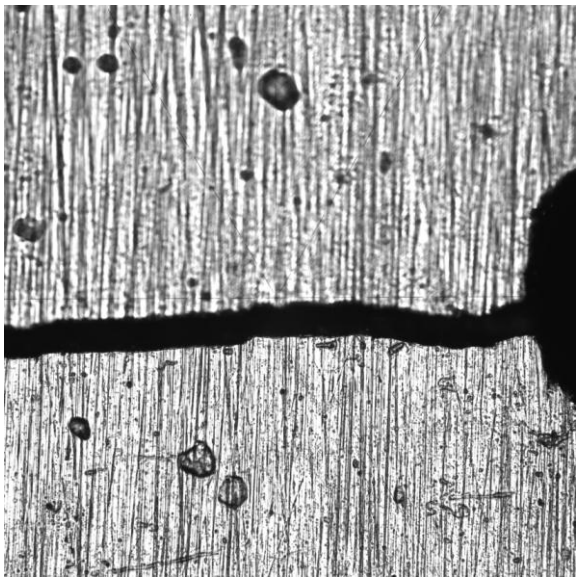

ST-350-2b

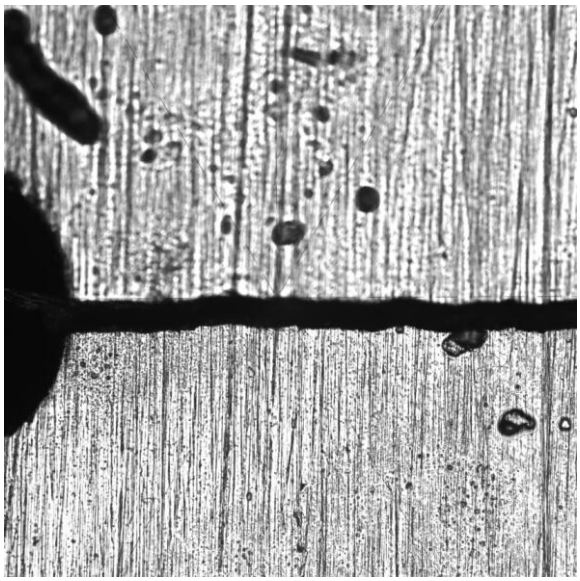

Specimen Number	Nominal Thickness (in)	Left Crack Length (in)	Right Crack Length (in)	Average Crack Opening (x1000 in)	Material
ST-350-2	0.350	0.958	0.957	1	304 SS

ST-350-3a

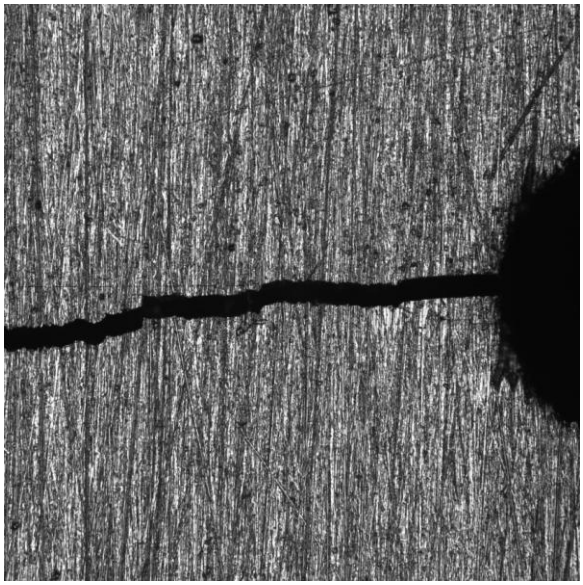

ST-350-3b

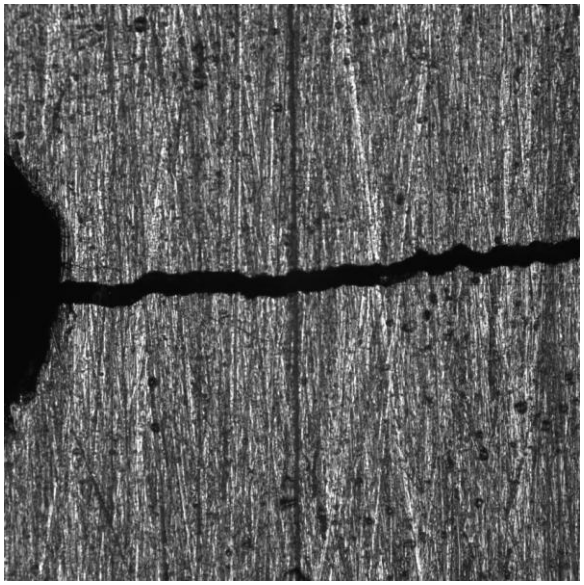

Specimen Number	Nominal Thickness (in)	Left Crack Length (in)	Right Crack Length (in)	Average Crack Opening (x1000 in)	Material
ST-350-3	0.350	0.150	0.152	1	304 SS

ST-350-4a

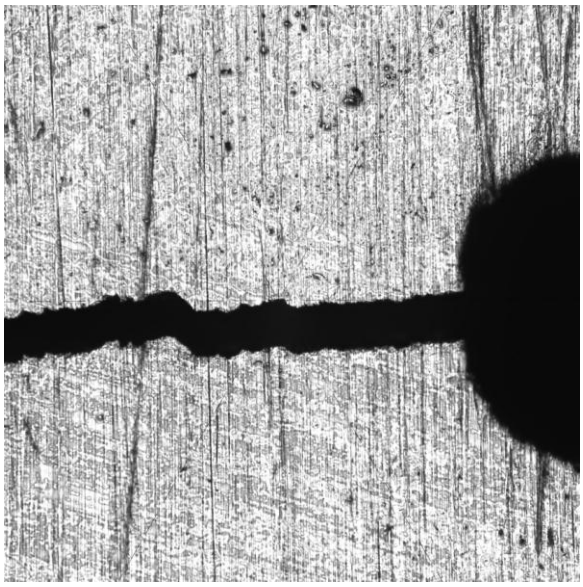

ST-350-4b

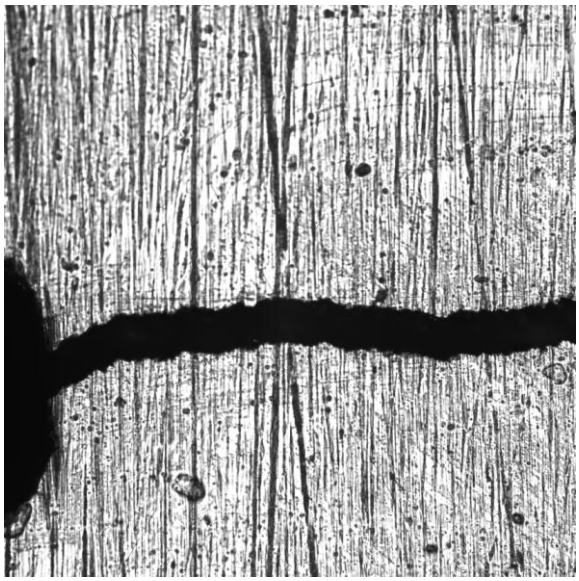

Specimen Number	Nominal Thickness (in)	Left Crack Length (in)	Right Crack Length (in)	Average Crack Opening (x1000 in)	Material
ST-350-4	0.350	0.305	0.303	1	304 SS

ST-350-5a

ST-350-5b

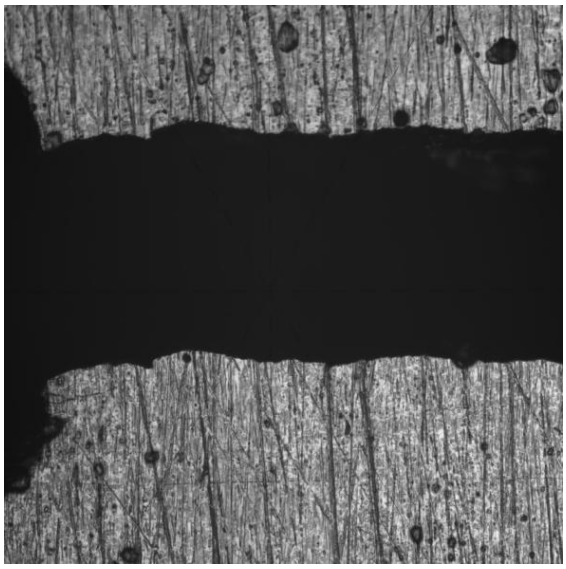

Specimen Number	Nominal Thickness (in)	Left Crack Length (in)	Right Crack Length (in)	Average Crack Opening (x1000 in)	Material
ST-350-5	0.350	0.951	0.947	10	304 SS

ST-350-6a

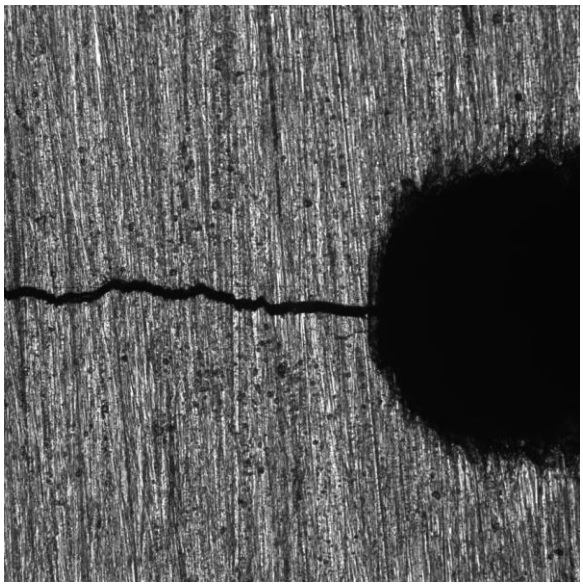

ST-350-6b

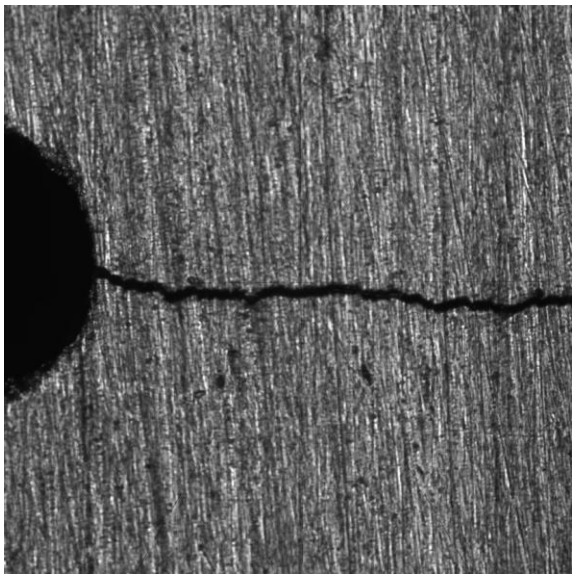

Specimen Number	Nominal Thickness (in)	Left Crack Length (in)	Right Crack Length (in)	Average Crack Opening (x1000 in)	Material
ST-350-6	0.350	0.151	0.150	1	304 SS

ST-350-3a

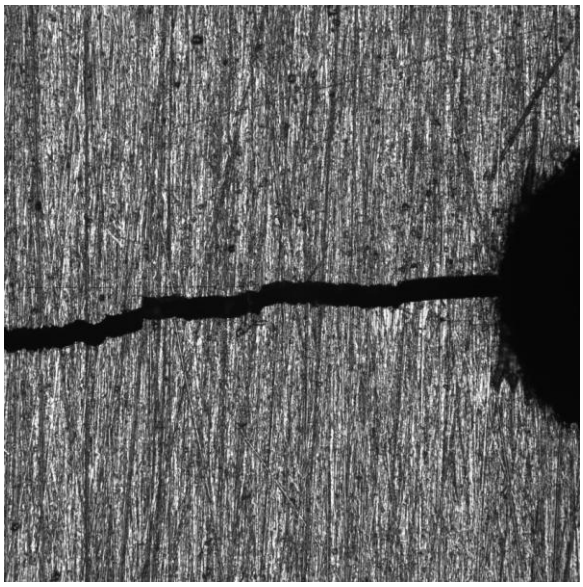

ST-350-3b

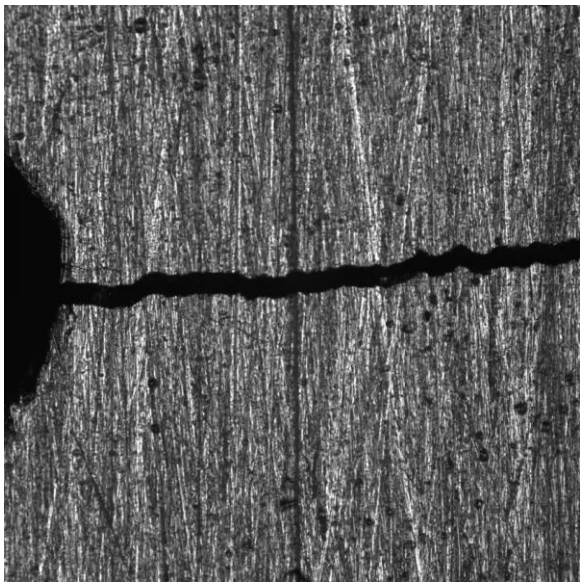

Specimen Number	Nominal Thickness (in)	Left Crack Length (in)	Right Crack Length (in)	Average Crack Opening (x1000 in)	Material
ST-350-3	0.350	0.150	0.152	1	304 SS

ST-350-4a

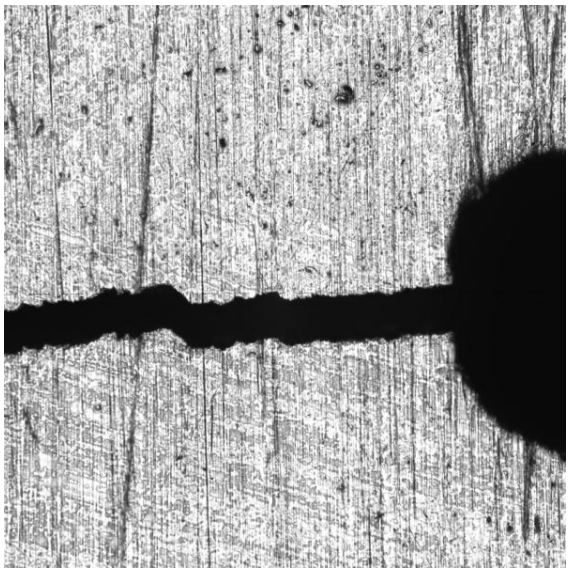

ST-350-4b

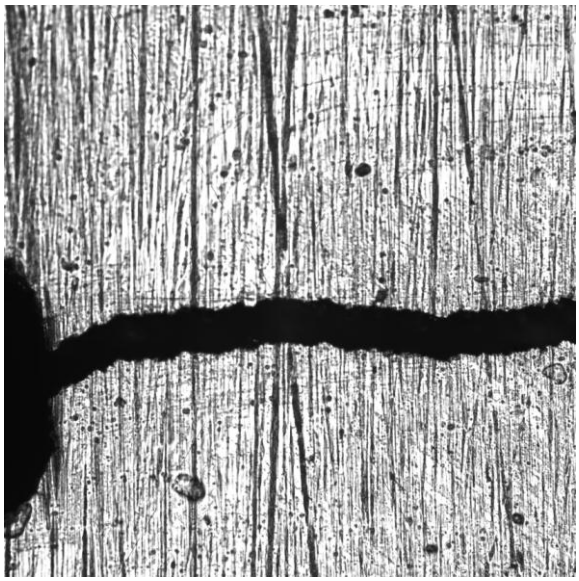

Specimen Number	Nominal Thickness (in)	Left Crack Length (in)	Right Crack Length (in)	Average Crack Opening (x1000 in)	Material
ST-350-4	0.350	0.305	0.303	1	304 SS

ST-350-5a

ST-350-5b

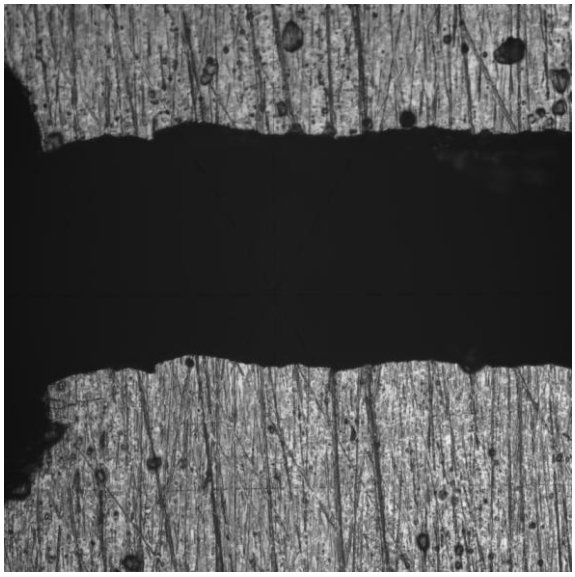

Specimen Number	Nominal Thickness (in)	Left Crack Length (in)	Right Crack Length (in)	Average Crack Opening (x1000 in)	Material
ST-350-5	0.350	0.951	0.947	10	304 SS

Appendix C

ImageJ Software Tools for the Evaluation of Computed Radiography Images

C1.0 INTRODUCTION

Computed Radiography (CR) images are often evaluated using signal-to-noise ratio (SNR) and contrast-to-noise ratio (CNR) as an indicator of image quality. CNR is similar to SNR, but subtracts off a term before taking the ratio, which is important when there is a significant bias in the image. Off-the-shelf radiography image analysis application software may inherently provide these image quality measurements, but, unfortunately, this is not always the case. For example, Software A provides a SNR measurement and Region of Interest (ROI) statistics allowing the CNR to be manually derived without too much difficulty. However, the Software B application provides neither SNR nor a convenient method to obtain ROI statistics. In order to assure that SNR and CNR can be obtained on any computed radiography image available on this program, independent of how the image was acquired or what vendor workstation the image resides, UDRI has developed a vendor-independent approach for acquiring these image quality measurements. In doing so UDRI hopes to achieve two main goals: 1) assure that image quality can be measured on all project-related CR images, and 2) allow SNR and CNR to be determined using one well-defined algorithm for each technique, insuring an "apples-to-apples" comparison of CR image quality. In addition, UDRI has developed a third image quality measurement, defect-to-noise ratio (DNR), permitting the evaluation of noise relative to a known crack response.

UDRI's vendor-independent image analysis approach has been implemented by creating image analysis plugins for the ImageJ public domain application. ImageJ is a general-purpose image processing application written in Java that can be hosted on Windows- or Linux-based computer systems. It supports a variety of image file formats allowing images from Software A or Software B to be imported. Aso, there are no licensing fees and they can be used at no additional cost. The remainder of this document will provide a brief overview of ImageJ, followed by a detailed description of the image quality applications developed.

C2.0 IMAGEJ APPLICATION

ImageJ is a public-domain, open-source image processing application developed by the National Institute of Health. There are no licensing fees associated with ImageJ, which can be downloaded and installed from "http://rsbweb.nih.gov/ij/". As downloaded, ImageJ provides basic image processing capability such as display, edit, analyze, process, display, and print on 8-bit, 16-bit, and 32-bit images read from a variety of formats including .tiff, .png, .pgm, .gif, .jpeg, .bmp, .dicom, and .fits. Image processing functions include logical and arithmetic operations between images, contrast enhancement, convolution, and Fourier analysis, to name a few. A variety of image analysis operations including: measure area/mean/lengths/angles, standard deviation, min/max, histogram generation, particle analysis, and profile/surface plots are provided. Geometric operations sup-

port image crop, scale, resize, rotate, and flip. ROI operations are supported within rectangular, elliptical, or irregular areas. A typical ImageJ application toolbar appears in Figure C1.

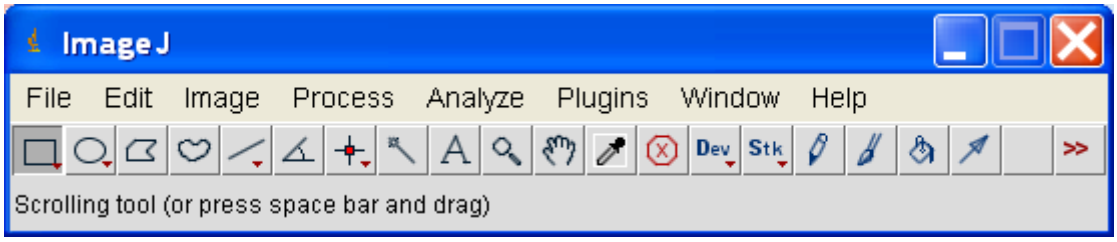

Figure C1. Typical ImageJ Toolbar

Although ImageJ provides typical image processing functions available in many off-the-shelf packages, the real power of ImageJ is the ability to expand this capability through the development of custom plugins. The open-architecture design and open-source availability of ImageJ allow custom Java plugins to be developed and integrated to meet the specialized needs of a particular application. Many plugins have been developed by third parties which can be downloaded and installed, allowing the capability of ImageJ to be expanded to suit a particular need. UDRI has taken advantage of this feature and developed three plugin modules suited for x-ray/CR image quality evaluation: SNR, CNR, and DNR plugins.

C2.1 ImageJ Operation

The steps required to use ImageJ in preparation for the desired image quality measurement is fairly straightforward. After invoking the ImageJ application, the CR image must be imported. This is easily accomplished by dragging the image from Windows Explorer onto the ImageJ application window. ImageJ will automatically recognize the file format and perform the necessary conversions to translate the file and display the image in a window. Software A and Software B export image files using the DICOM format. When ImageJ imports DICOM, it is converted to a 16 bit image.

A plugin is activated using the ImageJ "Plugins" pull-down menu. The menu should list a submenu called XRay which, when selected, displays three image quality (noise) plugins: "Image SNR", "Image CNR", and "Image DNR". Selecting one of these noise plugins from the submenu automatically assigns it to the currently active image. Only one noise plugin can be concurrently assigned to an image. Attempting to select a second plugin will invoke the error message shown in Figure C2.

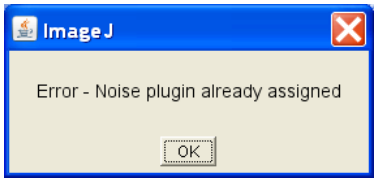

Figure C2. ImageJ Error Message

Once the noise plugin is active, a dialog will appear and one or more ROI"s will be displayed in the image. The ImageJ toolbar will now appear as shown in Figure C3, where there is now an additional button labeled "N". This button must be depressed for the current noise plugin to be selected and active. The operation of the selected plugin is the subject of Section C3.0.

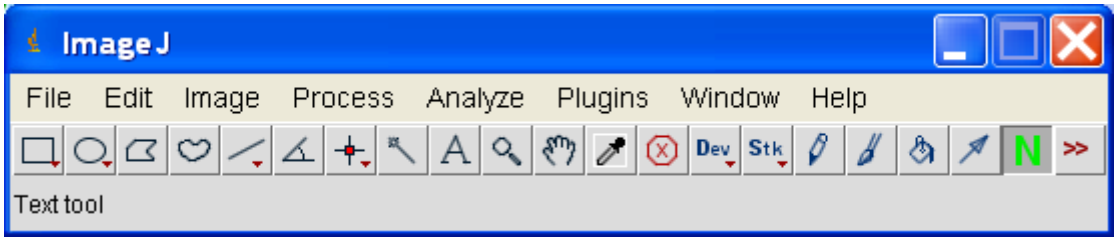

Figure C3. X-Ray Image Processing Plugin Selection

C3.0 IMAGEJ PLUGIN DEVELOPMENT

As mentioned, UDRI has developed three plugins for ImageJ that can be used for the evaluation of image quality of radiographic images. One purpose for developing these plugins is to insure that SNR and CNR can be measured on all CR images required for this program, independent of the workstation where the images may reside. Because ImageJ supports the input of images in the DICOM format, images from both the Software A and Software B workstations can be analyzed using plug-ins from within ImageJ. Secondly, using a single image analysis source for measuring these image quality indicators insures that the same algorithm is used on all images. Although SNR and CNR can be derived on the Scanner A workstation, performing these measurements using ImageJ insures consistent results. This approach guarantees an "apples-to-apples" comparison between workstations images. The operation of the Signal-to-Noise, Contrast-to-Noise, and Defect-to-Noise plugin is given in the following subsections. Insight into each noise algorithm is also provided.

C3.1 Signal-to-Noise Plugin

The signal-to-noise plugin is named "Image SNR" and listed in the XRay subMenu under the ImageJ "Plugins" menu item. Upon selecting "Image SNR", the SNR dialog box appears as shown in Figure C4. A green box defining an ROI appears in the active image, as shown in Figure C5, indicating the pixel neighborhood used for the statistics calculation. The box can be moved about the image by positioning the mouse cursor within the box, holding down the left mouse button, and dragging the box to a new location.

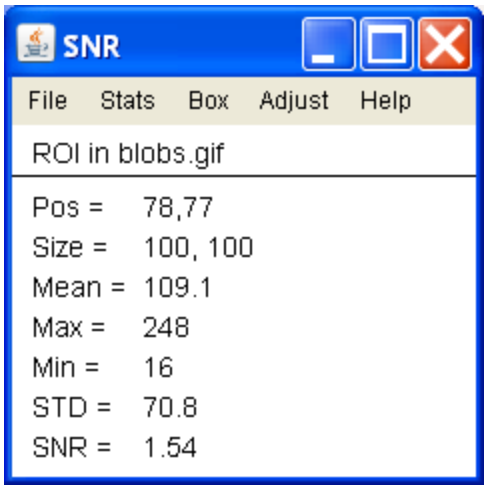

Figure C4. Image SNR Dialog Box

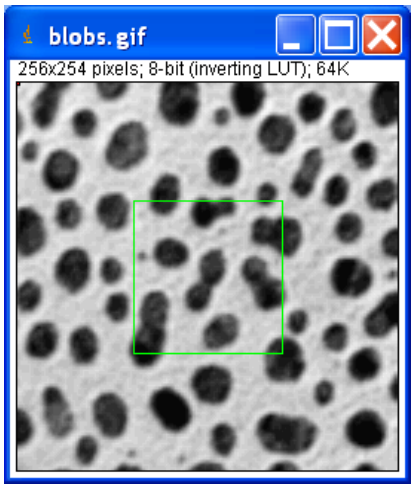

Figure C5. SNR ROI Indicated by Green Box

C3.1.1 SNR Dialog

The SNR dialog contains a menu and statistics display area. The statistics display area is defined by a white background and begins by displaying the name of the image where the ROI is displayed. A horizontal line separates the image name from the statistics listed. The statistics automatically update as the box is moved about the active image. The statistics are defined below:

Pos – the position of the upper left hand corner of the ROI box.
Size – the width and height of the ROI box in pixels.
Mean – the average pixel value of each pixel within the ROI box area.
Max – the maximum pixel value within the ROI box area.
Min – the minimum pixel value within the ROI box area.
STD – the standard deviation of the pixel values with the ROI box area.
SNR – the signal-to-noise ratio of the pixel values within the ROI box area.

SNR is calculated using the standard definition for images:

$$\mathrm{SNR} = \frac{\mu}{\sigma} \tag{1}$$

Where μ is the mean pixel value and σ is the standard deviation of the pixel values over a specified neighborhood.

The SNR dialog menu contains five menu items: “File”, “Stat”, “Box”, “Adjust” and “Help”:

1. The “File” item contains one submenu item,
   a. “Quit” which is used to terminate the plugin.
2. The “Stat” item contains one submenu item,
   a. “Save”, which causes current statistics to be saved to the statistics log dialog.
3. The “Box” item contains a series of submenu items used for modifying the size, position and boundary color of the box area.

4. The “Adjust” item contains a series of submenu items which are used to adjust the contrast of the image based on the ROI.
   a. “default”, returns the image to the original contrast settings
   b. “1 sigma”, adjust image contrast where new pixel range = μ +/- σ
   c. “2 sigma”, adjust image contrast where new pixel range = μ +/- 2σ
   d. “1 sigma drag”, adjust image contrast as b. when ROI is moved.
   e. “2 sigma drag”, adjust image contrast as c. when ROI is moved.
   f. “Off drag”, turns off drag if e. or f. are active.
5. The “Help” item contains one submenu item
   a. “About” which describes the plugin version and provides brief operating instructions.

C3.1.2 SNR Statistics Logging

The SNR Statistics dialog, shown in Figure C6, appears the first time the Save submenu item is selected from within the SNR dialog. As mentioned, current statistics are saved to this dialog where they are listed in the order they are collected. The first column of the display data simply maintains a count of the number of rows of data logged. The remaining columns contain the statistical data that appears in the display area of the SNR dialog and captured when “Save Item” is selected. The data listed can be saved to a file in a comma-delimited format by selecting the “Save As…” submenu item under the “File” menu.

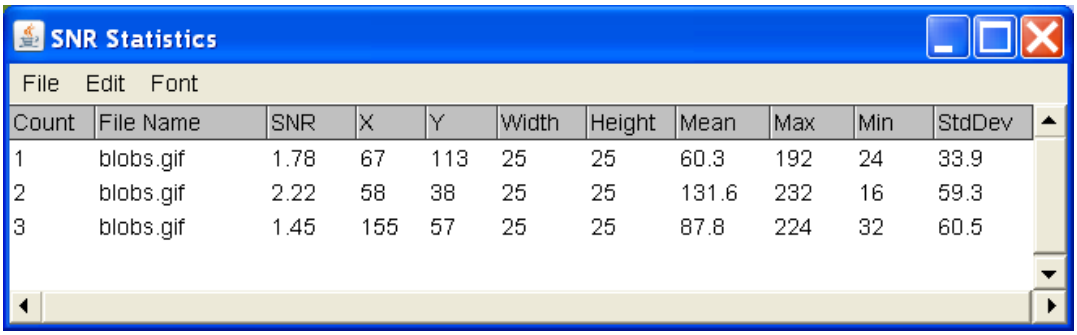

Figure C6. SNR Statistics Dialog Box

C3.2 Contrast-to-Noise Plugin

The contrast-to-noise plugin is named “Image CNR” and listed in XRay subMenu under the ImageJ “Plugins” menu item. Upon selecting “Image CNR” the CNR dialog box appears as shown in Figure C7. A green box and a red box defining two ROIs appear in the active image, as shown in Figure C8, indicating the pixel neighborhoods used for the statistics calculation. The boxes can be moved about the image by positioning the mouse cursor within a box, holding down the left mouse button, and dragging the box to a new location. The green box can be immediately moved to the mouse cursor location by holding down the “Ctrl” key and clicking the left mouse button. The red box is immediately moved by holding down the “Shift” key and clicking the left mouse button.

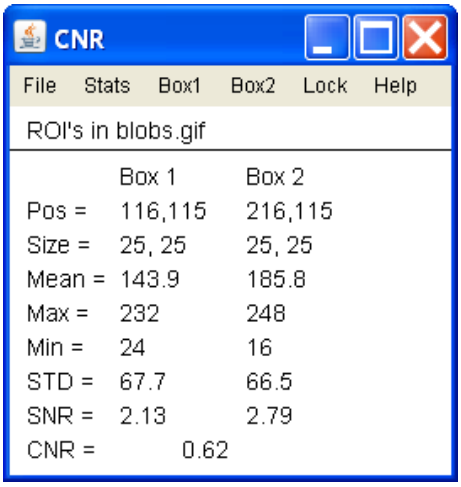

Figure C7. ImageJ CNR Dialog Box

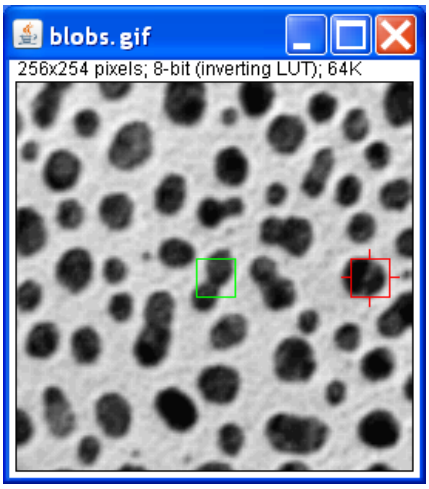

Figure C8. ImageJ CNR ROI Shown by Red Box in Image

C3.2.1 CNR Dialog. The CNR dialog contains a menu and statistics display area. The statistics display area is defined by a white background and begins by displaying the name of the image where the ROI is displayed. A horizontal line separates the image name from the statistics listed. The statistics automatically update as each box is moved about the active image. The green box is labeled "Box 1" and the red box is labeled "Box 2". The common statistics for each box are defined below:

Pos – the position of the upper left hand corner of the ROI box.
Size – the width and height of the ROI box in pixels.
Mean – the average pixel value of each pixel within the ROI box area.
Max – the maximum pixel value within the ROI box area.
Min – the minimum pixel value within the ROI box area.
STD – the standard deviation of the pixel values with the ROI box area.
SNR – the signal-to-noise ratio of the pixel values within the ROI box area.

SNR is calculated using the standard definition for images:

$$\text{SNR} = \frac{\mu}{\sigma} \tag{2}$$

Where μ is the mean pixel value and σ is the standard deviation of the pixel values over a specified neighborhood.

CNR is displayed at the bottom of the display area and is calculated using statistics from each box as defined below:

$$\text{CNR} = \frac{|\mu_a - \mu_b|}{\sigma_a} \tag{3}$$

Where μ_a is the mean of Box 1, μ_b is the mean of Box 2, and σ_a is the standard deviation of Box 1.

The CNR dialog menu contains six menu items: "File", "Stat", "Box1", "Box2", "Lock", and "Help".

1. The “File” item contains one submenu item,
   a.“ Quit” which is used to terminate the plugin.
2. The “Stat” item contains one submenu item,
   a. “Save”, which causes current statistics to be saved to the statistics log dialog.
3. The “Box1” item contains a series of submenu items used for modifying the size, position and boundary color of each box area.
4. 3. The “Box2” item also contains a series of submenu items used for modifying the size, position and boundary color of each box area.
5. The “Lock” item contains two submenu items: Off and On.
   a. “Off” permits each box to be dragged independently uing the mouse.
   b. “On” causes the boxes to move as a pair. Dragging one box causes the other to move relative to the box being dragged.
6. The “Help” item contains one submenu item
   a. “About” which describes the plugin version and provides brief operating instructions.

C3.2.2 CNR Statistics Logging. The CNR Statistics dialog, shown in Figure C9, appears the first time the “Save” submenu item is selected from within the CNR dialog. As mentioned, current statistics are saved to this dialog where they are listed in the order they are collected. The first column of the display data simply maintains a count of the number of rows of data logged. The remaining columns contain the statistical data that appears in the display area of the CNR dialog and captured when “Save Item” is selected. The data listed can be saved to a file in a comma-delimited format by selecting the “Save As…” submenu item under the “File” menu.

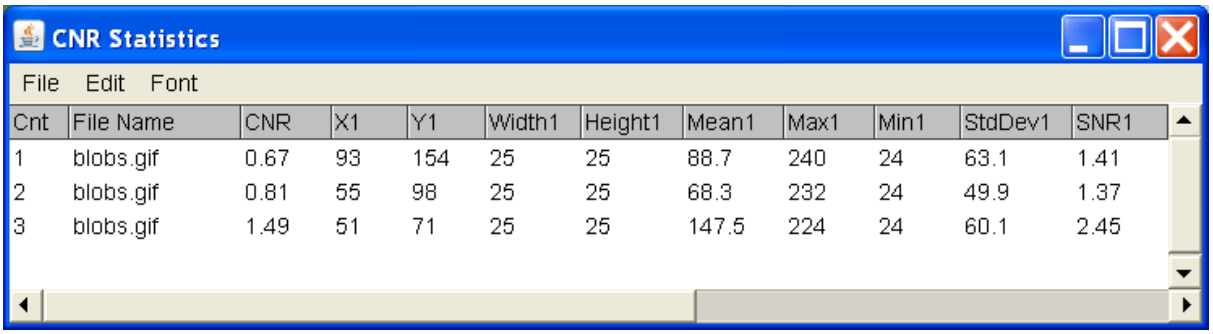

Figure C9. CNR Statistics Dialog Box

C3.3 Defect-to-Noise Plugin

The defect-to-noise plugin is named “Image DNR” and listed in the “XRay” submenu under the ImageJ “Plugins” menu item. Upon selecting “Image DNR”, the DNR dialog box appears as shown in Figure C10. A green box and a red box defining two ROIs appear in the active image, as shown in Figure C11, indicating the pixel neighborhoods used for the statistics calculation. The green box can be moved about the image by positioning the mouse cursor within the box, holding down the left mouse button, and dragging the box to a new location. The red box contains a line with three handles that can be used to resize, reposition, and reorient the box. The center handle repositions the box using the mouse. The end handles reorient and/or change the length of the

box using the mouse. The green box can be immediately moved to the mouse cursor location by holding down the "Ctrl" key and clicking the left mouse button. The red box is immediately moved by holding down the "Shift" key and clicking the left mouse button.

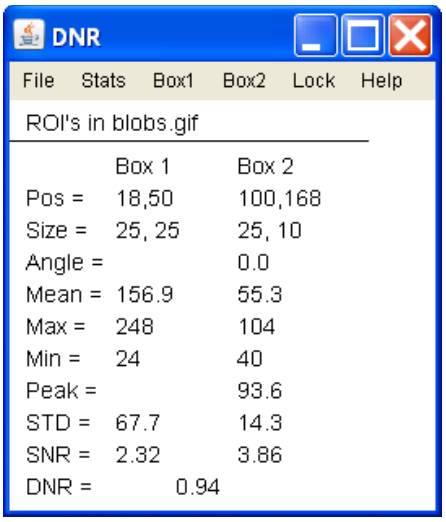

Figure C10. ImageJ DNR dialog box

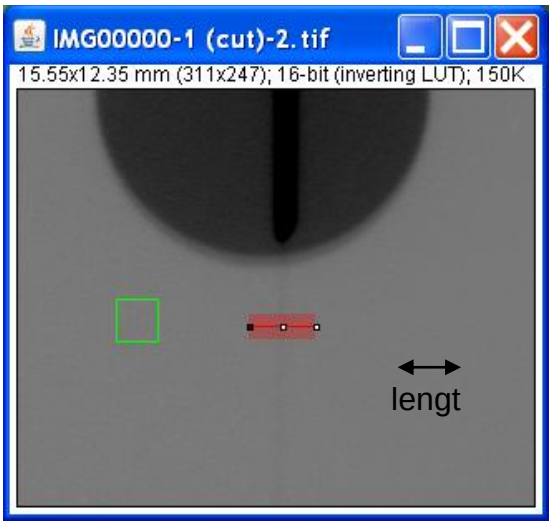

Figure C11. DNR Line Profiling Tool Shown by a Red Box

C3.3.1 Defect Processing. The defect-to-noise plugin contains specialized processing that attempts to locate a linear defect that has been selected using the red box ROI. For best results, the red box ROI should be oriented perpendicular to the suspected linear defect, as shown in Figure C11. Although referred to as a box, the red box ROI is actually a wide line defined as a series of single pixel lines running parallel to the length direction. If the box is of "width" equal to three, then the box consists of three adjacent lines of pixels, as shown in Figure C11. The number of pixels in each of the lines corresponds to the length of the box. The defect-to-noise averaging process is performed on corresponding pixels in each of the lines within the ROI. As a result of the analysis performed within the DNR tool, the "average intensity" perpendicular to the length direction is calculated and displayed on a plot whose abscissa is the pixel number in the length direction. The average of these adjacent lines is represented by the ROI Average Line displayed in the Line Profile graph shown in Figure C13. The abscissa of the plot is the pixel number in the ROI length direction and ordinate is the average intensity at that pixel location. The maximum value (i.e., peak) of this ROI Average Line is used to determine the Defect-to-Noise value defined in Section C3.3.2. The pixel number corresponding to peak value in the ROI Average Line determines the horizontal position of the red line that is drawn in the Line Image dialog shown in Figure C12. Additional information regarding the Line Image and ROI Average Line dialog boxes is contained in Section C3.3.3 below.

C3.3.2 DNR Dialog. The DNR dialog contains a menu and statistics display area. The statistics display area is defined by a white background and begins by displaying the name of the image where the ROI is displayed. A horizontal line separates the image name from the statistics listed. The statistics automatically update as each box is moved about the active image. The green box is labeled "Box 1" and the red box is labeled "Box 2". The common statistics for each box are defined below:

Pos – the position of the upper left hand corner of the box.
Size – the width and height of the box in pixels.
Angle – the orientation of box2 defined by the angle of the line about the origin (black handle)
Mean – the average pixel value of each pixel within the box area.
Max – the maximum pixel value within the box area.
Min – the minimum pixel value within the box area.
Peak – maximum value of the line profile (ROI Average Line).
STD – the standard deviation of the pixel values with the box area.
SNR – the signal-to-noise ratio of the pixel values within the box area.

SNR is calculated using the standard definition for images:

$$\text{SNR} = \frac{\mu}{\sigma} \tag{4}$$

Where μ is the mean pixel value and σ is the standard deviation of the pixel values over a specified neighborhood.

DNR is displayed at the bottom of the display area and is calculated using statistics from each box as defined below:

$$\text{DNR} = \frac{|\mu_a - \rho_b|}{\sigma_a} \tag{5}$$

Where μ_a is the mean of Box 1, ρ_b is the peak of the line profile (refer to Section C3.3.1) of Box 2 and σ_a is the standard deviation of Box 1.

The DNR dialog menu contains six menu items: File, Stat, Box1, Box2, Lock, and Help.

1. The "File" item contains one submenu item,
   a. "Quit" which is used to terminate the plugin.
2. The "Stat" item contains one submenu item,
   a. "Save", which causes current statistics to be saved to the statistics log dialog.
3. The "Box1" item contains a series of submenu items used for modifying the size, position and boundary color of the box area.
4. The "Box2" item contains a series of submenu items used for modifying the size, position and color of the box area as well as the box orientation.
5. The "Lock" item contains two submenu items: Off and On.
   a. "Off" permits each box to be dragged independently uing the mouse.
   b. "On" causes the boxes to move as a pair. Dragging one box causes the other to move relative to the box being dragged.
6. The "Help" item contains one submenu item
   a. "About" which describes the plugin version and provides brief operating instructions.

C3.3.3 Additional Defect Dialogs. Two additional dialog boxes are displayed that are associated with the red box ROI: the "Line Image" dialog and "Line Profile" dialog. Both boxes display information that is derived from the line profile described in Section C3.3.1. The "Line Image" dialog is simply a display of the ROI with a red line indicating where the line profile peak is located, as shown in Figure C12. The contrast of the Line Image display is automatically adjusted based on pixel content.

Figure C12. Line Image Display Box

The "Line Profile" dialog contains a graph of a line profile created from the ROI pixel information (described in Section C3.3.1), as shown in Figure C13. The horizontal axis indicates the length of the line in pixels and the vertical axis is the amplitude of each pixel value along the line. A significant peak within the line profile, as shown in Figure C13, is a good indication that a crack is present.

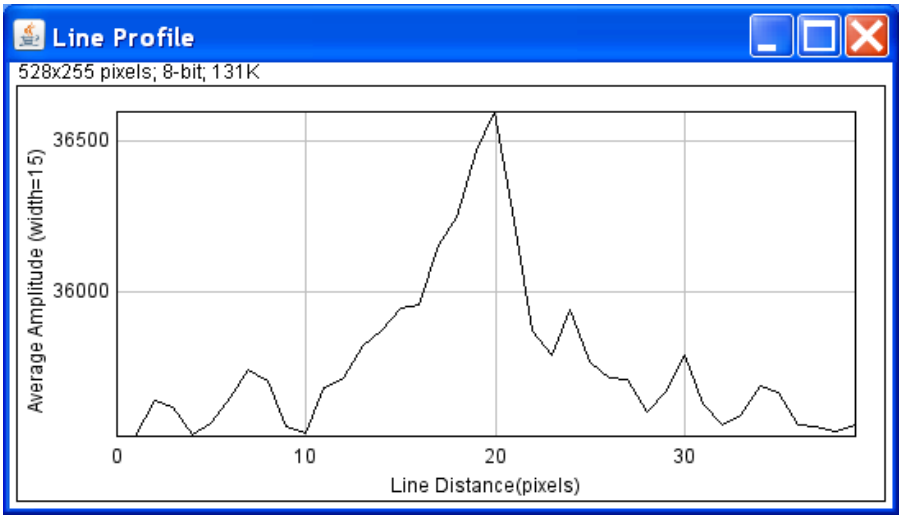

Figure C13. Line Profile Average Intensity

C3.3.4 DNR Statistics Logging. The DNR Statistics dialog, shown in Figure C14, appears the first time the "Save" submenu item is selected from within the DNR dialog. As mentioned, current statistics are saved to this dialog where they are listed in the order they are collected. The first column of the display data simply maintains a count of the number of rows of data logged. The remaining columns contain the statistical data that appears in the display area of the DNR dialog and captured when the save item is selected. The data listed can be saved to a file in a comma-delimited format by selecting the "Save As…" submenu item under the "File" menu.

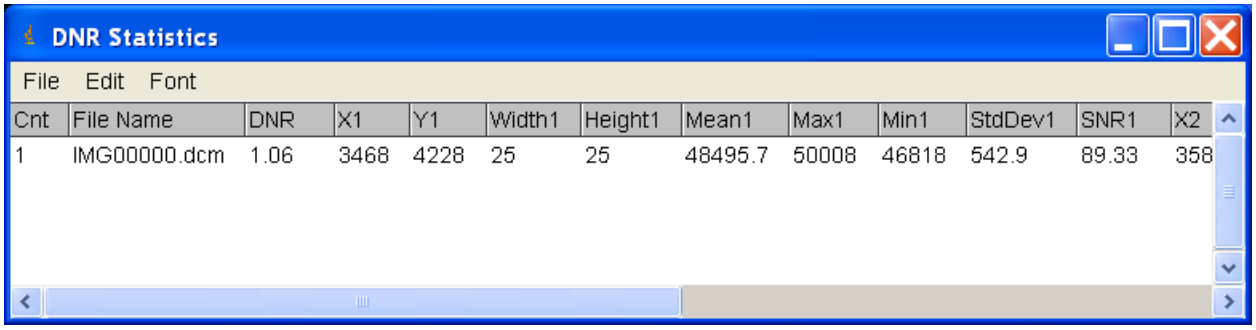

Figure C14. DNR Statistics Dialog Box

C4.0 SUMMARY

UDRI has successfully developed three Java plugins that expand the capability of the ImageJ image processing application allowing the measurement of signal-to-noise, contrast-to-noise, and – a new method – defect-to-noise, for determining the image quality of computed radiography images. This new software insures that a consistent and reliable approach for determining image quality is afforded to all project images, regardless of image format or vendor imaging workstation. And last, but not least, a proven approach for developing image processing tools has been explored and demonstrated, and can be easily expanded upon as new requirements demand new tools in the future.